

**CHARACTERIZATION OF PROTON EXCHANGE MEMBRANE
FUEL CELL AND PEM ELECTROLYZER USING
NON-STEADY STATE ELECTROCHEMICAL TECHNIQUES**

By

Yaritza M. López de Jesús

A thesis submitted in partial fulfillment of the requirements for the degree of

MASTER OF SCIENCE

in

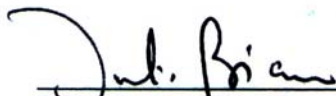
CHEMICAL ENGINEERING

UNIVERSITY OF PUERTO RICO

MAYAGÜEZ CAMPUS

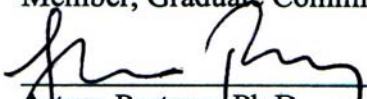
2004

Approved by:



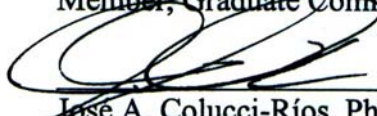
Julio G. Briano, Ph.D.
Member, Graduate Committee

12 Jul. 2004
Date



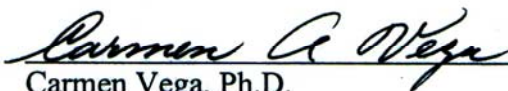
Arturo Portnoy, Ph.D.
Member, Graduate Committee

1/Julio/2004
Date



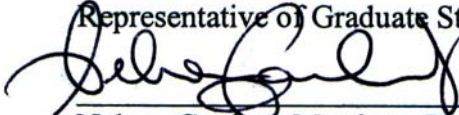
José A. Colucci-Ríos, Ph.D.
President, Graduate Committee

June 21, 04
Date



Carmen Vega, Ph.D.
Representative of Graduate Studies

1 de julio de 2004
Date



Nelson Cardona Martínez, Ph.D.
Chairperson of the Department

July 14, 2004
Date

ABSTRACT

Proton Exchange Membrane Fuel Cells (PEMFCs) and PEM Electrolyzer were characterized using Electrochemical Impedance Spectroscopy (EIS). Faradaic resistance (R_{Ω}), kinetic and mass transfer parameters such as charge transfer resistance, double layer capacitance and diffusion coefficient from Warburg's theory were obtained. The PEM electrolyzer and PEM fuel cell use *perfluorocarbon sulfonic acid (PFSA) ionomer* (Nafion™) as the electrolyte. The PEMFC showed more performance losses than the PEM Electrolyzer, these losses were corroborated with Warburg's theory. The PEMFC exhibited performance losses related with mass transfer. Two PEMFCs with different catalyst loading, 0.1 and 0.3mgPt/cm², were compared respectively, and the memory effects were analyzed. The PEMFC with 0.3mgPt/cm² presented better properties and less performances losses than the PEMFC with 0.1mgPt/cm². The memory effects of both PEMFCs were found to be related to the water content and management in the cells. This phenomenon was more evident at low applied potentials.

RESUMEN

Una celda de combustible y un electrolizador de membrana de intercambio protónico fueron evaluadas utilizando la técnica electroquímica de espectroscopía de impedancia. Se pudo obtener valores de la resistencia del electrolito, parámetros cinéticos y de transferencia de masa, como la resistencia de la transferencia de carga, capacitancia de doble capa y el coeficiente de difusión de la Teoría de Warburg. La celda de combustible y el electrolizador un monómero de ácido perfluorosulfónico (Nafion™) como electrolito. La celda de combustible demostró tener más pérdidas en la operación que la celda de electrólisis. La celda de combustible presentó pérdidas causadas por efectos de transferencia de masa, lo que fue corroborado por la teoría de Warburg. Se analizaron y compararon dos celdas de combustibles con diferentes cantidades de catalizador y se estudiaron los efectos de memoria de ambas celdas. La celda con $0.3\text{mgPt}/\text{cm}^2$ presentó menos pérdidas en la operación que la celda de $0.1\text{mgPt}/\text{cm}^2$. Se encontró que los efectos de memoria de ambas celdas de combustibles están relacionados con el contenido y manejo de agua en las celdas, lo que fue más evidente a bajos potenciales aplicados.

Copyright © 2004 by Yaritza M. López de Jesús. All rights reserved. Printed in the United States of America. Except as permitted under the United Copyright Act of 1976, no part of this publication may be reproduced or distributed in any form or by any means, or stored in a data base or retrieval system, without the prior written permission of the publisher.

... *“to God, because He provides me with health and intelligence to accomplish my work”*.

... *“to my beautiful family, just because they made me”*.

Yaritza

ACKNOWLEDGEMENTS

I want to thank God and Virgin María because they always drive my actions, giving me wisdom, forbearance and energy to finish and achieve everything I desire. I will like to thanks the University of Puerto Rico, Mayagüez Campus, specially, to the Chemical Engineering Department, for allowing the opportunity to do my Master in Science degree. The best stimulus was given by Dr. José A. Colucci, my advisor during my two year of studies, who trusted on me to do my research work. I appreciate his great knowledge and desire of teach everybody with excellence.

Thanks to my family; Mami, Papi, Moisés, Jose Gabriel, and Juan Carlos, who gave me the moral and economical support when I need it, I love them! Thanks to my love, Lob, because he always me with tender, love and happiness. Thanks for your patience and trust. Also, I want to thank his family, because they always supported me in my bad and good moments. Thanks to my friends Madeline, Marisel, Luna, and Ritsdeliz, because they encouraged me with their words and “jangeo” time. Thanks to the undergraduate students that worked with me hard during this research. Finally, I want to thank my beautiful and wonderful doggy, Groffy, because he always gave me love. Thanks to everyone that put their piece of rock in my student life.

TABLE OF CONTENTS

LIST OF TABLES	ix
LIST OF FIGURES	x
LIST OF APPENDIX	xv
CHAPTER I: INTRODUCTION	1
I.1 JUSTIFICATION	1
I.2 OBJECTIVES	2
CHAPTER II: LITERATURE REVIEW	4
CHAPTER III: THEORY	15
III.1 FUEL CELL TECHNOLOGY	15
III.1.a PEM FUEL CELL DESCRIPTION	16
III.1.a.i PEM FUEL CELL ELECTROCHEMICAL PROCESS	19
III.2 ELECTROCHEMISTRY	21
III.2.a FARADAIC AND NONFARADAIC PROCESS	21
III.2.b ELECTRODE REACTIONS	22
III.2.c THE ELECTRICAL DOUBLE LAYER	27
III.3 ELECTROCHEMICAL IMPEDANCE SPECTROSCOPY	30
III.3.a INTRODUCTION	30
III.3.b EXPERIMENTAL ANALYSIS THEORY	31
III.3.c SIMPLEST EQUIVALENT CIRCUIT	36
III.3.d NYQUIST PLOT	38

III.3.e BODE PLOT	40
III.3.f WARBURG IMPEDANCE	43
CHAPTER IV: MATERIALS AND METHODS	46
IV.1 MATERIALS	46
IV.2 METHODS	49
CHAPTER V: DISCUSSION OF RESULTS	52
V.1 PEM FUEL CELL MODE VERSUS ELECTROLYSIS MODE	52
V.2 MEMORY AND CATALYST LOADING EFFECTS	63
V.3 LINEAR POLARIZATION	78
CHAPTER VI: CONCLUSIONS	81
CHAPTER VII: RECOMMENDATIONS	83
BIBLIOGRAPHY	84
APPENDIX	88

LIST OF TABLES

Table 1. Fuel cell classifications and characteristics	15
Table 2. Impedance equation for simple electric circuits	37
Table 3. Results of the PEM Electrolyzer	62
Table 4. Results of the PEM Fuel cell	62
Table 5. Results for PEMFC of $0.1\text{mgPt}/\text{cm}^2$ with Wet Pretreatments	76
Table 6. Results for PEMFC of $0.1\text{mgPt}/\text{cm}^2$ with Dry Pretreatments	76
Table 7. Results for PEMFC of $0.3\text{mgPt}/\text{cm}^2$ with Wet Pretreatments	77
Table 8. Results for PEMFC of $0.3\text{mgPt}/\text{cm}^2$ with Dry Pretreatments	77
Table 9. Linear Polarization for PEMFC with $0.3\text{mgPt}/\text{cm}^2$.	80
Table E.1. Exchange current of PEMFC with $0.1\text{mgPt}/\text{cm}^2$	105
Table E.2. Exchange current of PEMFC with $0.3\text{mgPt}/\text{cm}^2$	105

LIST OF FIGURES

Figure 1. Schematic cross-section of a single polymer electrolyte fuel cell	17
Figure 2. Single PEM fuel cell	18
Figure 3. Fuel cell mode schematic and process diagram	20
Figure 4. Electrolysis cell mode schematic and process diagram	20
Figure 5. Helmholtz's electrical double layer model	28
Figure 6. Stern's double layer model schematic diagram	30
Figure 7. Applied potential (E) and resulting current sine waves	33
Figure 8. Impedance planar vector in rectangular and polar coordinates	35
Figure 9. Equivalent circuit of an electrochemical cell	37
Figure 10. Nyquist Plot	38
Figure 11. Bode Plot of simple electrochemical cell	41
Figure 12. Bode Plot for Warburg Impedance	44
Figure 13. Idealized Warburg Plot	45
Figure 14. Eco H ₂ /Air equipment	46
Figure 15. Demountable PEMFC	48
Figure 16. PARSTAT 2263	48
Figure 17. Nyquist Plot for the PEM Electrolyzer at different potentials	55
Figure 18. Nyquist Plot for the PEMFC for different overpotentials	55
Figure 19. PEM electrolyzer Ohmic Resistance from Nyquist Plot at different overpotentials	56

Figure 20. PEMFC Ohmic Resistance from Nyquist Plot at different overpotentials	56
Figure 21. Charge Transfer Resistance versus potential for PEM Electrolyzer	57
Figure 22. Charge Transfer Resistance versus potential for PEMFC	52
Figure 23. Warburg characteristic impedance plot for the PEMFC	59
Figure 24. Warburg diffusion coefficient for PEMFC	60
Figure 25. Warburg resistance for PEMFC	60
Figure 26. Double layer capacitance of the PEM Electrolyzer	61
Figure 27. Double layer capacitance of the PEMFC	61
Figure 28. Nyquist Plot for PEMFC 0.1mgPt/cm ² with dry pretreatment at OCP	64
Figure 29. Nyquist Plot for PEMFC 0.3mgPt/cm ² with dry pretreatment at OCP	64
Figure 30. Nyquist Plot for PEMFC 0.1mgPt/cm ² with wet pretreatment at OCP	65
Figure 31. Nyquist Plot for PEMFC 0.3mgPt/cm ² with wet pretreatment at OCP	65
Figure 32. Ohmic resistance for PEMFC with 0.1mgPt/cm ² for all initial conditions	67
Figure 33. Ohmic resistance for PEMFC with 0.3mgPt/cm ² for all initial conditions	68
Figure 34. R1 for PEMFC with 0.1mgPt/cm ² for all initial conditions	69
Figure 35. R1 for PEMFC with 0.3mgPt/cm ² for all initial conditions	69
Figure 36. Experimental Charge Transfer Resistance for PEMFC of 0.1mgPt/cm ²	71
Figure 37. Charge Transfer Resistance calculated using <i>i-η</i> equations for PEMFC of 0.1mgPt/cm ²	71
Figure 38. Experimental Charge Transfer Resistance for PEMFC of 0.3mgPt/cm ²	72
Figure 39. Charge Transfer Resistance calculated using <i>i-η</i> equations for PEMFC of 0.3mgPt/cm ²	72

Figure 40. Double Layer Capacitance versus overpotential for PEMFC of 0.1mgPt/cm ²	74
Figure 41. Double Layer Capacitance versus overpotential for PEMFC of 0.3mgPt/cm ²	75
Figure 41. Linear Polarization for PEMFC of 0.3mPt/cm ² with Dry Pretreatment.	79
Figure 43. Linear Polarization for PEMFC of 0.3mPt/cm ² with Wet Pretreatment.	80
Figure A.1. PEMFC Nyquist Plots at different overpotentials	89
Figure A.2. PEMFC Ohmic Resistance from Bode Plot at different overpotentials	89
Figure A.3. Charge Transfer Resistance versus overpotential for PEMFC from Bode Plot	90
Figure B.1. PEM Electrolyzer Nyquist Plots at different potentials	91
Figure B.2. PEM electrolyzer Ohmic Resistance from Bode Plot at different overpotentials	91
Figure B.3. Charge Transfer Resistance versus potential for PEM Electrolyzer from Bode Plot	92
Figure C.1. Nyquist Plots for PEMFC of 0.1mgPt/cm ² with dry pretreatment at OCP	93
Figure C.2. Nyquist Plots for PEMFC of 0.1mgPt/cm ² with wet pretreatment at OCP	93
Figure C.3. Nyquist Plots for PEMFC of 0.1mgPt/cm ² with dry pretreatment at $\eta = -0.05V$	94
Figure C.4. Nyquist Plots for PEMFC of 0.1mgPt/cm ² with wet pretreatment at $\eta = -0.05V$	94
Figure C.5. Nyquist Plots for PEMFC of 0.1mgPt/cm ² with dry pretreatment at $\eta = -0.10V$	95
Figure C.6. Nyquist Plots for PEMFC of 0.1mgPt/cm ² with wet pretreatment at $\eta = -0.10V$	95
Figure C.7. Ohmic resistance for PEMFC with 0.1mgPt/cm ² for all initial conditions from Bode Plot	96

Figure C.8. Experimental Charge Transfer Resistance from Bode Plot for PEMFC of 0.1mgPt/cm ²	96
Figure C.9. Charge Transfer Resistance calculated using $i-\eta$ equation for PEMFC of 0.1mgPt/cm ²	97
Figure C.10. Double Layer Capacitance versus overpotential for PEMFC of 0.1mgPt/cm ² from Bode Plot	97
Figure D.1. Nyquist Plots for PEMFC of 0.3mgPt/cm ² with dry pretreatment at OPC	98
Figure D.2. Nyquist Plots for PEMFC of 0.3mgPt/cm ² with wet pretreatment at OPC	98
Figure D.3. Nyquist Plots for PEMFC of 0.3mgPt/cm ² with dry pretreatment at $\eta = -0.02V$	99
Figure D.4. Nyquist Plots for PEMFC of 0.3mgPt/cm ² with wet pretreatment at $\eta = -0.02V$	99
Figure D.5. Nyquist Plots for PEMFC 0.3mgPt/cm ² with dry pretreatment at $\eta = -0.05V$	100
Figure D.6. Nyquist Plots for PEMFC of 0.3mgPt/cm ² with wet pretreatment at $\eta = -0.05V$	100
Figure D.7. Nyquist Plots for PEMFC of 0.3mgPt/cm ² with dry pretreatment at $\eta = -0.08V$	101
Figure D.8. Nyquist Plots for PEMFC of 0.3mgPt/cm ² with wet pretreatment at $\eta = -0.08V$	101
Figure D.9. Nyquist Plots for PEMFC of 0.3mgPt/cm ² with dry pretreatment at $\eta = -0.10V$	102
Figure D.10. Nyquist Plots for PEMFC of 0.3mgPt/cm ² with wet pretreatment at $\eta = -0.10V$	102
Figure D.11. Ohmic resistance for PEMFC with 0.3mgPt/cm ² for all initial conditions from Bode Plot	103
Figure D.12. Experimental Charge Transfer Resistance from Bode Plot for PEMFC of 0.1mgPt/cm ²	103

Figure D.13. Charge Transfer Resistance calculated using $i-\eta$ equation for PEMFC 0.1mgPt/cm ² from Bode Plot	104
Figure D.14. Double Layer Capacitance versus overpotential for PEMFC 0.3mgPt/cm ² from Bode Plot	104
Figure F.1. $E-i$ curve for PEMFC of 0.3mgPt/cm ² at dry condition	106
Figure F.2. $E-i$ curve for PEMFC of 0.3mgPt/cm ² at dry condition	107
Figure F.3. $E-i$ curve for PEMFC of 0.3mgPt/cm ² at wet condition	108
Figure F.4. $E-i$ curve for PEMFC of 0.3mgPt/cm ² at wet condition	109

LIST OF APPENDIX

APPENDIX A. PEMFC RESULTS FOR ELECTROLYSIS COMPARISON	89
APPENDIX B. PEM ELECTROLYZER	91
APPENDIX C. PEMFC with $0.1\text{mgPt}/\text{cm}^2$	93
APPENDIX D. PEMFC with $0.3\text{mgPt}/\text{cm}^2$	98
APPENDIX E. EXCHANGE CURRENT	105
APPENDIX F. LINEAR POLARIZATION PLOTS FOR PEMFC WITH $0.3\text{mgPt}/\text{cm}^2$	106
APPENDIX G. PROPERTIES OF NAFION [®]	110

CHAPTER I: INTRODUCTION

I.1 JUSTIFICATION

Depletion of fossil fuels and the environment degradation are two of the most important problems related to energy production. The need for efficient, non-polluting power sources for vehicles in urban environments, emphasized by recent legislative initiatives, has resulted in increased attention to the option of fuel cell powered vehicles of high efficiency and low tail pipe emissions [19]. This is recognized as a worldwide forward step in the protection of human health and the environment. Fuel cells continue to gain momentum as a clean and efficient potential future energy conversion technology.

Among the different types of fuel cells, the Proton Exchange Membrane Fuel Cell (PEMFC) is attracting much interest, because it is capable of producing high power densities working at low temperatures. The PEMFC uses hydrogen gas as fuel, which is considered the most suitable fuel for a fuel cell powered vehicle, since it provides the highest conversion efficiency [26]. PEMFCs are electrochemical reactors which complete direct conversion of the chemical energy of the reactants, hydrogen and oxygen, to electrical energy, water and heat with high efficiency and high environmental compatibility. There are also the reversible proton exchange membrane fuel cells (RFC), with high energy capacity and with potential for many weight-critical portable applications. The reversible proton exchange membrane (PEM) cells are capable of operating as fuel cell and electrolyzer. The PEM electrolyzer is another electrochemical cell which breaks down water into hydrogen and oxygen gas with an applied voltage,

which is the reversible process of the PEM fuel cell. The PEMFC and PEM electrolyzer performance losses are going to be evaluated and compared using electrochemical methods. This work will be focused in characterizing the performance of the PEM electrochemical cells using the Electrochemical Impedance Spectroscopy (EIS) technique.

I.2 OBJECTIVES

The commitment to find a non-polluting energy source has increased the attention of research and development of fuel cells and the different alternatives to produce and store the required fuel for these cells. The proton exchange membrane fuel cell and electrolyzer operated at different potentials could generate performance losses caused by physical properties, kinetics and transports phenomenon. Non-steady state electrochemical techniques, such as EIS, can be used to understand the fundamental and performance losses of the PEM electrochemical cells. EIS is a very useful tool to formulate a hypothesis, particularly when EIS data is converted to equivalent circuit models.

A key component of this work will be the comparison of the equivalent circuit elements that will be proposed from the oxygen electrode operating in fuel cell and electrolyzer mode. Also, emphasis will be given to understand memory related effects typically observed in electrochemical systems. In fuel cells and/or electrolyzer mode operation it is suspected that membrane humidification could play an important role in the memory of the cell. The equivalent circuits are expected to reflect their behavior. Spectrums will be generated within an overpotential range to accomplish electrochemical

impedance spectroscopy experiments. Analyses of the impedance data provide better understanding of the water management, proton and oxygen transport within the PEM fuel cell and PEM electrolyzer under operational conditions. The experiments for the proton exchange membrane fuel cell are going to be focused in the cathode oxygen reduction reaction (ORR) because the major contributions of the total energy losses due to high overpotential are created in the cathode. Also, the effects of catalyst loading will be studied with 0.1mgPt/cm^2 and 0.3mgPt/cm^2 .

CHAPTER II: LITERATURE REVIEW

The requirements for obtain high efficiency and good performance of the PEMFC direct the research and development field to study interfacial electrochemistry, electrochemistry and materials science aspects of membranes, carbon and metals, and mass/heat transport engineering. In most general terms, the target of these efforts in development of materials and components has been to achieve high PEMFC performance, long-term performance stability and low intrinsic cost.

There are several electrochemical methods and techniques to study phenomena occurring in the interfacial region between electrodes and electrolytes. In general, these techniques involve driving the electrode to a condition far from equilibrium and the response is observed usually as a transient signal. EIS has been recognized as a valuable tool in the study of electrochemical systems. EIS deals with materials for which ionic conductivity predominates, includes both supported and unsupported situations, and may involve either ionic motion and/or ion-vacancy motion [29].

Paganin et al. [31] studied several aspects related to the limiting polarization behavior of the polymer electrolyte fuel cells using ac impedance spectroscopy. They took into account the different types of potential losses caused by the interfacial reaction kinetics, the conductance of the electrolyte in the catalyst layer, the oxygen diffusion in the gas phase, in the thin film and in the distributed agglomerate regions of the gas diffusion electrodes and the balance of the water in the membrane. They found that the water transport plays an important role in establishing the limiting polarization behavior of the polymer electrolyte fuel cell, corresponding to the only limiting factor when pure

oxygen is employed as the cathode reagent. When the oxygen source is air, the diffusion of oxygen in the gas phase becomes a limiting factor, but for pressurized systems the diffusion of water can also be observed, especially for thick membranes.

Andreas et al. [1] investigated the physico-chemical origins of the performance loss in polymer electrolyte fuel cells operated at high current densities. They presented fuel cell impedance measurements varying the membrane thickness, the ionic density, and the humidification conditions of the reactants. They mentioned that there is strong evidence to support that the observed low frequency impedances might equally be attributed to an effect on the anode side. At high current densities, the anode side water content in the membrane may be strongly reduced when thicker membranes or materials with intrinsically lower water content are being used. In that case, not only the higher integral membrane resistance will lower the cell performance, but there could be a build-up of additional, non-negligible, activation overpotential for the hydrogen oxidation reaction (HOR). As most of the catalyst sites become inactive due to the low proton mobility in this dried out zone, and consequently the proton transport off the reaction site is inhibited.

Ayala [3] used impedance spectroscopy for the characterization and understanding of fuel cell performance losses. A H₂/O₂ Polymer Electrolyte Fuel Cell (PEFC) with a Pt/Ru-Nafion[®] 117 membrane-electrode assembly was used in a range of 3.4 to 9.6 and 1.6 to 5.1 mL/min for H₂ and O₂ flow rates, respectively. Cell temperatures were varied from 27 °C to 47°C. The sources and nature of the voltage losses and the kinetics effects were determined using impedance spectroscopy. Anode charge transfer

resistance values were around 0.019 ohms. Membrane resistance values (around 0.5 ohm-cm²) and charge transfer values as a function of overpotential were determined (Cathode charge transfer resistance values presented an average Tafel slope of 116 mv/dec). Other findings include the diffusion problems encountered when reactant gases are not fed stoichiometrically.

Parthasarathy et al. [33] performed ac impedance measurements in the frequency range of 0.05 Hz – 100 kHz for a platinum microelectrode/bulk Nafion interface. They observed two major features in the complex impedance plot. At lower frequency they found a feature associated with the charge transfer resistance in parallel with interfacial double layer capacitance. The other feature was found at higher frequency, typically in the 10 – 100 kHz frequency domain, and was attributed to grain boundaries in the ionomeric membrane electrolyte, i.e., to a bulk ionomeric electrolyte phenomenon. They found at higher cathode polarizations, kinetic semicircle approaches the real Z axis in the complex plot at the high frequency end with an angle of 45, which correspond to Warburg element. They showed a decrease in the charge transfer resistance with an increase in cathode overpotential.

Eikerling et al. [11] studied a macro-homogeneous model under stationary conditions to calculate the small-signal dynamic response of the cathode catalyst layer in polymer electrolyte fuel cells. Within this approach the effects of reaction kinetics and double layer capacitance at the dispersed catalyst/electrolyte interface, proton conductivity of the electrolyte network within the layer and oxygen diffusion through the gas-pore space were studied. The analytical expressions derived reveal relationships

between the structure of the layer and impedance spectra. Particularly strong dependences of the differential resistivity on the electrode composition appear if either proton transport or oxygen diffusion dominates the voltage losses. Due to proton transport limitations, a linear branch was seen in impedance spectra in the high frequency limit, whereas in the low frequency domain a semicircular part arises. These results helped to distinguish the contribution of the catalyst layer from the contribution of other fuel cell components and characterize it quantitatively.

Song et al. [36] studied polymer electrolyte fuel cell electrodes to find an optimal composition of the electrodes using AC impedance methods. The thickness and composition of the supporting layer were optimized on the basis of the information of the AC impedance measurements. The AC spectra for ORR at different cathodic potentials and various concentration of conventional Teflon demonstrated values for the ohmic resistance of 0.25-0.3 ohms-cm² for 3.5 mg cm⁻² catalyst loading. They found a low frequency arc in the impedance spectrum at high overpotentials, which is believed to reflect water related transport limitations.

Fischer et.al. [12] investigated and achieved better performance of the PEMFC at high electro-catalyst utilization. The PEMFC was equipped with thin film electrodes exploiting pore forming with additives in the electrode recipe formulation. They found better access of oxygen from air to the depth of the cathode. For air operation at ambient pressure and catalyst loading of 0.15 mg Pt cm⁻² a current density of 200 mA cm⁻² at 0.7 V cell voltages can be obtained with such electrodes. With oxygen no improvement in performance occurred at current densities up to 800 mA cm⁻² with dry cathode gases.

Recently, Jaouen et. al. [25] studied the behavior of a polymer electrolyte fuel cell cathode with 30 wt % Nafion and 70 wt % Pt/C using current-interrupt technique and electrochemical impedance spectroscopy. Steady-state polarization curves were also recorded. They investigated the effect of a varying oxygen pressure and humidity. A mathematical model was fitted to experimental data recorded at current densities in the range 1-400 mA cm⁻². Up to a current density of 200 mA cm⁻², the model could fit the data well. They determined the double-layer capacitance, Tafel slope, oxygen solubility, and the effective proton conductivity in the cathode. At higher current density, the model could not properly fit the data, possibly because of non-uniform electrode thickness or because the data, especially the impedance spectrum was affected by the anode. The anode was not taken into account in the model. By the impedance data they observed a low frequency loop attributed to the membrane behavior. The parameters obtained from the experimental data indicated that the electrode is limited by both diffusion and migration.

Guangehun and Pickup [21] studied the effect of Nafion catalyst loading in the cathode layer of the PEMFC electrodes using impedance spectroscopy, cyclic voltammetry and polarization techniques. The optimum Nafion loading was determined to be 30% mass by the need to balance the improved proton conductivity and oxygen permeability. The impedance results demonstrated that the ionic conductivity increased with the Nafion content, and this is the main factor responsible from the increase in performance up to 30% Nafion. The losses at higher Nafion content was attributed to increasing oxygen transport resistance, because the electronic resistance did not increase

significantly. The higher electronic resistances were found at low Nafion loadings, indicating that Nafion played a significant role.

Gode et. al. [18] investigated the Nafion content of the cathode, spanning from 10 to 70 wt%, influence on its structure and electrochemical performance using materials and electrochemical characterization techniques (polarization curves, EIS, and current pulse measurements). They found the cathode performance at lower Nafion content, less than 30 wt%, limited by poor kinetics due to poor wetting of Pt by Nafion, by proton migration throughout the cathode as well as diffusion of O₂ in the bulk. At medium Nafion content, from 35 to 45 wt. %, they explained the wetting of Pt by Nafion is almost complete and the mass transport limitations were due to O₂ diffusion in the agglomerates. At Nafion content of 45 wt. % they explained that the pore size and the overall porosity decreased becoming the cathode limited by O₂ diffusion through the agglomerates and the cathode.

Brett et al. [6] presented a method for measuring electrochemical impedance spectroscopy response over a frequency range of 0.1 Hz to 10 kHz as a function of position in a solid polymer fuel cell. Measurements have been made at both 0.8 and 0.6 volts vs. SHE. A distribution of impedance characteristics was seen along the channel with evidence of mass transport effects that are not evidence from localized dc measurements. The membrane conductivity did not change with positions at both potentials, as is expected from the fact that reactant gases were fully humidified. At low potentials and low frequency response dominates a time constant characteristic of convective transport within the flow channel. The response was attributed to the

consumption of reactant upstream of the point of which the measurement was made.

Genies et. al. [17] studied the ORR on Pt nanoparticles in alkaline solution using d.c. and a.c. techniques (EIS). The ORR impedance measurements on Pt particles using an active layer on a gas diffusion electrode instead of on a rotating disk electrode, showed inductive behavior characteristic of a two electrochemical step mechanism. They described the results with ECE mechanism (four-electron pathway) and with EEC mechanism (two-electron pathway followed by chemical decomposition of OH_2^- on the initial or another particle). The EEC mechanism was found preponderant on small nanoparticles.

Freire and González [13] have studied the effect of temperature, membrane thickness and humidification conditions on the impedance response. The impedance results were analyzed in terms of the high frequency resistance, the contribution of the charge transfer due to the oxygen reduction reaction and a low frequency relaxation process. They concluded that the low frequency relaxation process is mainly due to the flooding of the cathode with liquid water and the consequential shortage of oxygen for the oxygen reduction reaction due to its limited diffusivity in water. They compared the results for different membrane thicknesses and operation conditions at constant cell potential. But when different cell setups and operational conditions were compared in potentiostatic mode, the current density (reaction rate) differs and so did the anode and cathode overpotential as well as the production of water on the cathode side. They showed that thinner membranes present better characteristics of water management.

Wagner [39] characterized the membrane electrode assembly in polymer

electrolyte fuel cells using impedance spectroscopy. He proved the possibility of separate the cell impedance into electrode impedances and electrolyte resistance with varying the operational conditions, current density and gas supply of the fuel cell and by simulation of the measured EIS with an equivalent circuit. He calculated the i - E curves and voltage losses (overpotential) in the fuel cell integrating over current densities of the individual impedance elements. Also, he determined the rate determining reaction steps depending on current density and humidification.

Cho et. al. [7] determined the characteristics of the PEMFC brought to temperatures below 0°C . The characteristics were studied with thermal cycles during which the temperature of the environment chamber was cycled from 80 to 210°C . They found the cell performance was degraded due to the phase transformation and volume changes of water. They revealed with the AC impedance spectroscopy that charge transfer resistance and ohmic resistance were increased by the repetitive freezing and melting of water in PEMFC while proton conductivity was almost constant. Concluding, the increase in ohmic resistance was attributed to an increase in contact resistance between the membrane, the electrodes, and flow fields.

Gottesfeld and Zawodzinski [19] studied the losses in the Polymer Electrolyte Fuel Cells. They mentioned that the high overpotential at the PEFC cathode is the most important source of loss in the PEFC, as in all other low-temperatures fuel cells. This is reflected directly in a polarization curve of the PEFC by the open circuit voltage close to 1.0V , compared with a thermodynamically voltage expected, 1.23V at room temperature for H_2/O_2 fuel cell. They attributed the discrepancy to sluggish kinetics of the oxygen

reduction reaction process, resulting in an open circuit mixed potential. A cathode potential as low as 0.70-0.80V is required to reach an ORR current density of 1 A/cm² in a PEFC air cathode at 80°C, corresponding to a cell voltage loss of 400-500mV.

Lefebvre et. al. [27] interpreted impedance data for cathodes in proton exchange membrane fuel cells with the aid of a finite transmission-line model in which the ionic conductivity of the catalyst layer decreases with distance from the membrane. They purged the cathode compartment of the cell with nitrogen during measurements and found that the impedance response becomes dominated by charging of the catalyst's double layer through the layer's ionic resistance. With simulation of the experimental data they showed the variation of the catalyst layer's ionic conductivity with distance from the membrane. They compared data for electrodes with and without impregnated ionomer (Nafion[®]), and showed that the Nafion containing electrode has a much higher ionic conductivity and larger active catalyst area providing better fuel cell performance. They also explained that the ionic conductivity of the membrane decreases with distance from the membrane.

As seen in the previous work the transport phenomena of mass, energy, momentum and electrical charges play a significant role in PEMFCs. Costamagna [8] study a simulation model which allows the evaluation of the distribution of the physico-chemical parameters within the structure of a PEMFC reactor. The validated model was used to investigate the behavior of the reactor, with particular attention to critical operating conditions, flooding, membrane drying and degradation due to temperature peaks. Murgia et al. [30] presented a modified version of the well-known model of

Bernardi and Verbrugge which was developed to simulate the behavior of polymer electrolyte fuel cells. Such equations are analytically integrated in the reactive regions of the electrodes, eliminating the main nonlinear terms in the full mathematical model. It is shown that the modified Bernardi-Verbrugge model is as accurate as the original model. It allows an extension of the cell current density over which it is possible to find solutions, the full numerical procedure is very stable, and the simulations are up to three orders of magnitude faster than those performed with the original model.

The fuel cell handbook from the United States Department of Energy [35] mentioned the critical requirement of the PEMFCs to maintain a high water content in the electrolyte to ensure high ionic conductivity. The ionic conductivity of the electrolyte is higher when the membrane is fully saturated offering low resistance to current flow and increases overall efficiency. The leading factors affecting the water transport are the water drag through the cell, back diffusion from the cathode, and the diffusion of any water in the fuel stream through the anode. Water transport is a function of cell current and the characteristics of the membrane and the electrodes. Water drag refers to the amount of water pulled by osmotic action with the proton, between 1 and 2.5 molecules of water are dragged by proton of hydrogen. As a result, the ion exchanged can be envisioned as a hydrated proton, $H(H_2O)_n^+$. Water management has a significant impact on cell performance, because at high current densities mass transport issues associated with water formation and distribution limit cell output. Inadequate water management of water present adverse effects including dilution of reactant gases by water vapor, flooding of the electrodes, and dehydration of the solid polymer membrane. Dehydration

of the cell can cause adherence of the membrane to the electrode, which is very important because there is no free liquid electrolyte to form a conducting bridge. If there is too much humidification the electrode floods, which causes problems with diffusing the gas to the electrode.

CHAPTER III: THEORY

III.1 FUEL CELL TECHNOLOGY

Fuel cells are electrochemical reactors that convert the chemical energy from the reaction of hydrogen and oxygen directly into electrical energy and water. The basic physical structure of a fuel cell consists of an electrolyte layer in contact with a porous anode and cathode on either side. A fuel cell system which includes a "fuel reformer" can utilize the hydrogen from any hydrocarbon. Since the fuel cell relies on chemistry and not combustion, emissions from this type of a system would still be smaller than emissions from the cleanest fuel combustion processes. Fuel cells are classified by the type of electrolyte used and differ in operation temperature, efficiency, and its application. Table 1 summarizes the fuel cell types and its properties.

Table 1. Fuel cell classifications and characteristics [14]

Fuel cell	Electrolyte	Operating Temperature	Electrical efficiency	Fuel / Oxidant
Alkaline Fuel Cell (AFC)	Potassium Hydroxide Solution (KOH)	Room temperature to 90°C	60 - 70 %	H ₂ / O ₂
Proton Exchange Membrane Fuel Cell (PEMFC)	Proton Exchange Membrane	Room temperature to 80°C	40 - 60%	H ₂ / O ₂ , Air
Direct Methanol Fuel Cell (DMFC)	Proton Exchange Membrane	Room temperature to 130°C	20- 30 %	CH ₃ OH / O ₂ , Air
Phosphoric Acid Fuel Cell (PAFC)	Phosphoric Acid	160 - 220°C	0.55	Natural gas, bio gas, H ₂ / O ₂ , Air
Molten Carbonate Fuel Cell (MCFC)	Molten mixture of alkali metal carbonates	620 - 660°C	0.65	Natural gas, bio gas, coal gas H ₂ / O ₂ , Air
Solid Oxide Fuel Cell (SOFC)	Oxid ion conducting ceramic	800 - 1000°C	60 - 65%	Natural gas, bio gas, coal gas H ₂ / O ₂ , Air

III.1.a PEM FUEL CELL DESCRIPTION

The polymer electrolyte fuel cell contains an immobilized membrane sandwiched between the two electrodes. The PEFC is known as proton exchange membrane fuel cell, because its electrolyte is a membrane of protonic exchange. The proton exchange membrane utilized in most recent PEMFC technology is made of a *perfluorocarbon sulfonic acid (PFSA) ionomer*, *Nafion™*, made by DuPont, see Appendix G for DuPont technical specifications table. However, there are other similar materials produced commercially. The chemical and physical properties of perfluorocarbon sulfonate membranes give them superiority over any other membrane material. These membranes have chemical stability under oxidative and reductive environments. Well humidified membranes achieve high protonic conductivities or low resistance per area, of 0.05 ohm-cm² for a membrane of 50 μm thick [19]. The immobilized electrolyte membrane simplifies sealing in the production process, reduces corrosion, and provides for longer cell and stack life. PEFCs operate at low temperature, allowing for faster startups and immediate response to changes in the demand for power. The PEFC system is seen as the system of choice for vehicular power applications, but is also being developed for smaller scale stationary power.

A PEM fuel cell cross-section schematic is presented in figure 1. The central part of the cell is the membrane-electrode assembly (MEA). The MEA consists of an ionomeric membrane with thin catalyst layers bonded onto each of its two major surfaces. It has the generic structure of an electrochemical cell: electrode-electrolyte-electrode. The

electrode of the MEA is a thin film, 5-50 μm of thickness, which contains dispersed catalyst. The catalyst layer is in contact with a proton exchange membrane, as seen in the center of the figure 1, which serves as the electrolyte and the gas separator in the cell.

CROSS SECTION OF POLYMER ELECTROLYTE FUEL CELL

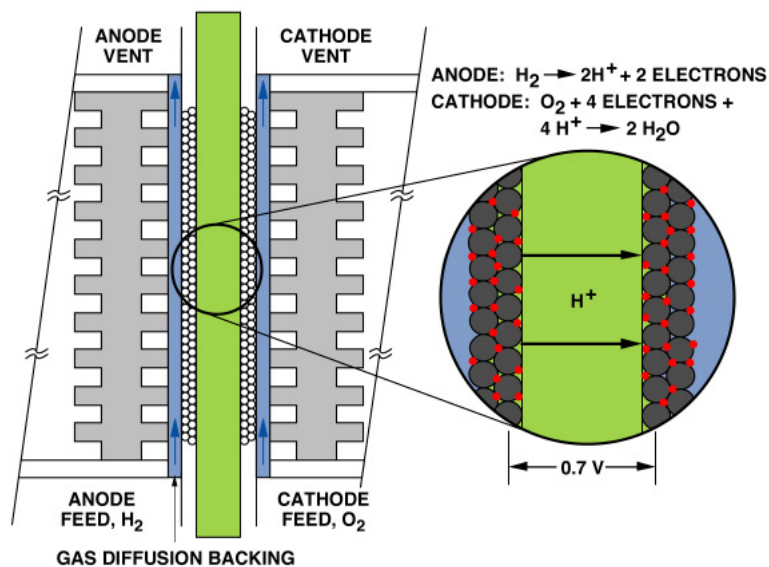


Figure 1 Schematic cross-section of a single polymer electrolyte fuel cell (PEFC) [19].

The proton exchange membrane is typically 50-175 μm thick. The catalyst layer of Pt as small circles supported on carbon as larger circles is magnified at the right of the PEMFC in figure 1. “Pt is an essential catalyst for the electrochemical conversion of hydrogen and oxygen at the anode and cathode of the fuel cell, respectively, into electric current” [19] The gas diffusers are the porous backing layer behind the catalyst (figure 1) made of *hydrophobized porous carbon paper*, or carbon cloth with 100-300 μm of thickness and are wet-proofed by treatment with *poly-tetrafluoroethylene (PTFE)*. “The role of these gas diffusers is to enable direct and uniform access of the reactant gases, hydrogen and oxygen, to the catalyst layers, without having to diffuse through films of

liquid water.” [19] The final elements of a fuel cell are the current collector plates which usually contain machined flow fields for effective distribution of reactant gases along the surfaces of the electrodes. These plates are the bipolar plates in the fuel cell stack made of high density graphite.

A schematic view of a single cell is presented below in Figure 2. The graphite blocks and the gas diffusers are explained above. The Teflon masks shown are gaskets that confine the gas flow to the active area and provide an effective seal. A single PEMFC operates approximately at 0.7V. To obtain higher voltage several single cells have to be assembled together.

SINGLE CELL HARDWARE

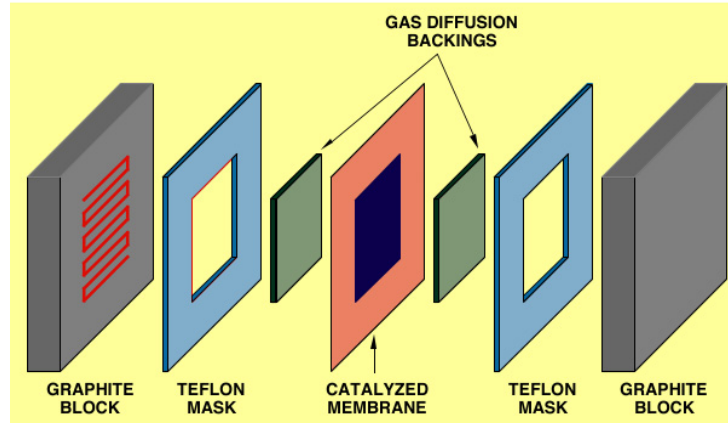


Figure 2. Single PEM fuel cell. [19]

III.1.b PEM FUEL CELL ELECTROCHEMICAL PROCESS

Hydrogen gas extracted from natural gas, or other hydrocarbon fuels, permeates the anode. Electrons and protons are stripped from the hydrogen gas aided by a catalyst in the anode. Hydrogen protons, which remain solvated with a certain number of water molecules, diffuse into the membrane. Since electrons cannot pass through the electrolyte they travel by an external circuit producing electricity. [14] At the cathode the hydrogen protons combined with the electrons react with oxygen gas to produce water and heat (Figure 2). The electrochemical half reactions, oxidation and reduction at the anode and cathode, respectively, are the followings;

Oxidation half reaction at the anode



Reduction half reaction at the cathode



The overall electrochemical process of a PEMFC is called “reverse hydrolysis” or opposite of hydrolyzing water from hydrogen and oxygen.

Overall reaction



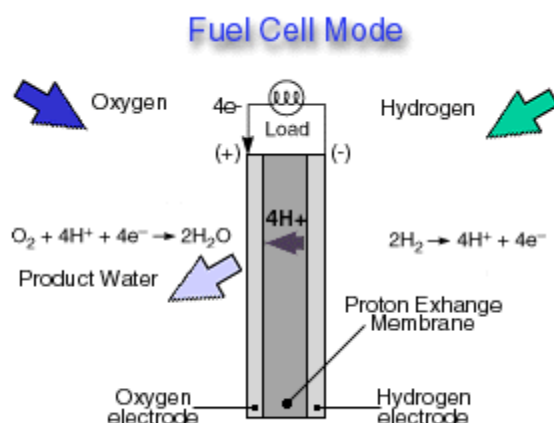


Figure 3. Fuel cell mode schematic and process diagram [23]

The hydrolysis is accomplished supplying electricity to the cell and water to the cathode (see Electrolyzer Cell Mode figure below) described by the half reactions, oxidation and reduction, at the cathode and anode, respectively. Certain fuel cell types are reversible, which can accomplish the electrochemistry associated with processes, the production of electricity from fuel and oxidant and the production of fuel and oxidant from water when supplied with electricity.

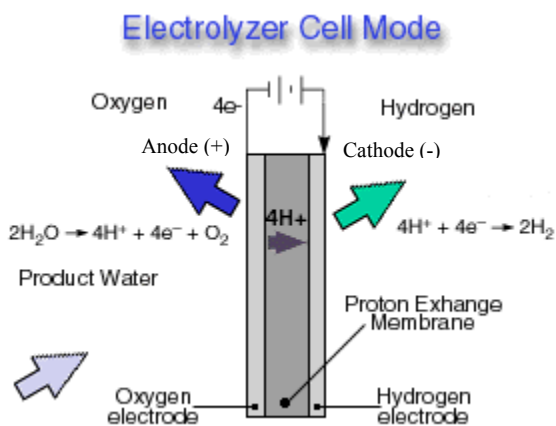


Figure 4. Electrolysis cell mode schematic and process diagram. [23]

Oxidation half reaction at the anode



Reduction half reaction at the cathode



Overall reaction



The reversible fuel cell concept is one that incorporates a fuel cell that can accomplish both, hydrolysis and reverse hydrolysis, in the same cell. This allows one to consider the completely renewable production of electricity by using a renewable energy supply (e.g., solar, wind) to produce hydrogen and oxygen from water which can subsequently be used to produce electricity through the same fuel cell from the fuel and oxidant produced previously.

III.2 ELECTROCHEMISTRY

III.2.a FARADAIC AND NONFARADAIC PROCESS

There are two types of process at the electrode surface. One kind is comprised of reactions in which charge are transferred across the metal-solution interface. Electron transfer causes oxidation or reduction to occur. These reactions are governed by Faraday's Law, where the amount of chemical reaction caused by the flow of current is proportional to the amount of electricity passed. The electrodes at which faradaic process

occurs are called charge transfer electrodes. The nonfaradiac processes occur at a given electrode-solution interface that show a range of potentials where no charge transfer reaction take place because of such things as changing of the double layer. Another example, adsorption and desorption can occurs and the interface structure can change with changing the potential or solution composition. Although charge does not cross the interface, external currents can flow when the potential, electrode area or solution composition changes. [4]

Electrochemical cells at which faradic process is occurring are classified as galvanic or electrolytic cells. The electrolytic cell is one in which reaction are affected by the imposition of an external voltage greater than the open circuit potential of the cell. These cells are employed to carry out the desired chemical reactions by expending electrical energy. The galvanic cell is one in which the reaction occurs spontaneously at the electrode when they are connected externally by a conductor. These cells convert the chemical energy into electrical energy, unlike the electrolytic cells. Commercially, there exist different types of galvanic cells the primary cell (non-rechargeable), secondary cells (rechargeable), and fuel cells. In electrolytic cells, the cathode is negative with respect to the anode, but in galvanic cells the cathode is positive with respect to the anode. For both types of cells the cathode is the reduction electrode and the anode is the oxidation electrode [4].

III.2.b ELECTRODE REACTIONS

The electrode process occurring at the electrode-electrolyte interface is a heterogeneous reaction which is more complex to interpret than a homogeneous reaction

which occurs in solution or in a gas phase. Generally, the heterogeneous reaction rate is described in units of mol per unit area.

$$Rate \left[\frac{\text{mol}}{\text{s} \cdot \text{cm}^2} \right] = \frac{i}{nFA} = \frac{j}{nF} \quad (7)$$

where

i = current (amperes, A)

F = Faraday constant, 9.64853×10^4 C

A = electrode surface area (cm^2)

n = number of electron transferred

j = the current density (A/cm^2)

The rate of the following simple electrode reaction $O + ne^- \leftrightarrow R$ depends on various surface effects in addition to the usual kinetics variables. This reaction is composed of a various steps to convert the dissolved oxidized species to the reduced form. In general the current or electrode reaction rate is governed by the following processes; mass transfer – from bulk solution to the electrode surface; electron transfer at the electrode surface; chemical reactions preceding or following the electron transfer; other surface reactions, adsorption, desorption or crystallization [4]

Each value of current density, j , is driven by the overpotential, which can be considered as a sum of terms associated with different reaction steps; mass transfer (η_{mt}), charge transfer (η_{ct}), and the overpotential associated with a preceding reaction (η_{rxn}). The electrode reaction can be expressed or represented by a resistance, R , composed of a series of resistance representing the reaction steps; R_{mt} , R_{ct} , R_{rxn} , etc. A fast reaction step

is represented by a small resistance or impedance, while a slow step is represented by high resistance or impedance. [4]

The potential affects the kinetics of reactions occurring on electrodes surface, for example, Hydrogen evolves rapidly at some potentials, but not at others. The Butler-Volmer equation describes the current density vs. overpotential relationship under electron transfer control. At equilibrium the net current is zero, the electrode adopts the potential based on the bulk concentrations of the oxidant and reduction agent as dictated by Nerst equation.

$$E_{eq} = E^{0'} + \frac{RT}{nF} \ln \frac{C_O^*}{C_R^*} \quad (8)$$

where,

C_O^* = bulk concentration of oxidant agent

C_R^* = bulk concentration of reduction agent

$E^{0'}$ = formal potential

R = Ideal gas constant, 8.314 J/mol-K

T = Temperature in Kelvin

F = Faradays constant, 9.64853×10^4 C

n = transferred electron number

The current – overpotential equation can be written as

$$i = i_0 \left[\frac{C_O(0,t)}{C_O^*} e^{-\alpha n f \eta} - \frac{C_R(0,t)}{C_R^*} e^{(1-\alpha) n f \eta} \right] \quad (9)$$

where

η = Overpotential, $E - E_{eq}$, Volts

$f = F/RT = 38.92 \text{ V}^{-1}$ at 298.13K

α = partition coefficient, normally is 0.5

i_0 = exchange current, Amperes (A)

$C_O(0,t)$ = concentration of the oxidant agent at electrode surface

$C_R(0,t)$ = concentration of the reduction agent at electrode surface

Approximate forms of i - η Equation are developed when η is small and when η is large, where Tafel behavior is predicted. The approximations are made considering no mass transfer effects, where surface and bulk currents do not differ. [4]

$$\frac{C_O(0,t)}{C_O^*} \approx \frac{C_R(0,t)}{C_R^*} \approx 1 \quad (10)$$

Equation 10 becomes

$$i = i_0 \left[e^{-\alpha n f \eta} - e^{(1-\alpha) n f \eta} \right] \quad (11)$$

At small overpotentials, a linear characteristic of i - η is expected, this relationship can be linearized via the approximation $e^x = 1 + X$ to give; [40]

$$i = -i_0 n f \eta \quad (12)$$

The ratio $-\eta/i$ has units of resistance and is known as charge transfer resistance, R_{ct} .

$$R_{ct} = \frac{RT}{nFi_0} \quad (13)$$

This parameter is the negative reciprocal slope of the i - η curves when the curve passed through the origin ($\eta = 0, i = 0$). The linear behavior is expected as far as 20mV. For

large overpotential, positive or negative, one bracket terms become negligible in equation

11. For reduction, at large negative η ;

$$i = i_0 e^{-\alpha n f \eta} \quad (14)$$

$$\eta = \frac{RT}{\alpha n F} \ln i_0 - \frac{RT}{\alpha n F} \ln i \quad (15)$$

The charge transfer resistance at higher overpotentials can be founded with the derivative of the equation 14, $\frac{di}{d\eta}$, which have units of reciprocal to resistance.

$$\frac{di}{d\eta} = \frac{1}{R_{ct}} = -\alpha n i_0 f e^{-\alpha n f \eta} \quad (16)$$

Therefore

$$R_{ct} = \frac{e^{\alpha n f \eta}}{n \alpha i_0 f} \quad (17)$$

When mass transfer is considered the relationship of i - η at small overpotentials can be expressed as;

$$\eta = -i(R_{ct} + R_{mt,c} + R_{mt,a}) \quad (18)$$

where

$R_{mt,c}$ = resistance of mass transfer effects related to the cathode

$R_{mt,a}$ = resistance of mass transfer effects related to the anode [4]

The current potential, i - E , curves are called polarization curves. An electrode at which no charge transfer can occurs across the metal-solution interface, regardless the potential imposed, is called an ideal polarized electrode (IPE). The polarization curve of

an IPE shows a very large change in potential with an infinitesimal current passage. An IPE is expected to presents a horizontal region of an i - E curve. Thus, an ideal non-polarizable electrode is an electrode whose potential does not change upon a passage of current, i.e. an electrode of fixed potential. Polarization curves of a non-ideal polarizable electrode are characterized by a vertical region. A real electrode can not behave as an IPE over whole potential range, but it can reach the ideality over a limited potential. Since charge transfer cannot pass through the IPE interface when the potential across is changed, the behavior of the electrode-solution interface is analogous to that of a capacitor. The capacitor accumulates charge (q) on its metal plates until q satisfies the following equation.

$$\frac{q}{E} = C \quad (19)$$

where,

q = charge stored on the capacitor (coulombs, C)

E = potential across the capacitor (volts, V)

C = capacitance (farads, F)

The charge on the capacitor consists of an excess of electrons on one plate and a deficiency of electrons on the other. [4]

III.2.c THE ELECTRICAL DOUBLE LAYER

The electrode/electrolyte interface disrupts the electrolyte solution where the electron transfer reaction occurs. The interactions between the solid and the electrolyte

will be considerably different to those in solution. Electrodes under potentiostatic control will be influenced of the charge held at the electrode. Those factors result in strong interactions between the ions or molecules in solution and the electrode surface. This region is called the electrical double layer.

The Helmholtz model at 1850's was the first that puts forward the term “electrical double layer”. He assumed that no electron transfer reactions occur at the electrode and the solution is composed of the electrolyte only. The interactions at the electrode surface and solution were assumed to be electrostatic in nature and resulted from the fact that the electrode holds a charge density, which come up from an electrons deficiency or excess at the electrode surface. Helmholtz's view of this region is shown in the figure 5 below.

[37]

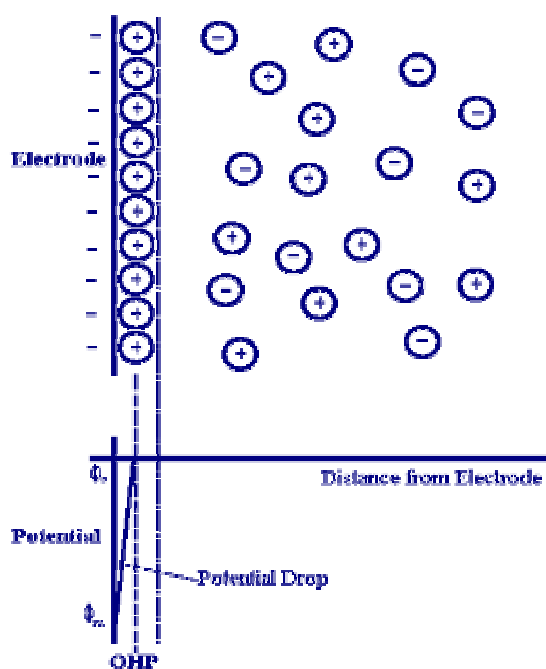


Figure 5. Helmholtz's electrical double layer model [37]

The attracted ions reach the electrode surface and form a layer balancing the electrode charge. The distance of this approach is assumed to be limited to the radius of the ion and a single sphere of solvation round each ion. This results on two layers of charge and a potential drop which is confined to only this region in solution. The result is absolutely analogous to an electrical capacitor which has two plates of charge separated by some distance with the potential drop occurring in a linear manner between the two plates. In the impedance analysis performed to electrochemical systems the response due to the electrolyte redistribution is modeled as capacitive elements. The Helmholtz's model does not account many factors such as, diffusion/mixing in solution, the possibility of adsorption on to the surface and the interaction between solvent dipole moments and the electrode. Stern's model addresses some of these limitations, assuming that the ions are able to move in solution and so the electrostatic interactions are in competition with Brownian motion. The result is a region close to the electrode surface, approximately 100×10^{-10} m, containing an excess of one type of ion but the potential drop occurs over the region called the diffuse layer (Figure 6).

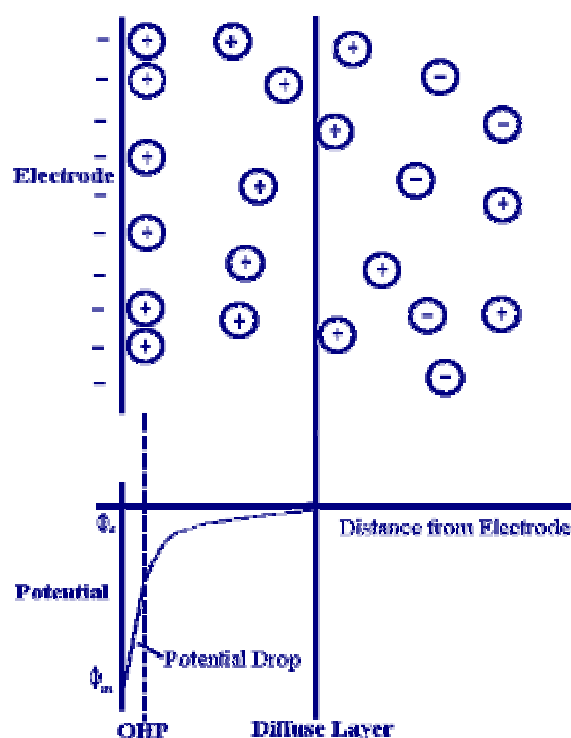


Figure 6. Stern's double layer model schematic diagram. [37]

III.3 ELECTROCHEMICAL IMPEDANCE SPECTROSCOPY

III.3.a INTRODUCTION

Electrochemical impedance spectroscopy (EIS) is a powerful technique for characterizing many of electrical properties of materials and their interfaces with electronically conducting electrodes [28]. EIS is helpful to understand chemical and physical processes in solutions as well as solids. It may be used to investigate the dynamics of bound or mobile charge in the bulk or interfacial regions of any material. For solution phase, electrochemistry of a complex sequence of coupled processes such as, electron transfer, mass transport and chemical reaction can all control or influence the output from an electrochemical measurement. Numerous microscopic processes take

place in an electrochemical cell when it is stimulated electrically. They include the transports of electrons through electronic conductors, the transfer of electrons at the electrode-electrolyte interfaces to or from atomic species which originate from the cell materials and its environment, and the flow of charged atoms or atoms agglomerates via defects in the electrolyte. The flow rate of charged particles, current, depends on the Ohmic resistance of the electrodes and the electrolyte and on the reaction rates at the electrode-electrolyte interfaces. A number of parameters can be derived from EIS spectrum; those pertinent only to the material itself, such as conductivity, dielectric constant, mobility of charges, equilibrium concentrations of the charged species, and the bulk generation-recombination rates; and those pertinent to an electrode-material interface, such as adsorption-reaction rates constants, capacitance of the interface region, and diffusion coefficient of neutral species in the electrode [28]. EIS considered these behaviors analogous to resistors, capacitors, and inductors which impede the flow of electrons in an ac circuit, while in dc theory the resistor is the only that impedes the electrons flow [5].

III.3.b EXPERIMENTAL ANALYSIS THEORY

An electrochemical cell can be considered as impedance to a small sinusoidal excitation. EIS uses alternate current (ac) signals to determine impedance over a range of frequencies. Electrochemical impedance theory is a branch of ac theory that describes the response of a circuit to an alternating current or voltage as a function of frequency. The performance of an electrochemical cell can be represented by an equivalent circuit of

resistors and capacitors. The Impedance is described by an analogous equation to the Ohm's law ($E = IR$), where E is dc potential, I is the current, and R is the resistance in direct current (dc);

$$E = I Z \quad (20)$$

E and I are here defined as potential (V) and current (A), respectively. Z is defined as impedance, the ac equivalent of resistance, ohms (Ω).

A typical plot of a potential sine wave (E) applied and the resultant ac current waveform (I) is shown in Figure 7. The potential applied equation is;

$$E(t) = E_0 \sin \omega t \quad (21)$$

where,

$E(t)$ = voltage as function of time (V)

E_0 = voltage amplitude (V)

ω = angular frequency (radians per second = $2\pi f$)

f = frequency in Hertz (1/s)

t = time in seconds

The resulting current sine wave equation:

$$I(t) = I_0 \sin(\omega t + \phi) \quad (22)$$

where

$I(t)$ = current as time function

I_0 = maximum amplitude

ϕ = phase shift in radians

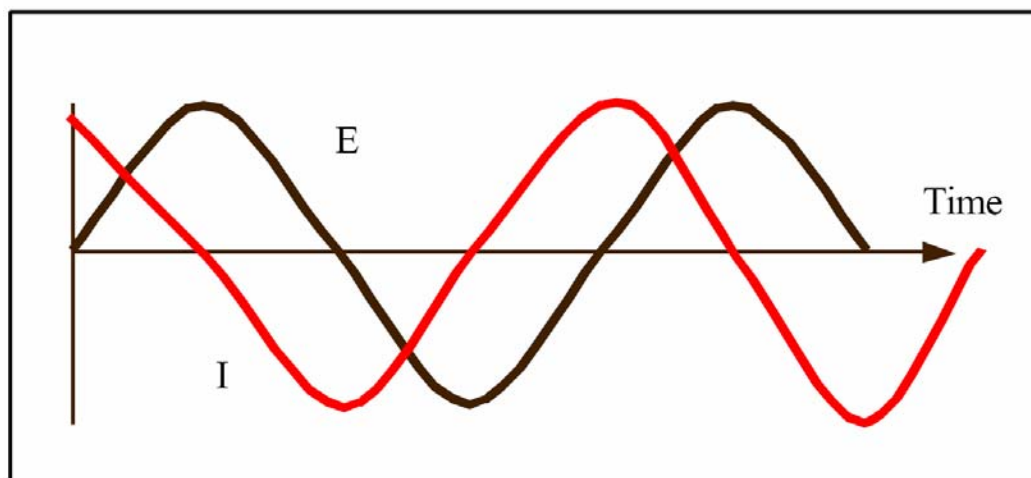


Figure 7. Applied potential (E), black, and resulting current (I), red, sine waves. [5].

Both sine waves are different in amplitude and are shifted in time implying that they are out of phase. In a purely resistive arrangement, the potential and the current sine waves would be exactly in phase, differing only in amplitude. [5] The impedance as function of time is;

$$Z(t) = \frac{E_0 \sin \omega t}{I_0 \sin(\omega t + \phi)} \quad (23)$$

In the EIS experiments the impedance is expressed as vector, where the raw data at each measured frequency consists of the real and imaginary components of the applied potential and the measured current; the real component of voltage (E'), the imaginary component of voltage (E''), the real component of current (I'), and the imaginary component of current (I''). The magnitude and direction of a planar vector in the right-hand of orthogonal system of axes can be expressed by the sum of the vectors components. For example, the impedance vector is;

$$Z(\omega) = Z' + jZ'' \quad (24)$$

where,

Z' = real part of the impedance vector $Z(\omega)$

Z'' = imaginary part of the impedance vector $Z(\omega)$

j = the imaginary number, $\sqrt{-1}$

The impedance vector can be plotted in plane with rectangular or polar coordinates, as shown in figure 8. The two rectangular coordinates values are;

$$Z' = |Z| \cos \phi \quad (25)$$

$$Z'' = |Z| \sin \phi \quad (26)$$

From this data the phase shift (ϕ) and the total impedance $|Z|$ for each applied frequency

The phase angle is;

$$\phi = \tan^{-1} \left(\frac{Z''}{Z'} \right) \quad (27)$$

and the absolute impedance is;

$$|Z| = \left[(Z')^2 + (Z'')^2 \right]^{1/2} \quad (28)$$

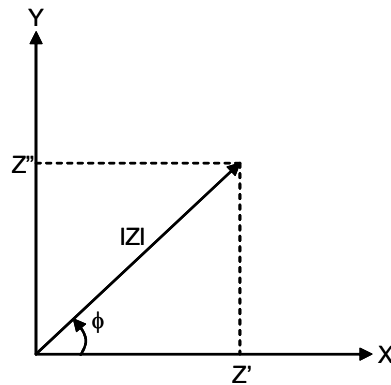


Figure 8. Impedance planar vector in rectangular and polar coordinates

In the polar form the impedance is expressed as;

$$Z(\omega) = |Z| \exp(j\phi) \quad (29)$$

This can be converted to the rectangular form using the Euler relation;

$$\exp(j\phi) = \cos \phi + j \sin \phi \quad (30)$$

For equation 29 the impedance complex number is expressed as;

$$Z(\omega) = |Z|(\cos \phi + j \sin \phi) \quad (31)$$

The real part of the impedance complex number is pure resistance and the imaginary component is a combined capacitance and inductance. The total impedance in a circuit is the combined opposition of all its resistors, capacitors, and inductors to the flow of electrons. The opposition of capacitors and inductors is given the same name reactance, symbolized by X and measured in ohms. Since the symbol for capacitance is C , capacitive reactance is symbolized by X_C . Similarly, since the symbol for inductance is L , inductive reactance is symbolized by X_L . [34] Capacitors and inductors affect not only the magnitude of an alternating current but also its time or phase dependent

characteristics. A circuit is said to be largely capacitive when most of the opposition to current flow comes from its capacitive reactance. When most of the opposition to current flow comes from its inductive reactance, a circuit is said to be inductive. In a capacitive circuit the current leads the applied voltage in phase angle, but in an inductive circuit the current lags the applied voltage in phase angle. In largely inductive circuits the potential and current sine waves have slight difference in phase angle.

The EIS data can be plotted in different formats. Each format has certain advantages for revealing particular characteristics of a chemical system. From the plots data it is possible to obtain an equivalent circuit for any electrochemical cell. The simplest circuit interpretations and the most significant plot formats will be discussed in the following sections.

III.3.c SIMPLEST EQUIVALENT CIRCUIT

The equivalent circuit for a simple electrochemical cell is known as the Randle's circuit. The Randle's circuit is pictured in the figure 9. The total current through the working interface is the sum of contributions of faradaic process, i_f , and double layer charging, i_c , given that the parallel elements of the circuit are introduced. The capacitance in the Randle's circuit, represented as C_{dl} , is the double layer capacitance which is nearly a pure capacitance. The faradaic process is a frequency dependent process therefore it can not be considered as simple linear circuit elements like, R and C. It has to be considered as general impedance Z_f . However as the current must pass through the solution resistance, it is represented as the Ohmic resistance, R_{Ω} , in an equivalent circuit. The simplest interpretation of the faradic process impedance is to consider a series

combination of series resistances, R_s , and a pseudo-capacity, C_s (figure 9). As seen in the figure 9 exists other interpretations where separates the pure resistance, the charge transfer resistance, R_{ct} , from another general impedance, Warburg impedance, Z_w , which represents resistance to mass transfer as explained in the next sections [4, 29].

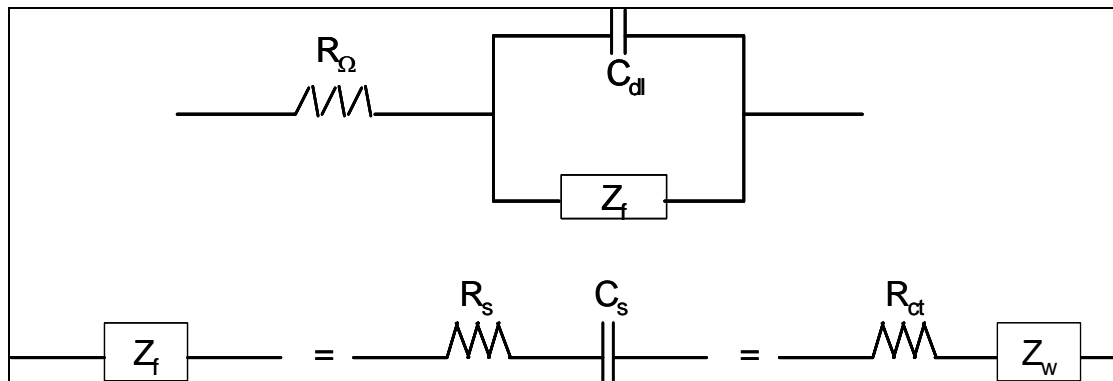
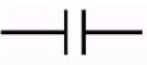
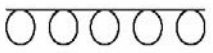
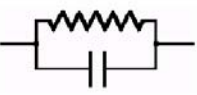


Figure 9. Equivalent circuit of an electrochemical cell

The impedance expressions for some electric circuits are presented in the following table. Determination of the total impedance needs to know the impedance values of each electric element in a circuit. To calculate the total impedance is very important to understand the combination of the electric elements, parallel or series.

Table 2. Impedance equation for simple electric circuits [5]

Circuit Element	Impedance Equation
	$Z = R + 0j$ $j = \sqrt{-1}$
	$Z = 0 - j / \omega C$ $\omega = 2\pi f$
	$Z = 0 + j \omega L$ $\omega = 2\pi f$
	$Z = \frac{R}{1 + \omega^2 C^2 R^2} - \frac{j \omega C R^2}{1 + \omega^2 C^2 R^2}$

III.3.d NYQUIST PLOT

A popular technique for evaluating ac impedance data is the Nyquist Plot which is a complex impedance plane diagram. As seen in the following figure, the imaginary component of impedance (Z'') is plotted vs. the real component of impedance (Z') at each excitation frequency. The plot in this figure illustrates the expected response of the equivalent circuit of a simple electrochemical cell, and could be used to compute the ohmic resistance R_Ω , the polarization resistance (R_p), and the double-layer capacitance, C_{dl} .

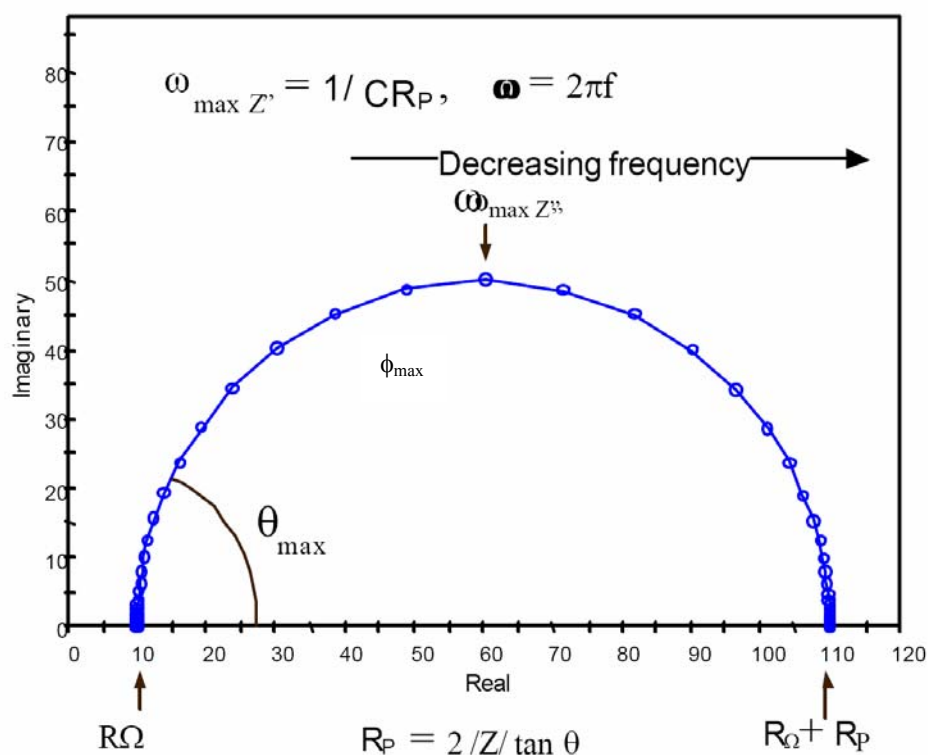


Figure 10. Nyquist Plot. Complex impedance diagram for an equivalent circuit of simple electrochemical cell. [5]

At high frequencies only the uncompensated resistance (Ohmic resistance, R_{Ω}) contributes to the real portion of impedance, whereas at very low frequencies the polarization resistance (R_p) or charge transfer resistance (R_{ct}) also contributes to this measurement. At higher frequencies the excitation waveform becomes much faster than the charge transfer rate becoming the R_p transparent to the technique. The Nyquist Plot shown in the figure 10 is for a simple cell, well known as Randles cell [5]. It can be interpreted as a simple circuit as Figure 9. As illustrated in the Nyquist Plot of the Randles cell in figure 9 at high frequencies the Z_{im} becomes zero, where the semicircle touches the x axis. The impedance at this high frequency is created by the Ohmic resistance, R_{Ω} . At the low frequency limit the semicircle intersects the Zre axis where the Z_{im} reach zero again. The impedance at this low frequency is governed by a pure resistance, but the value at these low frequencies is $R_{\Omega} + R_p$ or $R_{\Omega} + R_{ct}$. At intermediates frequencies de Nyquist Plot shows a maximum value of the imaginary part. At the frequency at which this maximum occurs the double layer capacitance can be calculated by the relation of;

$$C_{dl} = \frac{1}{\omega_{Z''_{max}} R_{ct}} \quad (32)$$

where,

ω = angular frequency (radians per second = $2\pi f$)

f = frequency in Hertz (1/s)

C_{dl} = Double layer capacitance (farads, F)

R_p = Polarization resistance (ohms, Ω)

R_Ω will represent constant impedance at high frequencies [4, 5, 29]. This is consistent with the fact that R_p can be measured by a dc technique while R_Ω cannot. For example, the polarization resistance can be used to calculate the corrosion rate of an electrode material in a given electrolyte.

Nyquist plot advantages.

- Is easy to extrapolate the value of the Ohmic resistance, R_Ω , when sufficiently high frequencies are used
- The plot format allows seeing the effects of the ohmic resistance.

Nyquist plot format disadvantages.

- Frequency does not appear explicitly.
- The ohmic resistance and polarization resistance can be easily read directly from the Nyquist plot, but the electrode capacitance can be calculated only after the frequency information is known.

III.3.e BODE PLOT

The Bode plot format allows the estimation of the absolute impedance, $|Z|$, and the phase angle, ϕ , as a function of frequency. The Bode plot has certain advantages over the Nyquist plot, since frequency appears as the independent variable, x axis. It presents how the impedance of a circuit or cell depends on the frequency. The frequency axis is in a logarithm scale to allow examining a very wide frequency range on one graph, but with each decade given equal weight. The Bode plot also shows the impedance magnitude, $|Z|$,

on a log axis to study wide impedance ranges on the same set of axes. Figure 11 shows a Bode Plot for the same data illustrated in the Nyquist plot in Figure 10.

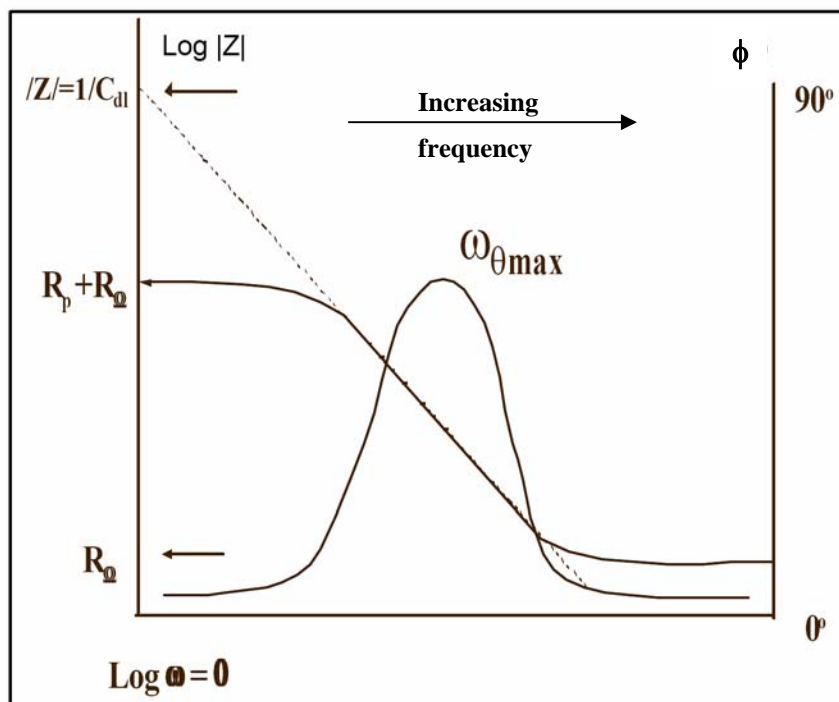


Figure 11. Bode Plot of simple electrochemical cell

The Bode plot is helpful to determine electrochemical parameters of a cell; the curve can yield values of R_p and R_Ω . As mentioned before at highest frequencies the ohmic resistance dominates the impedance and $\log |R_\Omega|$ can be read from the high frequency horizontal plateau. At lowest frequencies a $\log |R_\Omega + R_p|$ can be read from the low frequency horizontal plateau. At intermediate frequencies, this curve should be a straight line with a slope of -1, note that this slope value is for a simple electrochemical cell, for complex cells the slope value varies depending of the chemical or physical process in the cell. Extrapolating this line to the $\log |Z|$ axis at $\log \omega = 0$ ($\omega = 1$, $f =$

0.16 Hz), i.e. the intercept of the straight line at y axis, yields the value of the double layer capacitance, C_{DL} , from the relationship:

$$C_{dl} = \frac{1}{|Z|} \quad (33)$$

where,

$|Z|$ = impedance magnitude from the y axis intercept (ohms)

At the high and low frequency limits the phase angle is nearly zero (Princeton EIS). At intermediate frequencies the phase angle increases as the imaginary component of the impedance increases. The plot of the phase angle (ϕ) versus $\log \omega$ of a simple cell presents a peak at certain value of the frequency, in radians, at which the phase shift of the response is maximum. The slope of the straight line in the $\text{Log } |Z|$ vs. $\text{Log } \omega$ plot appears in the near frequencies of the frequency at which this peak occurs. The double-layer capacitance, C_{dl} , also, can be calculated from the following equation; [2]

$$C_{dl} = \frac{1}{R_p \omega_{max}^2 \left[1 + \frac{R_p}{R_\Omega} \right]} \quad (34)$$

Some of the advantages of the analysis are that it avoids longer measurement associated with low frequency R_p determinations. Furthermore, the $\log |Z|$ vs. $\log \omega$ plot sometimes allows a more effective extrapolation of data from higher frequencies. The Bode format is also desirable when data scatter prevents adequate fitting of the Nyquist semicircle. In general, the Bode plot provides a clearer description of the electrochemical system's frequency-dependent behavior than does the Nyquist plot, in which frequency values are implicit rather than explicit. [5]

III.3.f WARBURG IMPEDANCE

The rate of an electrochemical reaction can be influenced by diffusion of the reactive species towards or a product away from the electrode surface. The diffusion phenomenon can be present when the electrode is covered with reaction products, adsorbed solution components, or a prepared coating. For a diffusion-controlled electrochemical reaction mechanism, the impedance is known as the Warburg Impedance, where the current is 45 degrees out of phase with the applied potential [38]. “In terms of simple equivalent circuits, the behavior of Warburg impedance (45 degree phase shift) is midway between that of a resistor (0 degree phase shift) and a capacitor (90 degree phase shift). There is no simple electrical equivalent for the Warburg impedance.” [5]

The Warburg impedance, Z_w , is;

$$Z_w = \frac{\sigma\sqrt{2}}{\sqrt{\omega}} \quad (35)$$

where,

ω = angular frequency (radians per second = $2\pi f$)

f = frequency in Hertz (1/s)

σ = Warburg's coefficient

$$\sigma = \frac{RT}{n^2 F^2 A \sqrt{2}} \left(\frac{1}{D_o^{1/2} C_o^*} + \frac{1}{D_R^{1/2} C_R^*} \right) \quad (36)$$

where,

R = Universal gas constant (8.314 J/mol-K)

T = Temperature in Kelvin (K)

n = number of electron transferred

A = electrode area (cm^2)

D_o = oxidant specie diffusion coefficient

D_R = reduction specie diffusion coefficient

C_o^* = oxidant specie concentration in the bulk

C_R^* = reduction specie concentration in the bulk

The Warburg impedance is negligible at high frequencies, because the time is too short to impact the diffusion. An electrochemical cell is considered kinetic-controlled at “high” frequencies, since the surface concentrations are not affected by mass transfer effects. The latter are present at lower frequencies. The diffusion control can be detected experimentally by detection of a slope of $-1/2$ or $-1/4$ in the linear portion of the Bode plot, $\text{Log } |Z|$ vs. $\text{Log } \omega$, as shown in figure 12.

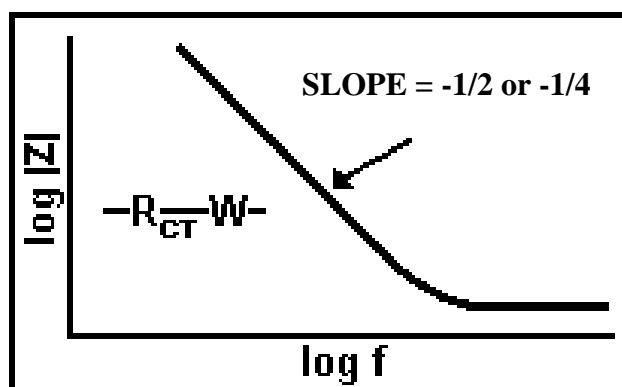


Figure 12. Bode Plot for Warburg Impedance [24]

An idealized Warburg plot of Z' and Z'' vs. $\omega^{-1/2}$ for a diffusion-controlled system is shown in the following figure.

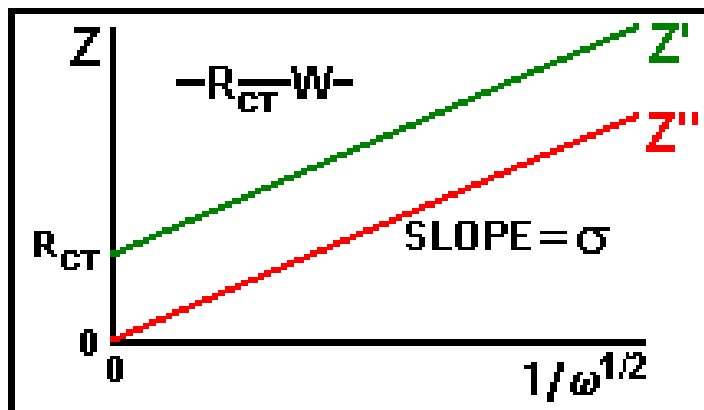


Figure 13. Idealized Warburg Plot [24]

In this plot the Z' and Z'' are linear functions in $\omega^{-1/2}$. The lines should be straight and parallel and the slope of both lines should be equal to the Warburg coefficient (σ). In the idealized Warburg Plot the line for the imaginary component, Z'' , should intersect the Z axis at zero, while the intercept for the real component, Z' , is the charge transfer resistance, R_{ct} . These results suggest a circuit of a charge transfer resistance in series with a Warburg Impedance. Thus, the linearity and slope of the Warburg plot can be used as a test of diffusion control. [24]

CHAPTER IV: MATERIALS AND METHODS

IV.1 MATERIALS

The next section provides a thorough description of the methodology and materials used in this study. Proton exchange membrane (PEM) cells were studied using different electrochemical techniques to characterize and understand their behaviors. The Eco H₂/Air equipment built with Nafion® membranes has the essential components of a completely renewable hydrogen energy system. Using the renewable energy produced from the solar panels, a PEM electrolyzer disassociates distilled water into its constituent components of hydrogen and oxygen. Energy is stored in the form of hydrogen which is then utilized by a PEM fuel cell. The Eco H₂/Air equipment is presented in figure 14.

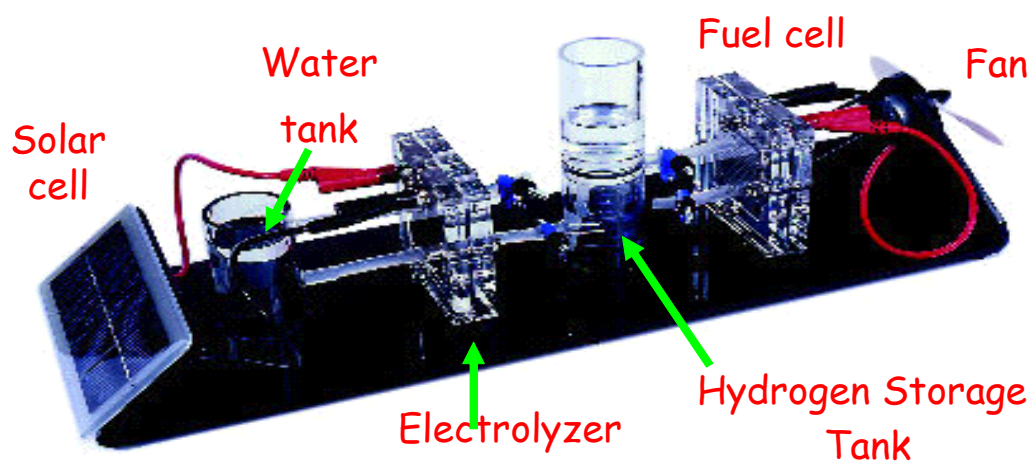


Figure 14. Eco H₂/Air equipment

The Eco H₂/Air device consists of:

- A solar cell with an area of 90 cm², a maximum power of 0.5 W, and the maximum current and voltage produced are 300 mA and 2.5 V, respectively.
- The PEM electrolyzer, built of Nafion® membrane loaded with platinum as a catalyst, has an electrode surface area of 16 cm², generates a maximum power of 2W, has an admissible voltage of 0-1.9 V, and admissible current of 0-2 A.
- A water storage tank made of acrylic with a water supply hose to the PEM electrolyzer.
- A hydrogen storage tank made of acrylic with maximum capacity of 40 cm³.
- The PEMFC built of Nafion® membrane loaded with platinum as a catalyst, has an electrode surface area of 16cm², generates a maximum power of 300 mW, and a voltage range of 0.3-0.9 V.
- The PEMFC physical dimensions are 175 x 530 x 150 mm (H x W x D).

An additional PEMFC was used to study the initial conditions influence in the impedance data and the memory related effects of the fuel cell. This PEMFC is a demountable fuel cell with membranes with different catalyst loading (figure 15). Two PEM were studied made of Nafion® 112 loaded with 0.1 and 0.3 mg Pt/cm² as catalyst with an electrode surface area of 9 cm². This fuel cell generates a maximum current of 1300 mA, and a voltage range of 0.4-0.9 V. The physical dimensions are 65 x 65 x 85 mm (W x H x D).



Figure 15. Demountable PEMFC [9]

A PARSTAT 2263 Advanced Electrochemical System was used to perform the experiments (Figure 16). It is a potentiostat, galvanostat and a frequency response analyzer that consists of hardware which is capable of ± 10 V scan ranges, has 200 mA current capabilities, and EIS measurements up to 1 MHz. The PARSTAT 2263 is DC powered to be operated with AC/DC converter, or with power supply for remote/field applications. It consists of Electrochemistry PowerSuite™ software, which has the ability to perform many of the standard techniques such as cyclic voltammetry, chronopotentiometry, chronoamperometry, Tafel plot, Electrochemical Impedance Spectroscopy (EIS), etc.



Figure 16. PARSTAT 2263 [32]

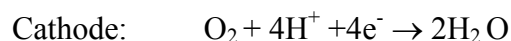
EIS technique is a powerful method to characterize many of the electrical properties of materials and their interfaces with electronically conducting electrodes. Normally, it is assumed that the properties of the electrode-material systems are time- invariant [28].

IV.2 METHODS

At the beginning of each experiment the production of hydrogen by an applied external voltage is needed. The solar cell of the H₂/Air equipment is powered with a spot halogen light of 75 Watts. The solar cell applies 1.5 volts to the PEM electrolyzer to start the electrolysis process. The PEM Electrolyzer breaks the water completing the followings reactions:



The water needed for the electrolysis was stored in the preceding tank and it flows to the electrolyzer controlled by a valve. The hydrogen produced by the electrolyzer was stored in the fuel tank and the oxygen came back to the water tank. The hydrogen stored was used by the PEM fuel cell to produce electrical energy by the reaction with oxygen from air. The electrochemical reactions PEM Fuel cells are the following:



To make the EIS measurement, ac voltage signal amplitude of 10 mV is applied to the PEM fuel cell and PEM electrolyzer over a frequency range of 1 mHz –100 kHz covering 36 points decade and varying the potential applied. The PARSTAT records the real and imaginary components of the impedance response. The raw data measured consists of the real and imaginary components of voltage, and ac current signal. From this data the phase angle and the total impedance for each applied frequency are determined. Depending upon the shape of the EIS spectrum, a circuit model or circuit description code and initial circuit parameters can be determined [4].

First, the cathode reduction reaction of the PEM fuel cell was studied using electrochemical impedance spectroscopy over the frequency range mentioned above. In the case of the proton exchange membrane fuel cell the cathodes give significant contributions the total energy losses due to high overpotential of the oxygen reduction reaction [23]. The anode of the PEM fuel cell was used as the reference and counter electrode, while the working electrode was the cathode. The cathode impedance spectrums, Nyquist Plot, Bode plot, and *i-v* plot were created as function of overpotential. The PEM electrolyzer was studied in the same frequency range of the PEM fuel cells. The working electrode of this cell was the anode; the reference and counter electrode were connected to the cathode. Impedance spectrums were generated as a function of overpotential. While the EIS experiments for the PEM fuel cell and the PEM electrolyzer were running, the hydrogen consumption and production was monitored.

To study the PEM fuel cell without control of the initial conditions, 10 levels for overpotential were used in the EIS technique. For these first runs the PEMFC of the Eco

H₂/Air was used. Before each experiment the PEM fuel cell was humidified and purged with hydrogen. The PEM electrolyzer experiments were investigated at constant potentials. To investigate the initial conditions and memory effects the dismountable PEM fuel cell was used. The experiments were performed with different initial conditions. One of the conditions was the dry membrane, 120 mL of H₂ only passed through anode. The other condition was the wet membrane when 120 mL of water were passed through the anode and then the 120mL of H₂ were delivered to the anode to begin the electrochemical reaction of the PEMFC. The experiments varying the initial conditions were performed next to hydrogen passed through the anode and to comprehend the memory effects experiments were carried out quickly after the other experiments finished. For all the experiments the impedance responses were analyzed. The membranes with different catalyst loading were changed to observe the effects in the impedance response due to distinct catalyst loading. The initial conditions, memory effects and catalyst loading effects in the demountable PEMFC were performed at five overpotentials (0.0, -0.02V, -0.05V, -0.08V, and -0.1V) for the membrane of 0.3 mg Pt/cm² and three overpotentials (0.0, -0.05V, and -0.1V) for the membrane of 0.1mg Pt/cm².

CHAPTER V: DISCUSSION OF RESULTS

The research focused on comparisons between the PEM fuel cell and PEM Electrolysis mode. Also, memory effects of the PEMFCs were analyzed, as well catalyst loading effects. The memory effects were studied varying the initial conditions making different pretreatments to the PEMFCs as explained in chapter IV section 2. The impedance results were analyzed in terms of the contribution of the ohmic resistance (electrolyte resistance), double layer capacitance, and charge transfer resistance for the oxygen reduction reaction. Linear Polarization technique was used to compare the charge resistance obtained by the electrochemical impedance spectroscopy results.

V.1 PEM FUEL CELL MODE VERSUS ELECTROLYSIS MODE

A PEM fuel cell and a PEM Electrolyzer with the same electrode area and membrane properties were used to compare the impedance results. The Nyquist plots of both cells show a high frequency semicircle (100 kHz – 180 Hz) as seen in figures 17 and 18 independent of the potential superimposed to a low frequency semicircle dependent of potential. The first intercept with the real axis of the Nyquist plot, i.e. at high frequencies when the imaginary component of the impedance is zero, indicates the value of the electrolyte resistance (R_{Ω}). PEM Electrolyzer average values of the ohmic resistance were estimated at 0.15 - 0.20 Ω (Figure 19) and for the PEM fuel cell were 0.23 - 0.52 Ω (Figure 20). It is well known that the resistance of the membrane is reduced with good water management [13]. The PEM fuel cells require intensive water management for stable and continuous operation [17]. Unlike PEMFCs, the PEM Electrolyzer did not

suffer the last problem because it is in contact with water to perform the electrolysis. This may explain the difference of the membrane resistance values between the two systems specifically; the high values observed for the PEMFC were caused by poor water management.

In order to understand the behavior of the high frequency semicircle the Electrochemistry PowerSuite™ software was used to identify the resistances present on the system. In the high frequency semicircle, the program identified a second intercept with the real axis which is named here as $R_1 + R_\Omega$. The values of R_1 did not change with potential. Some authors attributed the value of this resistance to the grain and boundaries resistance which include electrode geometry, surface irregularities, grain dispersion, and electrode electronic properties [3, 12, 28, and 31]. The unchanged value of R_1 indicates that the grains and boundaries properties are unchanged in all the experiments for each cell. The values of R_1 for the PEM Electrolyzer were $0.06 - 0.15\Omega$, and for the PEMFC were $0.1 - 0.2\Omega$. The slight differences may be caused by the extrapolations performed by the program.

A second semicircle appears at the low frequencies range. This semicircle is characteristic of the charge transfer process associated with the heterogeneous oxygen reduction reaction [3, 13, 31]. The third intercept of the Nyquist Plot indicates the value of the charge transfer resistance (R_{ct}). The value of this intercept is $R_1 + R_\Omega + R_{ct}$. The value of the charge transfer resistance is potential dependent. High values of R_{ct} indicate sluggish kinetics where mass transfer is a significant factor and in some cases the limiting factor, where adsorption of reactant species can be occurring [15]. The values of the

charge transfer resistance for the electrolysis mode are lower than the fuel cell mode values. For electrolysis R_{ct} varied from 0.15 - 0.65 Ω while for fuel cell mode operation R_{ct} varied from 1.8 - 4.3 Ω . As expected, for both operation modes the charge transfer resistance decreased as potential applied was increased. In impedance experiments any effect of oxygen diffusion in the electrode should be revealed in the charge transfer resistance, the low frequency arc should decrease in size as the overpotential is increased, because the kinetics of the ORR becomes faster. Lack of this behavior indicates oxygen diffusion or mass transfer effects. As seen in the plots of R_{ct} vs. overpotential in figures 21 and 22, the R_{ct} calculated from the Nyquist Plot low frequency semicircle were higher than the R_{ct} calculated by $i-\eta$ equations. The Tafel slope of the PEM Electrolyzer from the experimental values was 65.68mV/dec and the PEMFC Tafel slope was 156.67mV/dec, while the Tafel slope calculated using the equation 15 was 12.85mV/dec. The differences attained between the theoretical Tafel slope and the experimental ones suggest another process besides charge transfer kinetics. It is important to remind that the slope calculated assuming the Tafel behavior does not account with mass transfer effects.

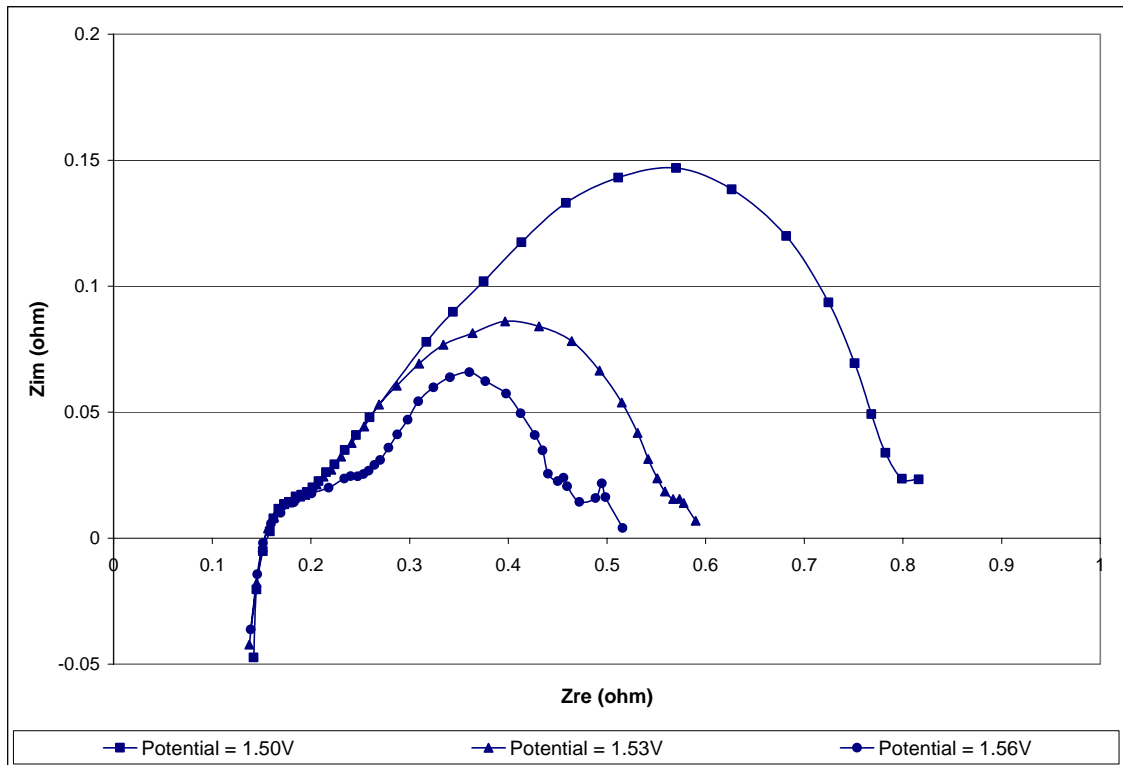


Figure 17. Nyquist Plot for the PEM Electrolyzer at different potentials

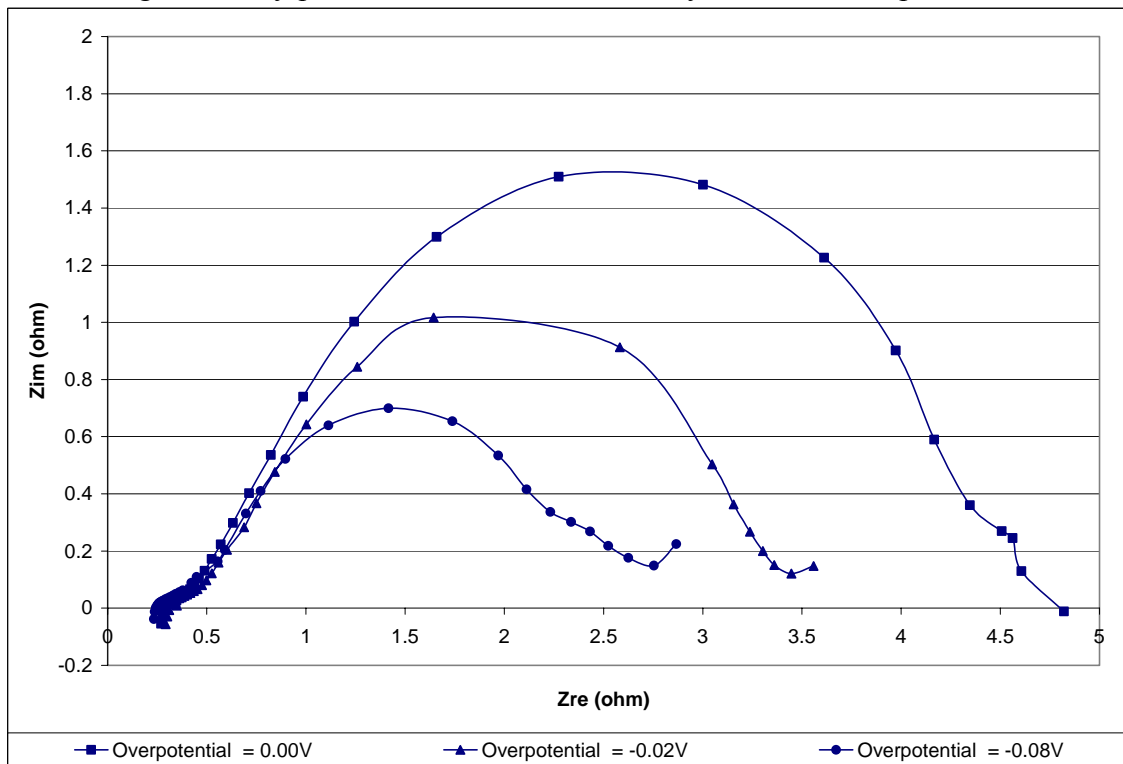


Figure 18. Nyquist Plot for the PEMFC for different overpotentials

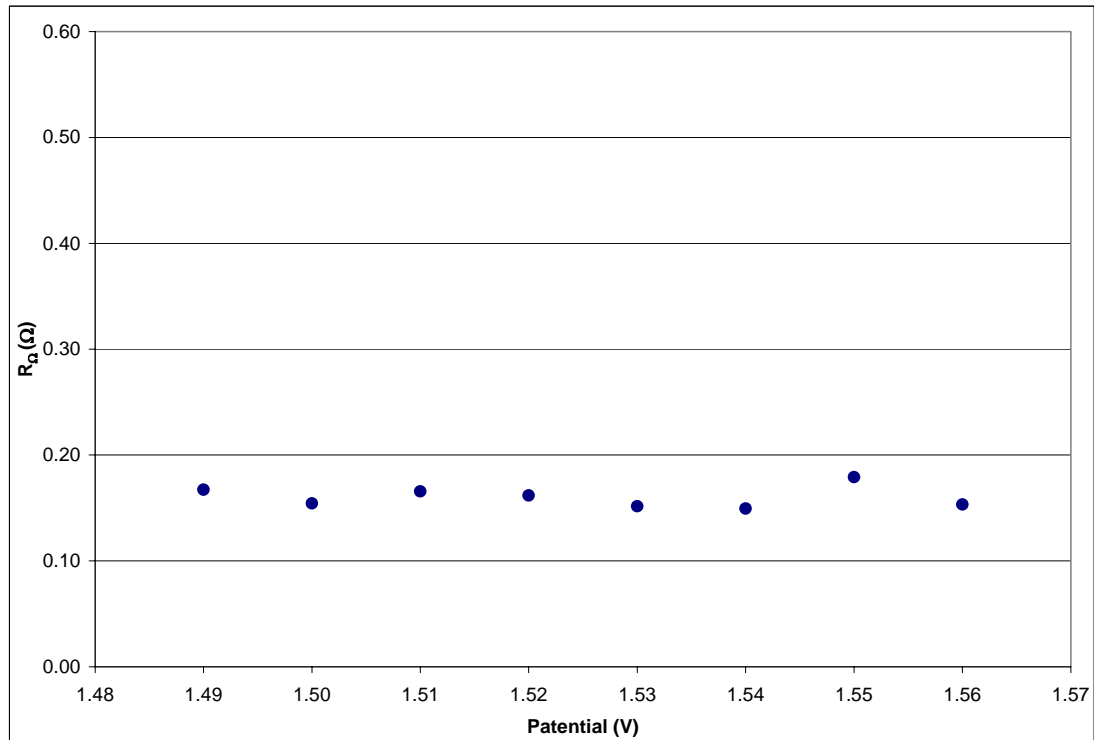


Figure 19. PEM electrolyzer Ohmic Resistance from Nyquist Plot at different overpotentials

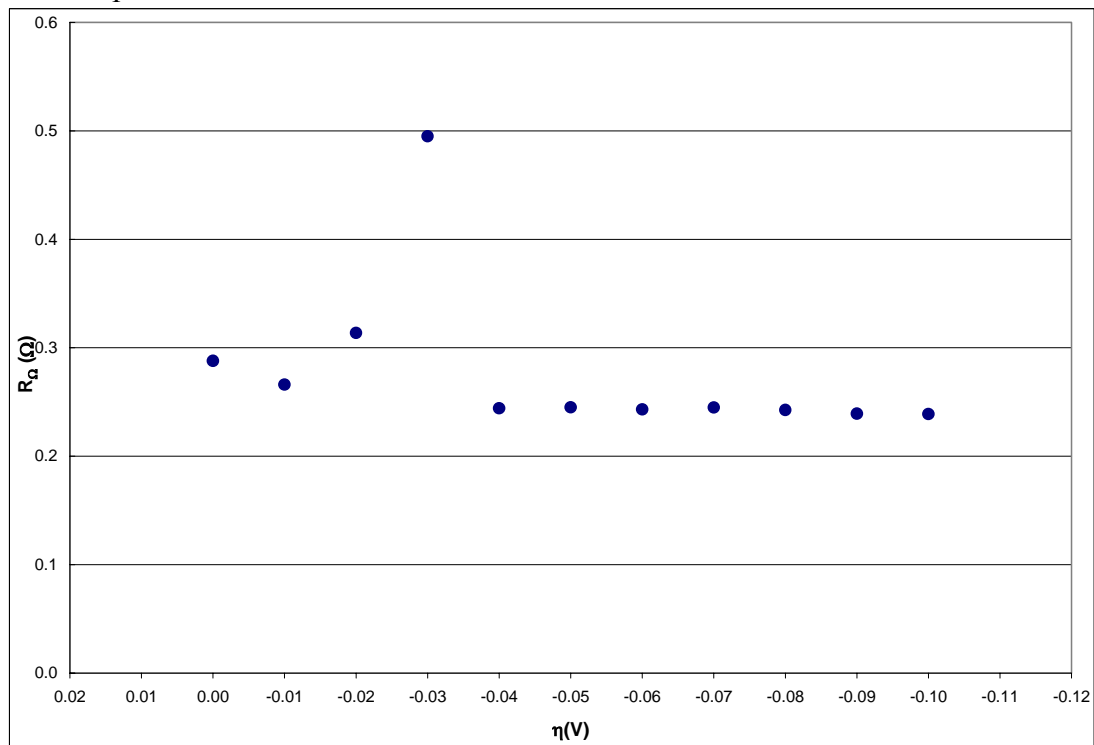


Figure 20 PEMFC Ohmic Resistance from Nyquist Plot at different overpotentials

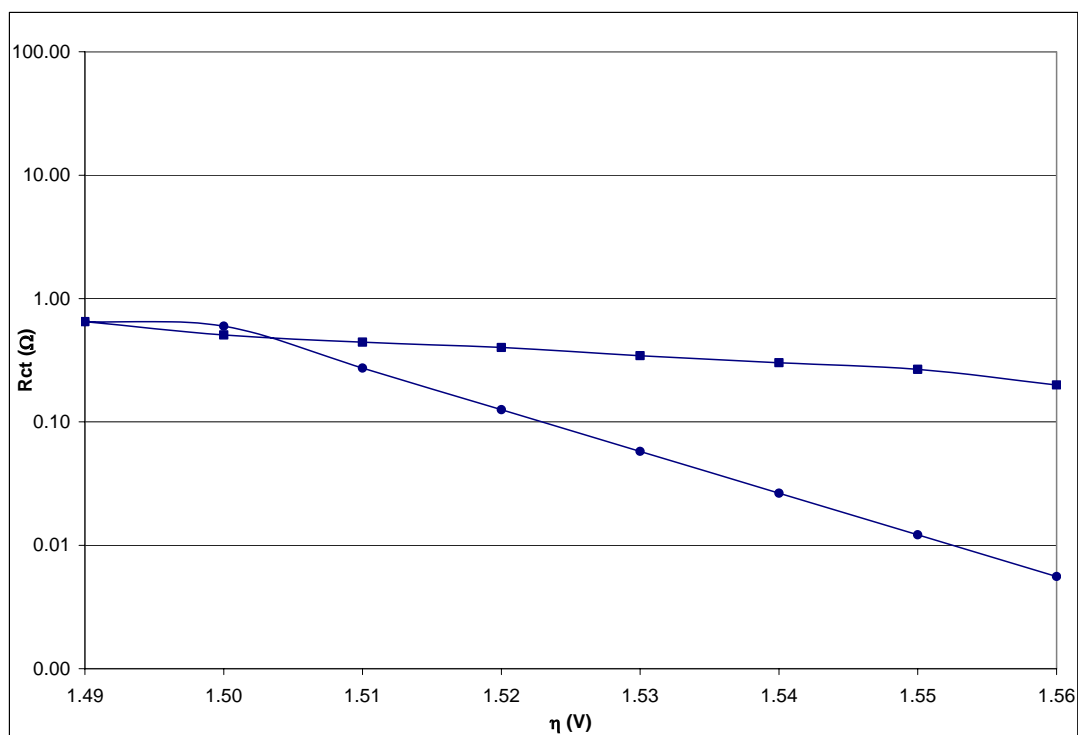


Figure 21. Charge Transfer Resistance versus potential for PEM Electrolyzer; (■) from experimental data; (●) calculated using i - η equations

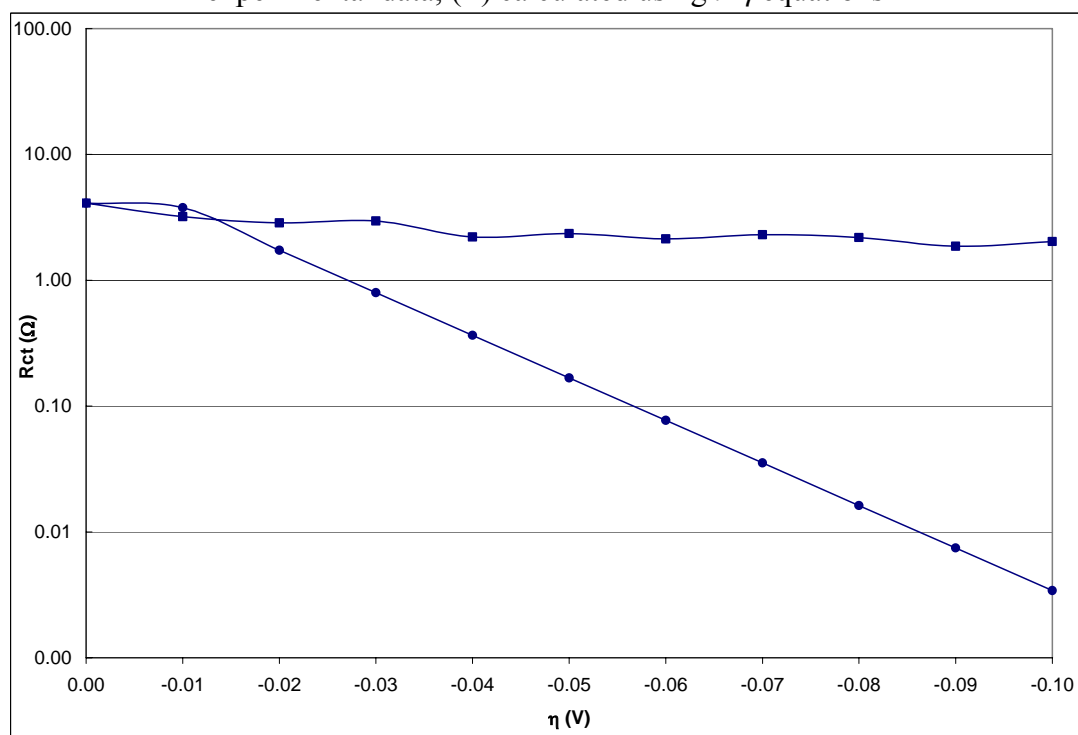


Figure 22. Charge Transfer Resistance versus potential for PEMFC; (■) from experimental data; (●) calculated using i - η equations

If the apparently phenomenon is caused by diffusion control effects a line of 45° (slope = 1) should be appear in the Nyquist Plot which indicates a Warburg impedance influence [4]. As mentioned in chapter III section 2 b.3, the Warburg impedance can be determined by plotting Z_{re} and Z_{im} versus $1/\omega^{1/2}$, where both lines should be parallel and the intercept of the Z_{re} is the charge transfer resistance. For the PEMFC the Warburg characteristic impedance was found in the frequency range of 900mHZ – 6Hz while for the electrolyzer was not estimated. An example of a Warburg plot for the PEMFC is presented in figure 23. The estimated average slope was 1.042 (figure #24) which is the Warburg coefficient (σ). In contrast to the theory the intercept of the impedance real component in the Warburg plot is much less than the charge transfer resistance calculated from the Nyquist Plot and Bode Plot. Although the intercept of the impedance imaginary part tend to be zero, as seen in figure 21. The average magnitude of the intercept of Z_{re} is 0.36Ω (figure 25). The Warburg coefficient and resistance from the PEMFC versus overpotential for the ORR is shown in figures 24 and 25, respectively. By close inspection the Warburg resistance R_w , apparently is the sum of the ohmic resistance and R_1 . More studies should be performed to understand the origin of R_1 and Warburg resistance, R_w .

Another parameter calculated from the impedance experiments was the double layer capacitance C_{dl} . The double layer capacitance values are greater for the PEM Electrolyzer than for the PEMFC. For the PEM Electrolyzer C_{dl} average values vary from 450 - 2600mF (figure 26) and for the PEM fuel cell the average values vary from 340 - 640mF (figure 27). The high value of C_{dl} in supported catalyst masks the effect of

the oxygen diffusion within the electrode on the impedance response. The values double layer capacitance reported for the PEM Electrolyzer had more variations than the values of the PEMFC. In the PEM fuel cell C_{dl} seems to be constant with overpotential. Other capacitive property was calculated from the high frequencies semicircle. This capacitance values are very small with respect to the double layer capacitance. The mass transport effects of the oxygen diffusion are expected to be seen in the Nyquist Plot where a third semicircle at very low frequency appears [13]. The mass transport semicircle was not seen, neither for PEMFC and PEM Electrolyzer. The values of R_{Ω} , R_{ct} , and C_{dl} were confirmed with the values obtained from the Bode Plots.

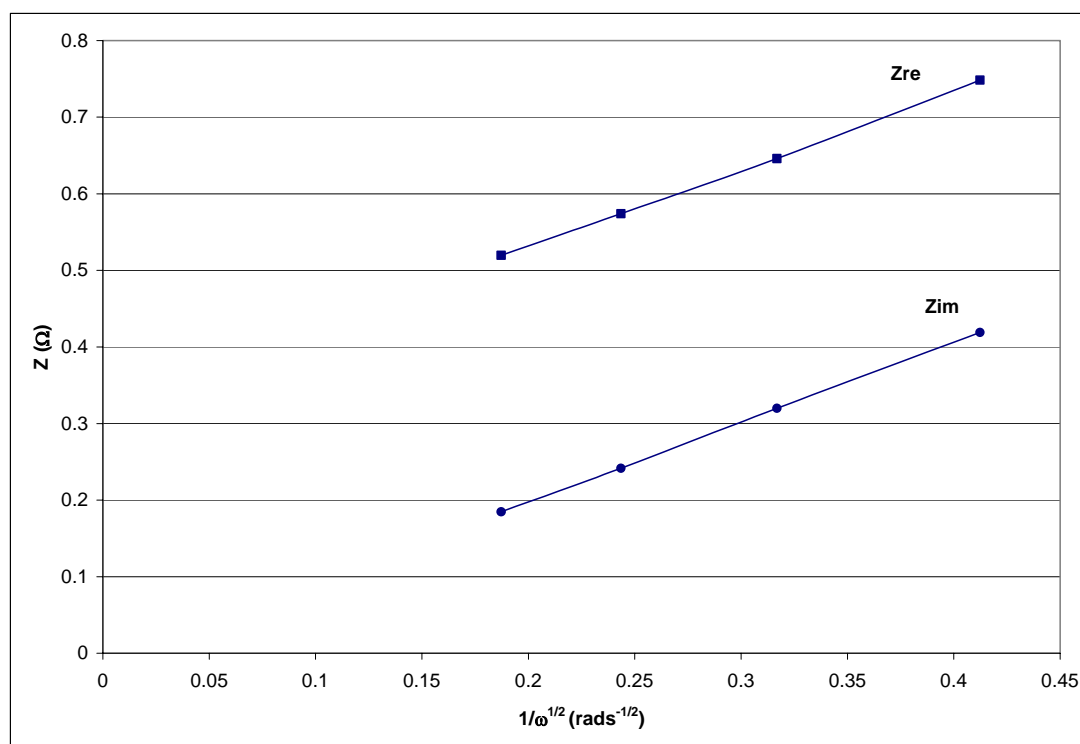


Figure 23. Warburg characteristic impedance plot for the PEMFC; (■) impedance real component (●) impedance imaginary component

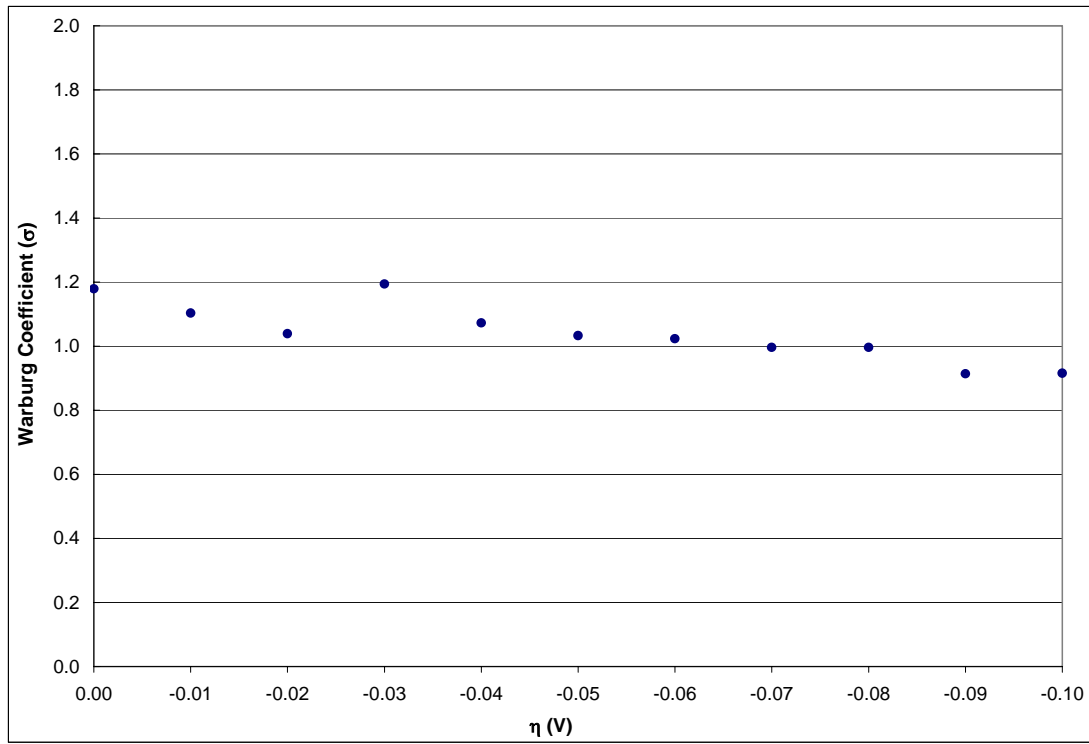


Figure 24. Warburg diffusion coefficient for PEMFC

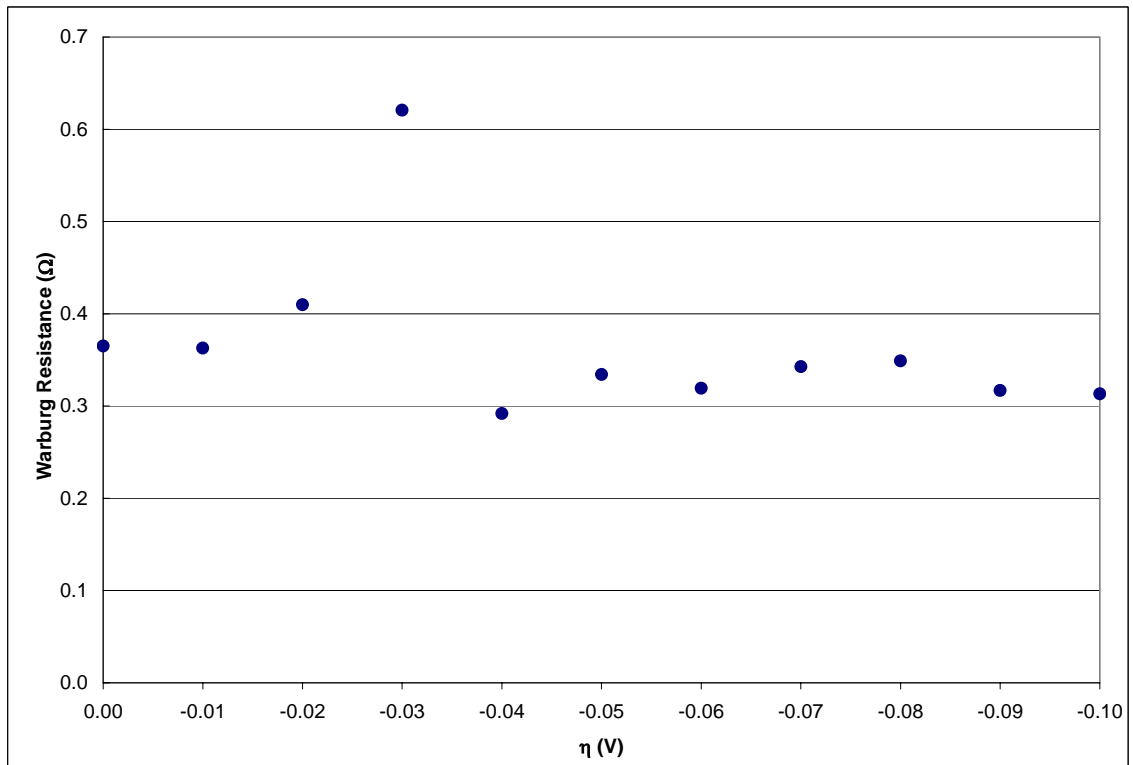


Figure 25. Warburg resistance for PEMFC

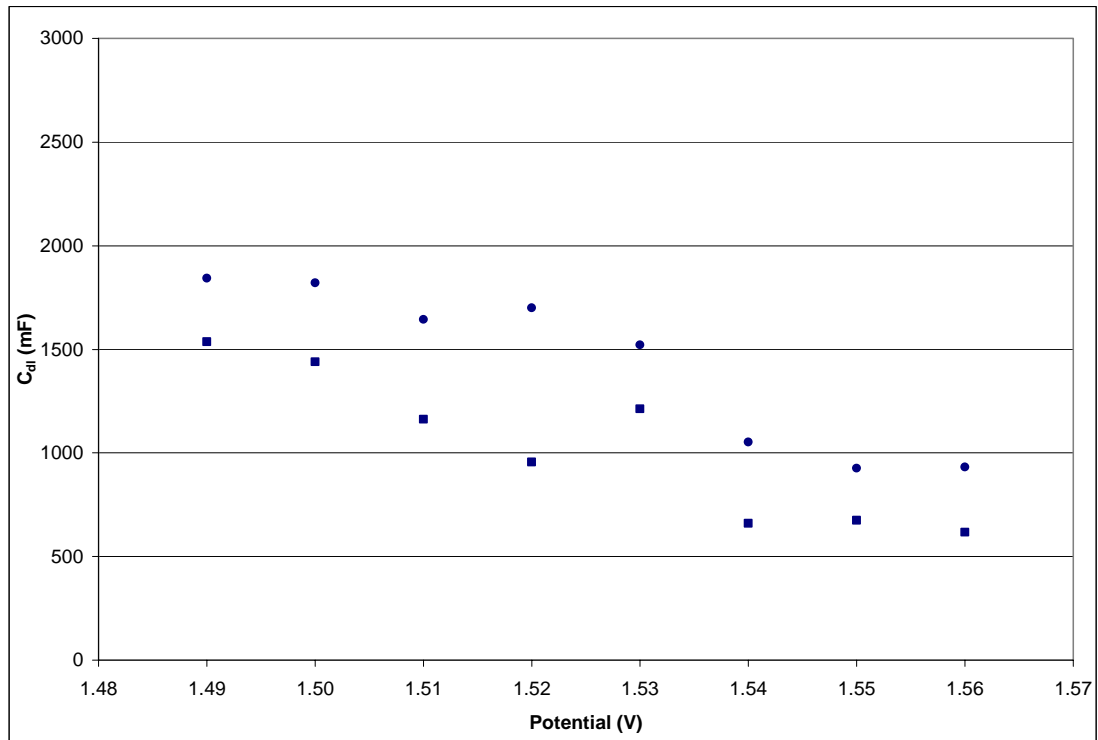


Figure 26. Double layer capacitance of the PEM Electrolyzer; (■) calculated from Nyquist Plot (●) calculated from Bode Plot.

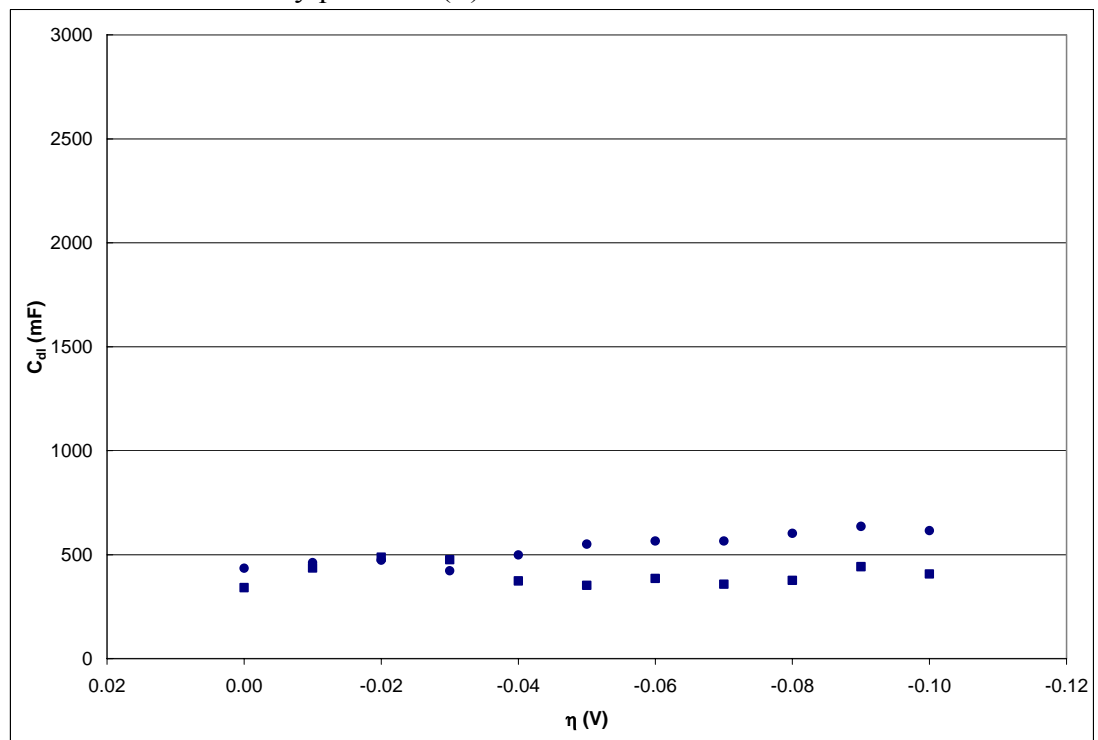


Figure 27. Double layer capacitance of the PEMFC; (■) calculated from Nyquist Plot (●) calculated from Bode Plot.

Summary of the PEM Electrolyzer and PEM Fuel cell results, R_{Ω} , R_1 , R_{ct} , and C_{dl} , calculated from Nyquist Plot and Bode

Plot are presented in table 2 and 3, respectively.

Table 3. Results of the PEM Electrolyzer

Voltage	1.49	1.50	1.51	1.52	1.53	1.54	1.55	1.56
Nyquist Plot Results								
R_{Ω} (ohm)	0.1673	0.1544	0.1656	0.1619	0.1516	0.1494	0.1792	0.1533
R_1 (ohm)	0.0611	0.1480	0.0573	0.0576	0.0789	0.0760	0.0618	0.1040
R_{ct} (ohm)	0.6496	0.5072	0.4427	0.4010	0.3445	0.3022	0.2663	0.1993
C_{dl} @ high freq (mF)	1.7934	1.7420	3.2104	2.0466	4.2654	2.1787	2.2350	0.6141
C_{dl} @ low freq (mF)	962.6685	2596.8473	1163.0613	839.4532	839.0586	500.3102	544.2431	453.0811
Bode Plot Results								
R_{Ω} (ohm)	0.1919	0.1854	0.1697	0.1581	0.2045	0.1955	0.1937	0.1753
R_{ct} (ohm)	0.5736	0.5634	0.4901	0.4253	0.3466	0.3240	0.3031	0.3075
C_{dl} @ ϕ_{max} (mF)	2404.5580	2034.6646	1643.6336	1700.6758	1759.8173	1561.0873	1827.1468	1769.8378

Table 4. Results of the PEM Fuel cell

Overpotential (V)	0.00	-0.01	-0.02	-0.03	-0.04	-0.05	-0.06	-0.07	-0.08	-0.09	-0.10
Nyquist Plot Results											
R_{Ω} (ohm)	0.2880	0.2660	0.3138	0.4951	0.2443	0.2452	0.2431	0.2450	0.2427	0.2393	0.2390
R_1 (ohm)	0.1563	0.1680	0.2017	0.1977	0.1267	0.1411	0.1159	0.1110	0.1244	0.1297	0.1201
R_{ct} (ohm)	4.1118	3.2050	2.8634	2.9612	2.2081	2.3508	2.1355	2.3060	2.1905	1.8661	2.0335
C_{dl} @ high freq (mF)	3.3510	2.4215	5.8159	2.3886	2.4297	2.1782	1.5667	1.2792	1.9389	2.3849	2.5610
C_{dl} @ low freq (mF)	341.3241	435.6003	487.3557	475.6686	373.2729	351.9502	385.9590	357.5879	376.4175	441.8671	406.4518
Bode Plot Results											
R_{Ω} (ohm)	0.3352	0.2671	0.2367	0.5194	0.2661	0.2598	0.2430	0.2617	0.3131	0.3114	0.2913
R_{ct} (ohm)	4.2669	2.9689	2.8805	2.8689	2.2247	2.3279	2.0446	2.3509	2.0505	1.7687	1.9812
C_{dl} @ ϕ_{max} (mF)	435.0519	461.2898	473.4934	422.1681	498.5079	550.2213	564.9507	565.5366	602.2752	635.9174	615.3888
Warburg Plot Results											
slope = σ	1.179	1.103	1.039	1.194	1.072	1.033	1.023	0.996	0.996	0.914	0.915
R_w (ohm)	0.365	0.363	0.410	0.621	0.292	0.334	0.319	0.343	0.349	0.317	0.313

V.2 MEMORY AND CATALYST LOADING EFFECTS

Two PEMFC with the same electrode area and membrane thickness were used to study the effect of catalyst loading. The memory effects were analyzed in terms of the initial conditions of the PEMFCs including the anode humidity and the operation conditions. The initial conditions are named as 1st run and after run; the 1st runs were controlled by the humidity of the anode, passing water through the anode (wet) or passing only hydrogen to the anode (dry). The “after runs” were performed after the ones mentioned above without controlling the initial condition.

Analyzing the impedance results for both PEMFC, one with 0.1mgPt/cm² and the other with 0.3mgPt/cm², two semicircles were also noted in the Nyquist Plot. The high frequency semicircle is superimposed to the lower frequency arc. The magnitude of the former is independent on overpotential. This behavior was observed in the majority of the runs. The high frequency arc was absent in some experiments. As explained before the R_{Ω} , R_1 , R_{ct} , and Cdl can be estimated from the Nyquist Plots. The values of R_{Ω} , R_{ct} , and Cdl were confirmed with the values obtained from the Bode Plot (Appendix C & D). The Nyquist Plots were analyzed at each applied potential, to see the effect of the initial condition or pretreatments. In figures 28 and 29 are presented the Nyquist Plots for both PEMFC open circuit potential for dry pretreatment. The Nyquist Plot squared marked is for after run condition and the circle marked is for 1st run condition. In figure 30 and 31 wet pretreatment Nyquist Plot for both fuel cell are presented.

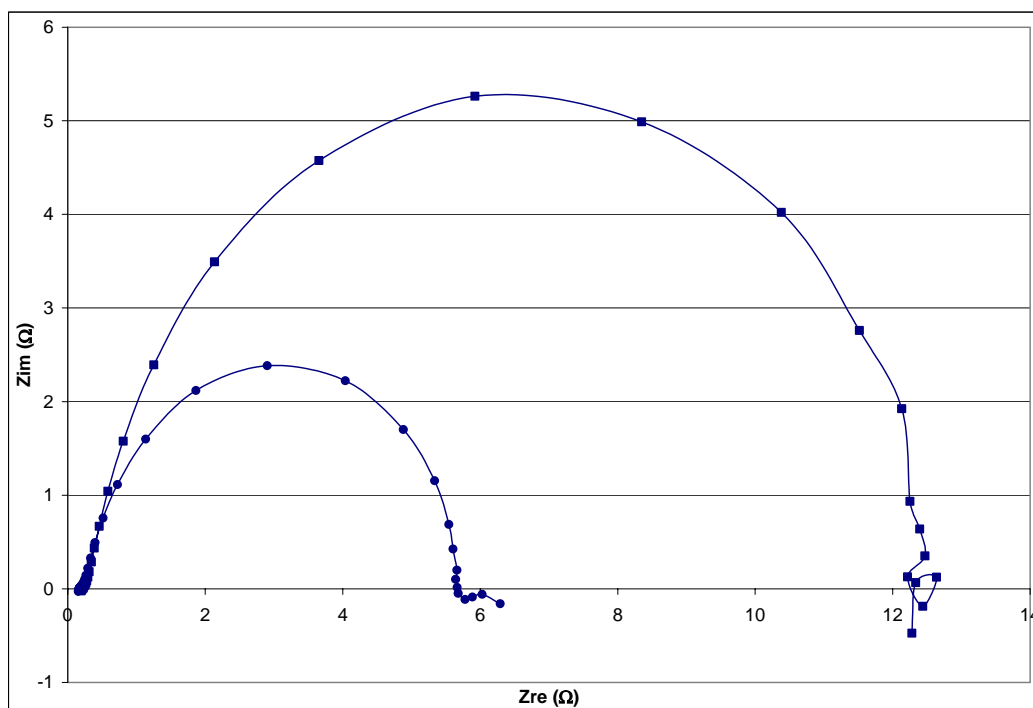


Figure 28 Nyquist Plot for PEMFC of 0.1mgPt/cm² with dry pretreatment at OCP; (■) for after run; (●) for 1st run.

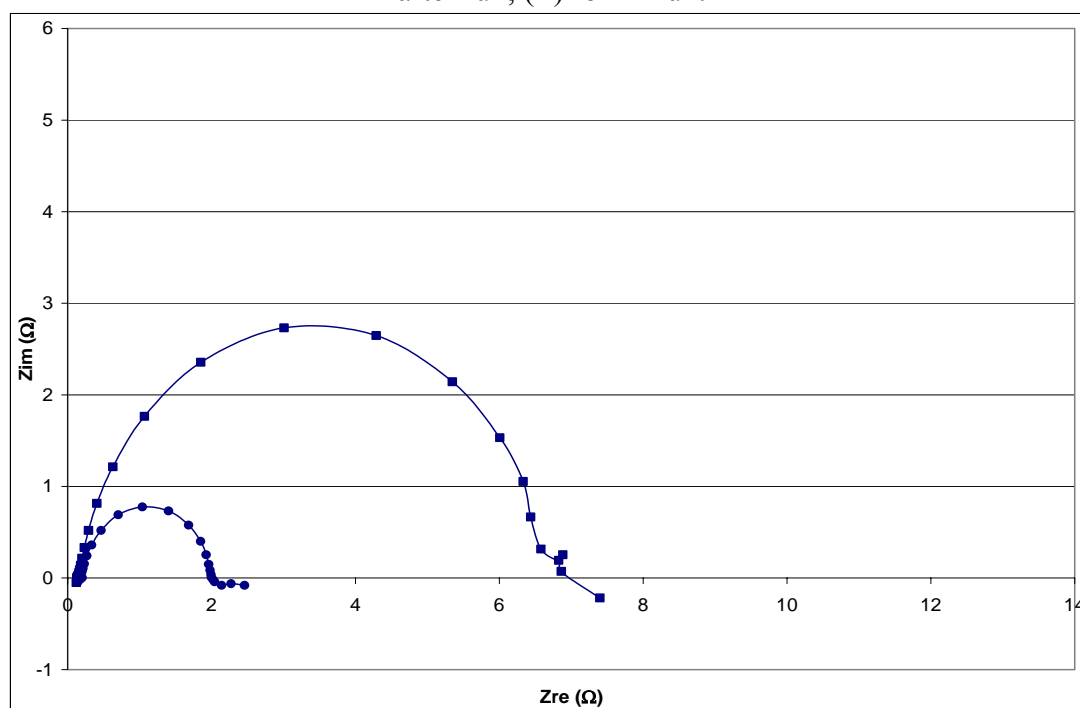


Figure 29 Nyquist Plot for PEMFC of 0.3mgPt/cm² with dry pretreatment at OCP; (■) for after run; (●) for 1st run.

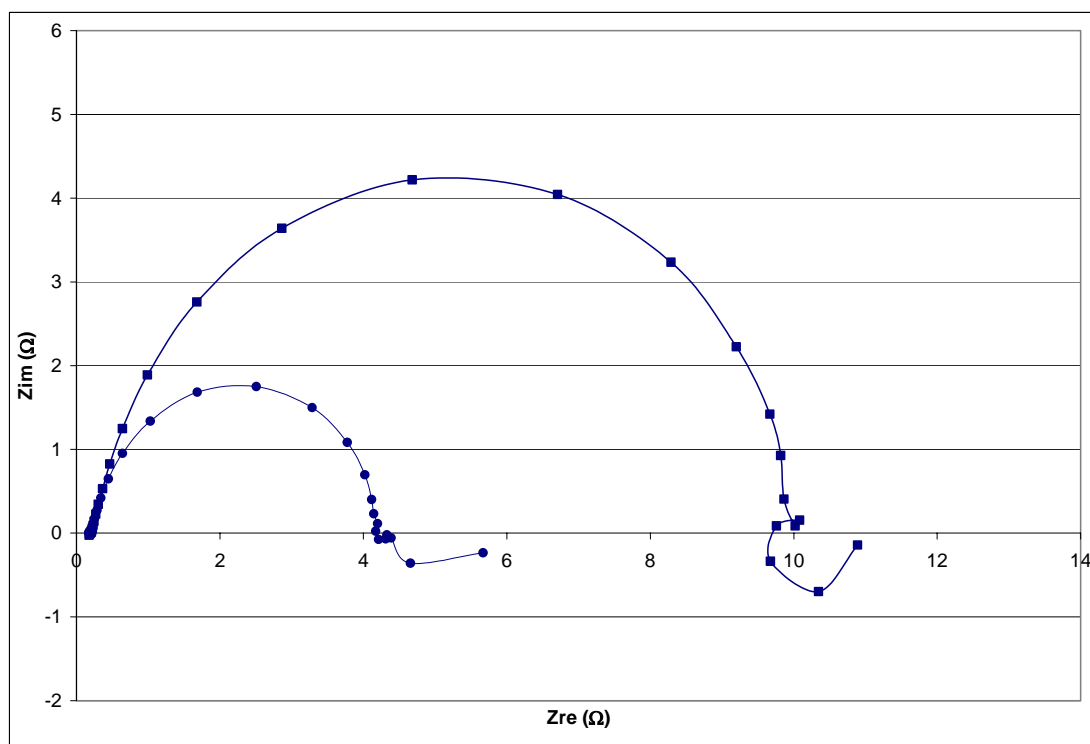


Figure 30 Nyquist Plot for PEMFC of 0.1mgPt/cm² with wet pretreatment at OCP; (■) for after run; (●) for 1st run.

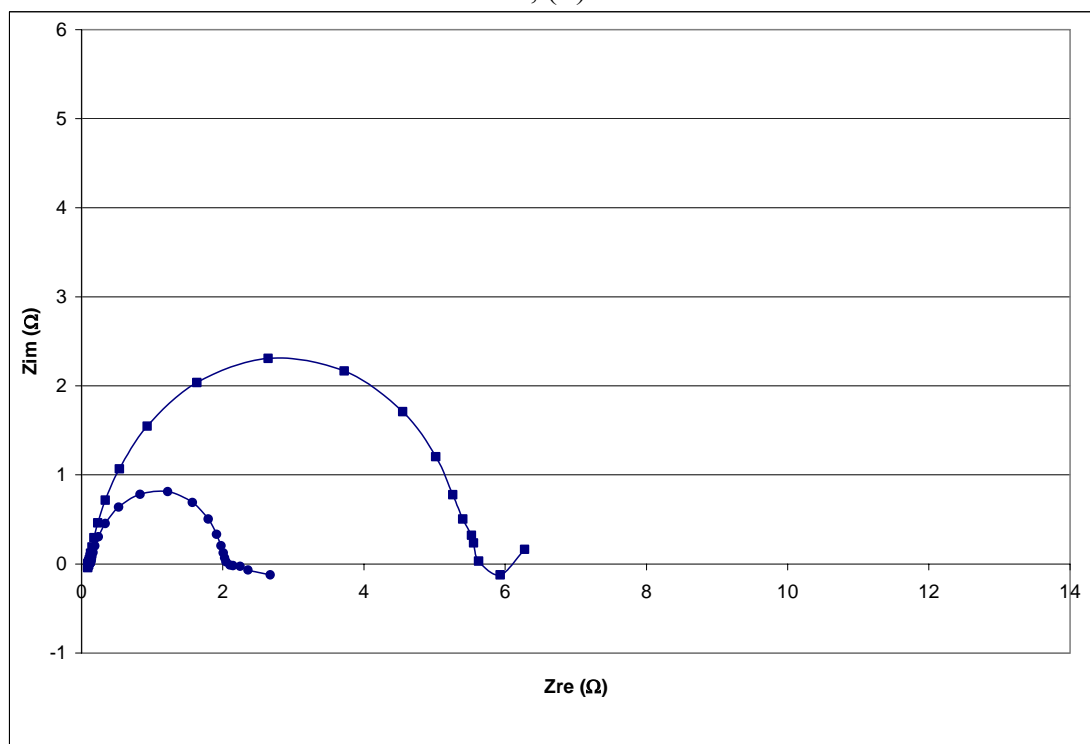


Figure 31 Nyquist Plot for PEMFC of 0.3mgPt/cm² with wet pretreatment at OCP; (■) for after run; (●) for 1st run.

As seen in the Nyquist Plots from both PEMFCs the 1st runs have the smaller charge transfer resistance semicircle. The wet 1st runs presented the smaller charge transfer resistance arcs for both cells. This indicates that this pretreatment is the best one to improve the cell performance. The larger values of R_{ct} for the dry 1st runs could be caused by lack of water, which inhibit the proton transport through the membrane. The biggest charge transfer resistances are obtained for the “after runs”. It can be caused by poor water management practices. For the wet after runs it can be caused by the water produced by the cell reaction at the cathode, which can flood the electrode inhibiting the oxygen diffusion through the cathode. The dry after runs gave the larger R_{ct} because its need of water to facilitate the proton conductivity or may be caused by the same cause of the wet after runs. These results were obtained for the overpotential range of 0.0 to 50mV. Overpotentials above 0.05V present distortion in the path as seen in Appendixes C and D.

Comparing the catalyst loading it seems that the charge transfer resistance semicircles are smaller for the PEMFC with catalyst loading of $0.3\text{mgPt}/\text{cm}^2$ and show less distortion in the Nyquist Plots and in the explained path. The charge transfer resistance semicircle could be influenced by the mass transport resistance demonstrating more mass transfer losses for the PEMFC with low catalyst loading caused by the grain dispersions of the catalyst. Also, the kinetics will be affected because this PEM has less active site to perform the reaction.

From the Nyquist and Bode plots at different overpotentials the ohmic resistances (R_{Ω}) were obtained for both PEMFCs. The results of the ohmic resistances for both cells

are presented in figures 32 and 33. The ohmic resistances average values are $0.11 - 0.24\Omega$ for the PEMFC with $0.3\text{mgPt}/\text{cm}^2$ for all conditions, and $0.16 - 0.32\Omega$ for the PEMFC with $0.1\text{mgPt}/\text{cm}^2$. The R_{Ω} values are very similar for both cells consistent with the fact that both cells have the same membrane thickness. It, also, demonstrates that the catalyst loading did not affect the ohmic resistance values. The variability of the values from 0.11 to 0.24Ω and $0.16 - 0.32\Omega$ can be attributed to the anode water management, where for some runs the anode was humidified with water, while for other runs the anode was “dry”.

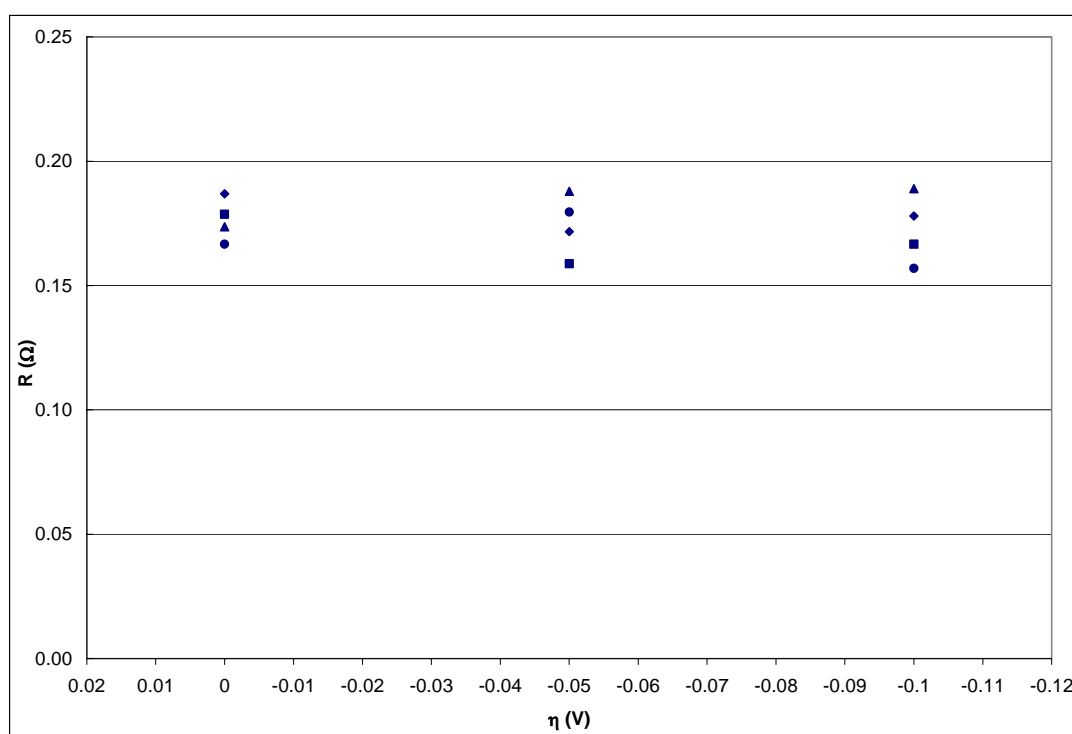


Figure 32 Ohmic resistance for PEMFC with $0.1\text{mgPt}/\text{cm}^2$ for all initial conditions; (■) wet 1st run; (●) wet after run; (▲) dry 1st run; (◆) dry after run.

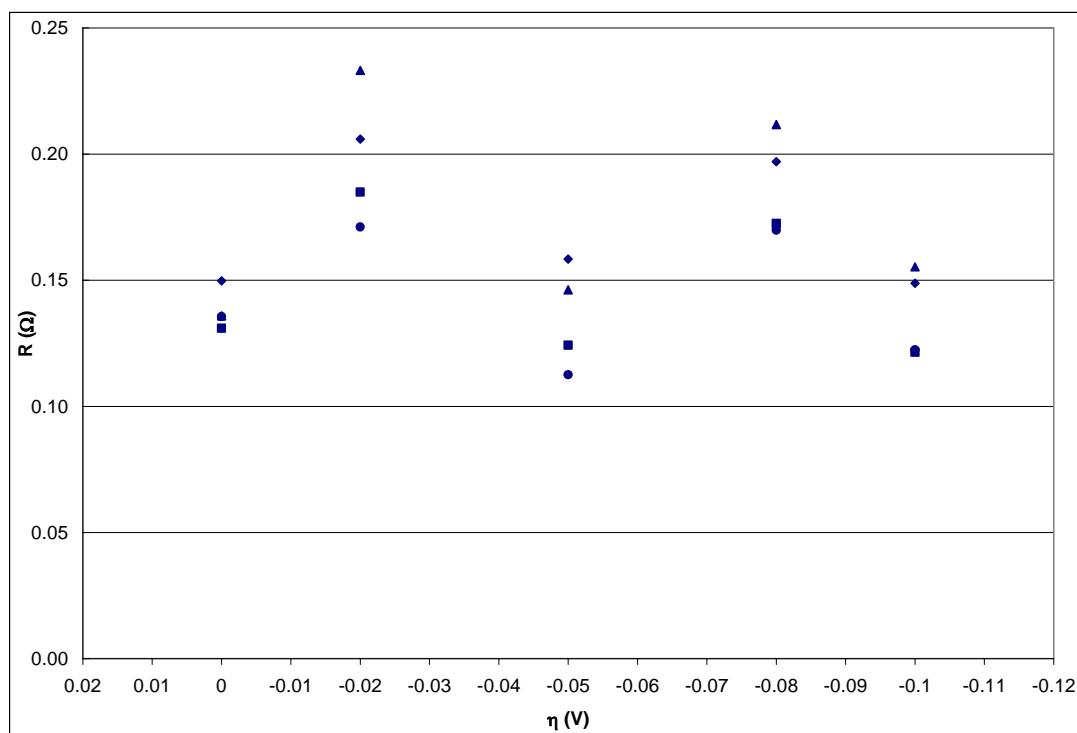


Figure 33. Ohmic resistance for PEMFC with $0.3\text{mgPt}/\text{cm}^2$ for all initial conditions; (■) wet 1st run; (●) wet after run; (▲) dry 1st run; (◆) dry after run.

The values of R_1 were obtained from correlations obtained from the high frequencies semicircles with the Electrochemistry PowerSuite™ software. [2] The values are presented in figures 34 and 35. For the PEMFC with less catalyst loading the average values of R_1 were from $0.034 - 0.16\Omega$, whereas for the PEMFC with high catalyst loading the average values were from 0.0063 to 0.067Ω . The average value of R_1 is less for the PEMFC with $0.3\text{mgPt}/\text{cm}^2$. The higher values of the resistance R_1 for the membrane with less catalyst implicates higher performance losses due to higher catalyst dispersion, less active sites than the other fuel cell and less protons traveling through the membrane.

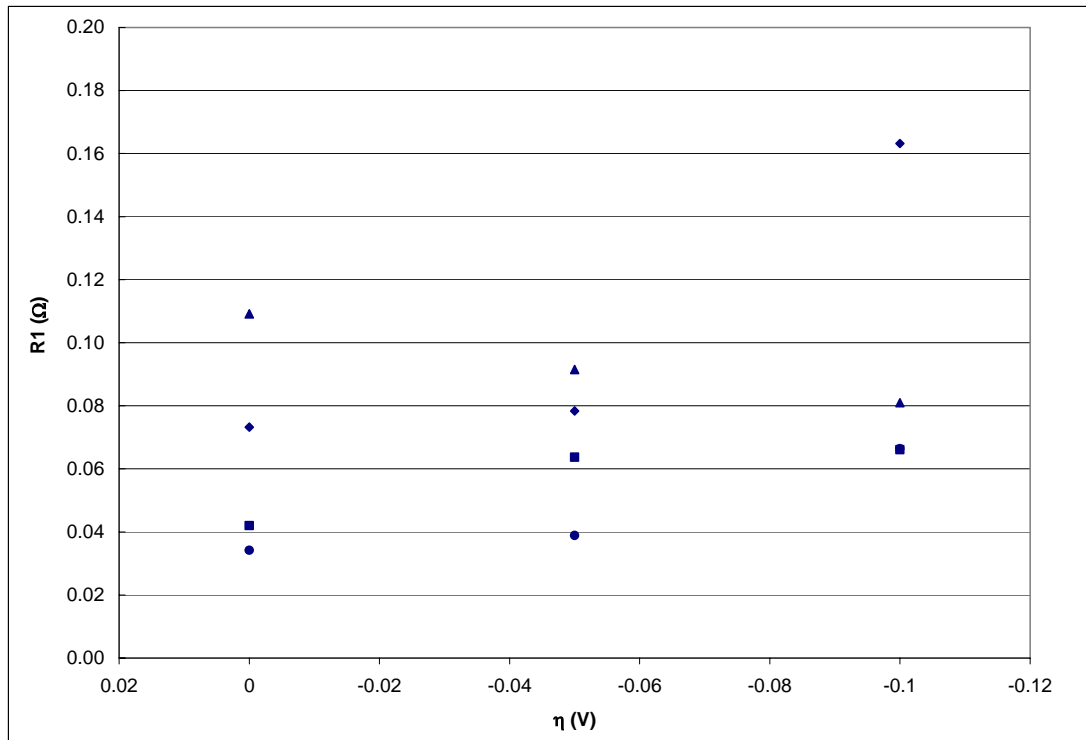


Figure 34. R1 for PEMFC with 0.1mgPt/cm² for all initial conditions; (■) wet 1st run; (●) wet after run; (▲) dry 1st run; (◆) dry after run.

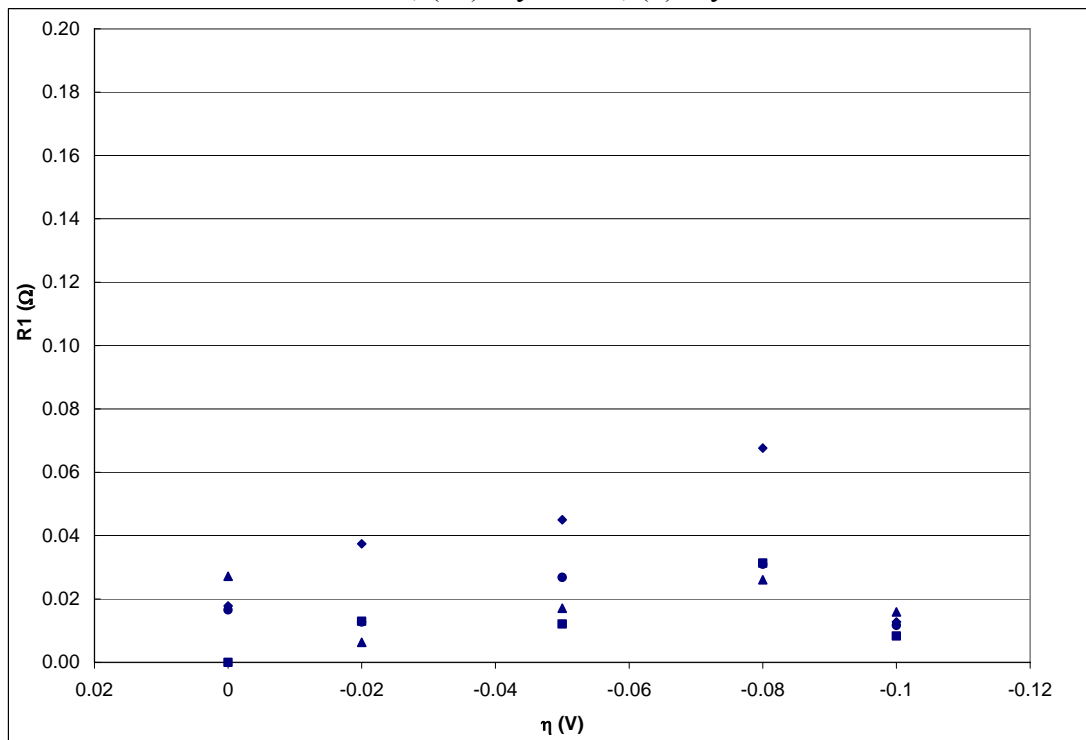


Figure 35. R1 for PEMFC with 0.3mgPt/cm² for all initial conditions; (■) wet 1st run; (●) wet after run; (▲) dry 1st run; (◆) dry after run.

The charge transfer resistance was calculated for all conditions and compared with R_{ct} calculated from $i-\eta$ equations. The charge transfer resistance for both cells decreased with increases in overpotential, as expected, but it did not decrease to the levels calculated by the Tafel equation. In figures 36 and 37 R_{ct} versus overpotential for the PEMFC with $0.1\text{mgPt}/\text{cm}^2$ is shown and in figures 38 and 39 for the PEMFC with $0.3\text{mgPt}/\text{cm}^2$. Figures 36 and 38 show R_{ct} from experimental results, while the charge transfer resistance calculated using $i-\eta$ equations is shown in 37 and 39. The Tafel slopes of the experimental values are smaller than calculated by the Tafel equation. This may be caused by mass transport effects not seen in the Nyquist Plot. In some cases the R_{ct} and mass transport resistances fall in the same frequency region. The mass transfer resistance semicircle could be superimposed to the R_{ct} semicircle producing higher values of R_{ct} as viewed in figures 36 and 38. The R_{ct} values obtained showed R_{ct} larger for the PEMFC of $0.1\text{mgPt}/\text{cm}^2$ than for the PEMFC $0.3\text{mgPt}/\text{cm}^2$. As mentioned above the charge transfer resistance semicircle could be influenced by the mass transport resistance demonstrating more mass transfer losses for the PEMFC with low catalyst loading. It could obtain R_{ct} higher values because sluggish kinetics originated by less active sites to accomplish the ORR. The PEMFC with low catalyst loading has the greater grain dispersion and less active site becoming slower the hydrogen oxidation and less proton transport through the membrane, showing apparently mass transport performance loss.

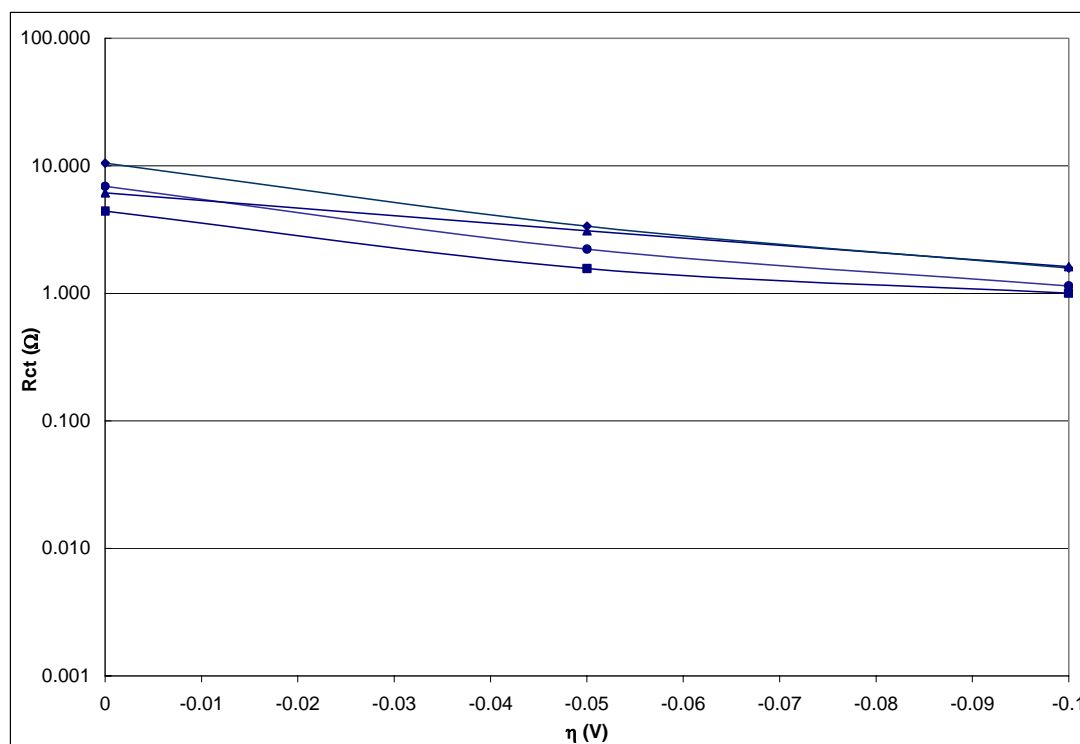


Figure 36. Experimental Charge Transfer Resistance for PEMFC of $0.1\text{mgPt}/\text{cm}^2$; (■) wet 1st run; (●) wet after run; (▲) dry 1st run; (◆) dry after run.

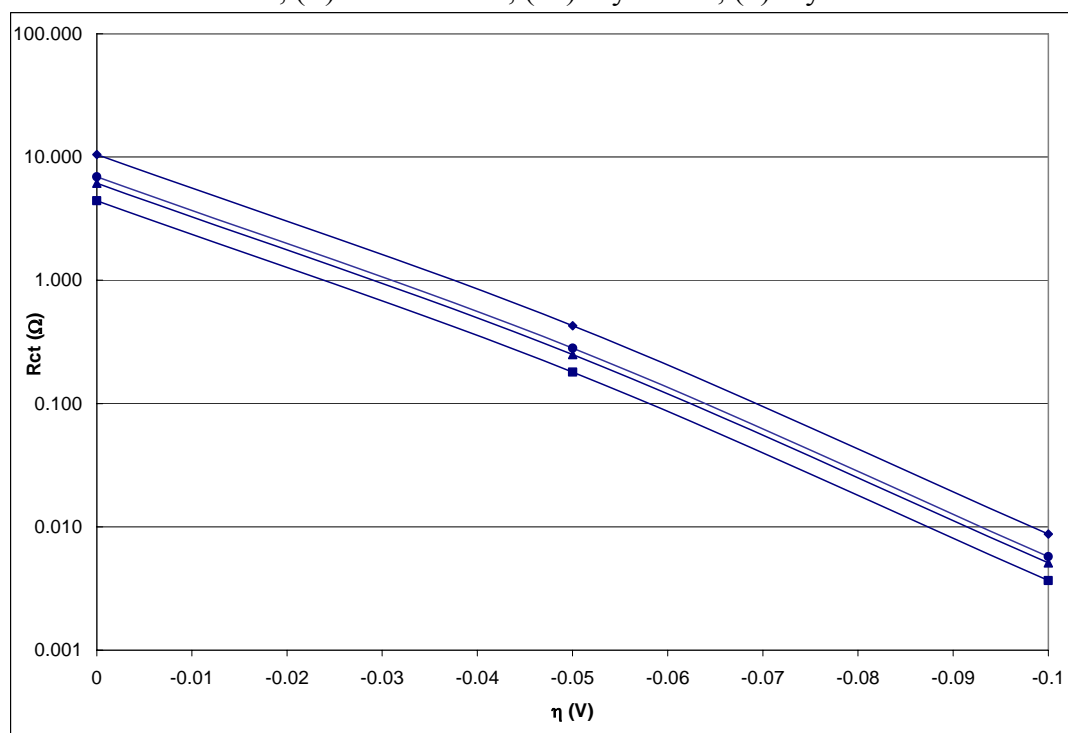


Figure 37. Charge Transfer Resistance calculated using i - η equations for PEMFC of $0.1\text{mgPt}/\text{cm}^2$; (■) wet 1st run; (●) wet after run; (▲) dry 1st run; (◆) dry after run.

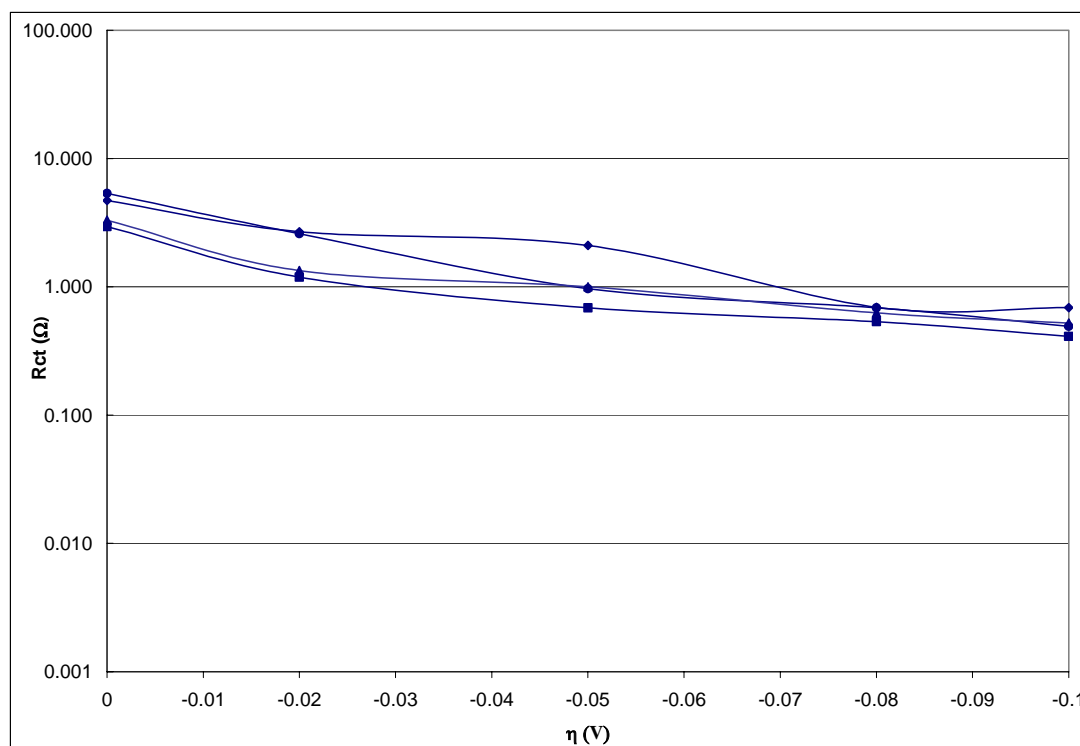


Figure 38. Experimental Charge Transfer Resistance for PEMFC of $0.3\text{mgPt}/\text{cm}^2$; (■) wet 1st run; (●) wet after run; (▲) dry 1st run; (◆) dry after run.

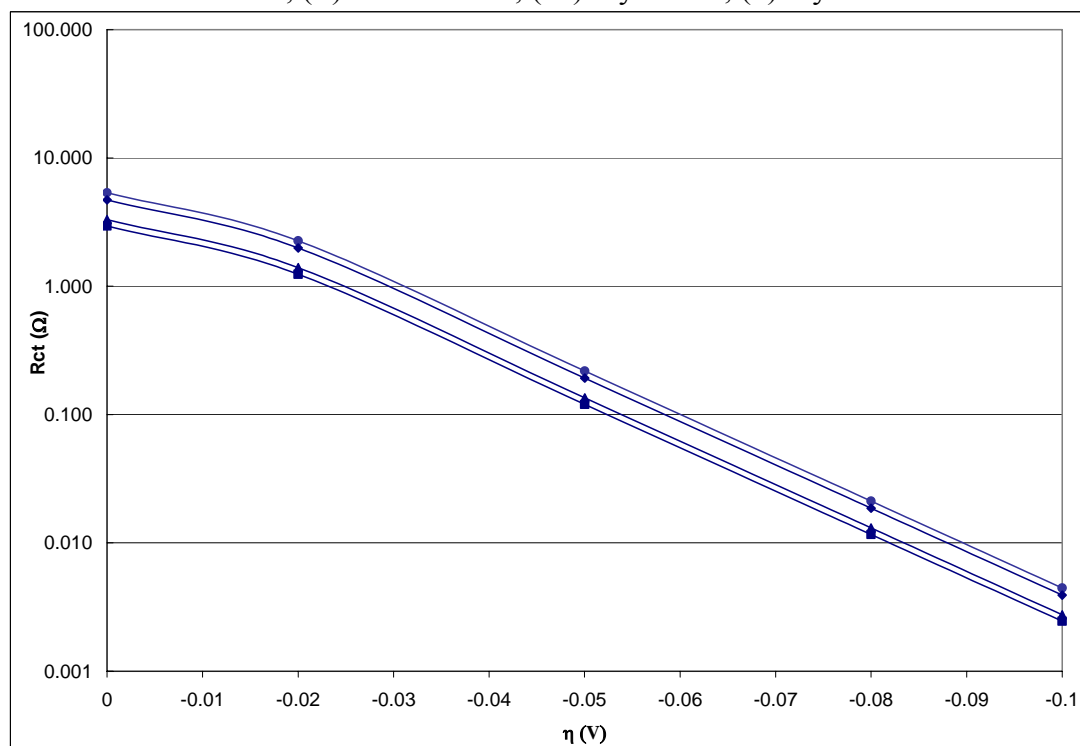


Figure 39. Charge Transfer Resistance calculated using Tafel equation for PEMFC of $0.3\text{mgPt}/\text{cm}^2$; (■) wet 1st run; (●) wet after run; (▲) dry 1st run; (◆) dry after run.

The memory effects of the PEMFC can be analyzed using the R_{ct} as a critical variable. Each PEMFC has its own behavior with respect to the charge transfer with the initial conditions as independent variables. The PEMFC with $0.1\text{mgPt}/\text{cm}^2$ presents higher average values of R_{ct} for after runs conditions especially for the dry after run pretreatment (figure 36). At higher overpotentials the higher R_{ct} average values were for the dry pretreatments. For overpotential of 50mV the after run pretreatment presented higher value than the other conditions, but for the 100mV of overpotential both, dry 1st and after run, pretreatment presented similar values. For wet pretreatments the high R_{ct} was exhibited by the after run condition, which is indicative of better proton conductivity. The ORR was improved by the wet 1st run pretreatment for all overpotentials.

At open circuit potential the cell with $0.3\text{mgPt}/\text{cm}^2$ presents the after run condition with higher R_{ct} values, but different from the other PEMFC the wet after run has the higher average value than 1st run (figure 38). At higher overpotentials, greater than 50mV , the average values of the R_{ct} were independent of potential. This could be caused because at high overpotentials the low frequency arc of the Nyquist Plot should decrease due to the increasing driving force, high current density (reaction rate), but it was not reflected.

The after runs for dry and wet are the best indicators of how the PEMFCs behave after they were operating, in both cells the after runs conditions present higher values than their 1st run conditions, dry and wet. This observation can help us to conclude that the PEMFCs acquire more resistance properties after they operate, even as the anode was wet or dry.

The Double Layer Capacitance, C_{dl} , were also measured in the Nyquist Plot and corroborated by the Bode Plot in order to obtain more accurate values. Contrary to the resistance properties the PEMFC with more catalyst loading has the highest average values for the C_{dl} , 100 – 200mF (figure 41), while the PEMFC with $0.1\text{mgPt}/\text{cm}^2$ C_{dl} average values were 25 – 50mF (figure 40). Higher values are preferred as shown in equation 33. The higher catalyst loading is more efficient minimizing losses associated with double layer charging effects. With respect to the initial conditions the C_{dl} was independent of these conditions.

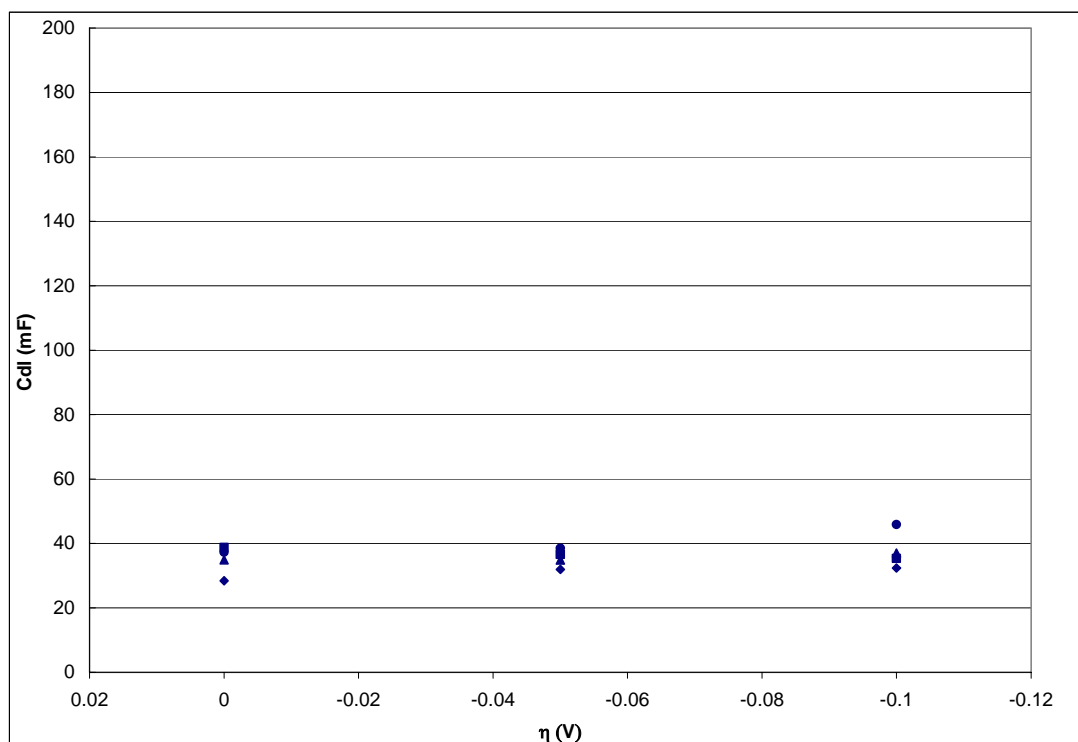


Figure 40. Double Layer Capacitance versus overpotential for PEMFC of $0.1\text{mgPt}/\text{cm}^2$; (■) wet 1st run; (●) wet after run; (▲) dry 1st run; (◆) dry after run.

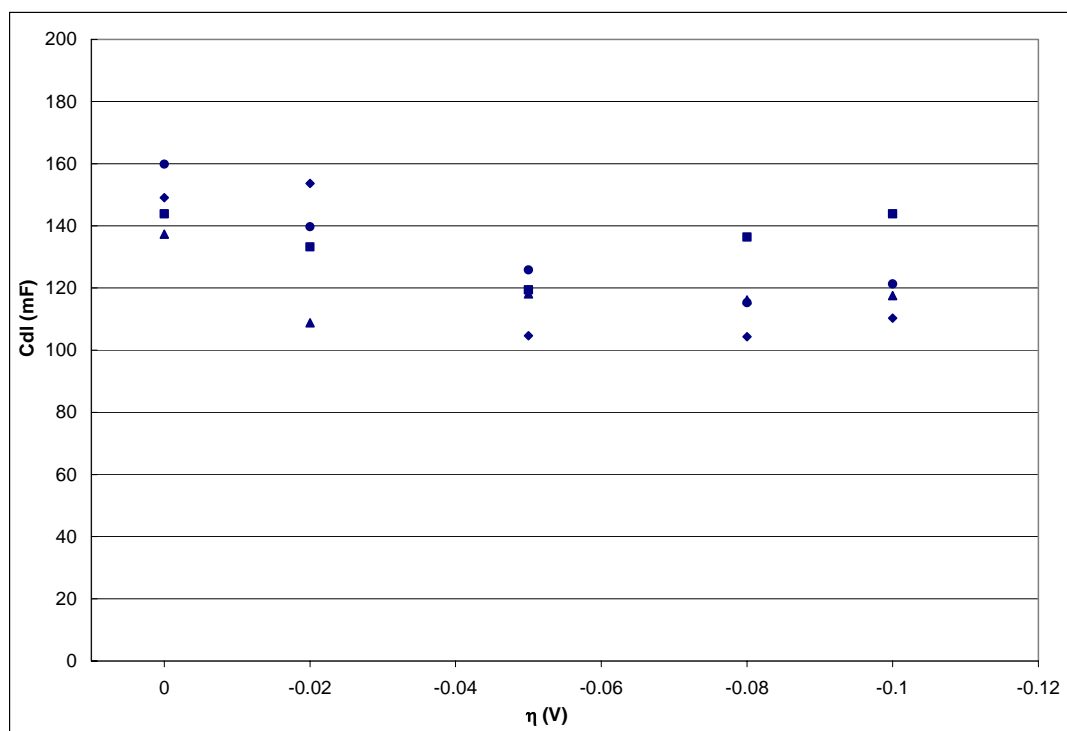


Figure 41. Double Layer Capacitance versus overpotential for PEMFC of $0.3\text{mgPt}/\text{cm}^2$; (■) wet 1st run; (●) wet after run; (▲) dry 1st run; (◆) dry after run.

The Warburg characteristic impedance was not obtained for none of these PEM fuel cells. The mass transport, oxygen diffusion or proton transport could be masked by the double layer capacitance or by the charge transfer resistance at medium and low frequencies.

The summary of the values of R_{Ω} , R_1 , R_{ct} , and C_{dl} are shown in table 4 and 5 for the PEMFC of $0.1\text{mgPt}/\text{cm}^2$ and table 6 and 7 for PEMFC of $0.3\text{mgPt}/\text{cm}^2$. The best fit data is tabulated in Tables 5 and 6.

Table 5. Results for PEMFC of 0.1mgPt/cm² with Wet Pretreatments

	Wet					
	1st run			After run		
Overpotential (V)	0	-0.05	-0.1	0	-0.05	-0.1
Nyquist Plot Results						
R _Ω (ohm)	0.1786	0.1588	0.1666	0.1796	0.1570	0.1717
R ₁ (ohm)	0.0420	0.0637	0.0661	0.0342	0.0389	0.0664
R _{ct} (ohm)	4.4160	1.5627	1.0018	6.9074	2.2238	1.1435
C _{dl} @ high freq (mF)	5.5355	6.1806	8.3921	3.1501	0.1131	6.1177
C _{dl} @ low freq (mF)	38.7626	36.6008	35.3427	37.2634	38.5370	45.9094
Bode Plot Results						
R _Ω (ohm)	0.2259	0.2173	0.2170	0.2580	0.2316	0.2128
R _{ct} (ohm)	4.3236	1.5722	1.0168	6.9615	2.1889	1.1465
C _{dl} @ φ _{max} (mF)	37.2533	39.3833	40.7500	32.2767	28.3733	48.8900

Table 6. Results for PEMFC of 0.1mgPt/cm² with Dry Pretreatments

	Dry					
	1st run			After run		
Overpotential (V)	0	-0.05	-0.1	0	-0.05	-0.1
Nyquist Plot Results						
R _Ω (ohm)	0.1737	0.1879	0.1890	0.1869	0.1717	0.1780
R ₁ (ohm)	0.1092	0.0915	0.0810	0.0732	0.0783	0.1632
R _{ct} (ohm)	6.1301	3.0932	1.6219	10.4867	3.3635	1.5817
C _{dl} @ high freq (mF)	5.2821	6.4825	3.2072	2.4343	5.0528	6.3505
C _{dl} @ low freq (mF)	34.9667	34.8715	37.0588	28.3931	31.9714	32.3804
Bode Plot Results						
R _Ω (ohm)	0.2176	0.3221	0.2597	0.2764	0.2813	0.2574
R _{ct} (ohm)	5.9929	3.0159	1.6444	10.3487	3.3050	1.6478
C _{dl} @ φ _{max} (mF)	32.7733	25.3500	22.2019	26.4600	29.1200	37.5900
Warburg Plot Results						

Table 7. Results for PEMFC of 0.3mgPt/cm² with Wet Pretreatments

	Wet									
	1st run					After run				
Overpotential (V)	0	-0.02	-0.05	-0.08	-0.1	0	-0.02	-0.05	-0.08	-0.1
Nyquist Plot Results										
R _Ω (ohm)	0.1310	0.1849	0.1242	0.1725	0.1214	0.1356	0.1712	0.1126	0.1699	0.1224
R ₁ (ohm)	0.0000	0.0129	0.0121	0.0313	0.0083	0.0166	0.0127	0.0268	0.0310	0.0117
R _{ct} (ohm)	2.9470	1.1891	0.6854	0.5344	0.4131	5.3546	2.5971	0.9662	0.6870	0.4916
C _{dl} @ high freq (mF)	0.0000	5.4762	11.2370	2.4740	4.9188	2.0922	0.7663	0.1680	1.0206	2.6424
C _{dl} @ low freq (mF)	143.8694	133.2070	119.4223	136.4330	143.9050	159.8546	139.7117	125.8253	115.3296	121.3279
Bode Plot Results	0.0000	0.0000	0.0000	0.0000	0.0000	0.0000	0.0000	0.0000	0.0000	0.0000
R _Ω (ohm)	0.1318	0.1962	0.1303	0.2063	0.1284	0.1337	0.1907	0.1358	0.2147	0.1288
R _{ct} (ohm)	2.6770	1.0284	0.6761	0.5219	0.3962	5.1814	2.4838	0.9010	0.6599	0.4871
C _{dl} @ φ _{max} (mF)	143.2667	159.3667	121.3550	194.0000	154.7750	127.8500	131.2667	99.8575	133.8325	136.0000

Table 8. Results for PEMFC of 0.3mgPt/cm² with Dry Pretreatments

	Dry									
	1st run					After run				
Overpotential (V)	0	-0.02	-0.05	-0.08	-0.1	0	-0.02	-0.05	-0.08	-0.1
Nyquist Plot Results										
R _Ω (ohm)	0.1358	0.2332	0.1462	0.2117	0.1553	0.1498	0.2060	0.1584	0.1970	0.1488
R ₁ (ohm)	0.0272	0.0063	0.0171	0.0261	0.0160	0.0178	0.0374	0.0450	0.0677	0.0127
R _{ct} (ohm)	3.3080	1.3372	0.7281	0.6259	0.5224	4.7108	2.6833	2.1023	0.6921	0.6880
C _{dl} @ high freq (mF)	1.5155	0.0475	5.8307	5.7838	10.4479	0.0000	26.7694	33.1159	9.4111	6.5001
C _{dl} @ low freq (mF)	137.3563	108.8069	118.1298	116.1758	117.5540	149.0625	153.6663	104.6445	104.3215	110.2557
Bode Plot Results	0.0000	0.0000	0.0000	0.0000	0.0000	0.0000	0.0000	0.0000	0.0000	0.0000
R _Ω (ohm)	0.1390	0.2265	0.1566	0.2407	0.1590	0.1395	0.2181	0.1561	0.2171	0.1435
R _{ct} (ohm)	3.0833	1.3262	0.7184	0.5762	0.5320	4.5781	2.5858	2.0670	0.7483	0.6775
C _{dl} @ φ _{max} (mF)	132.9333	156.9000	147.0333	156.3000	129.4667	114.2750	159.0333	117.0000	177.0333	135.1667

V.3 LINEAR POLARIZATION

Linear Polarization technique was performed to the PEMFC with higher catalyst loading, $0.3\text{mgPt}/\text{cm}^2$, to compare the charge transfer resistance values at different conditions. Three consecutively runs for each condition, wet and dry were carried out. The values of the R_{ct} calculated from the linear portion of the $i-\eta$ curves are shown in figures 42 and 43 and Appendix F. Figures 42 and 43 present the linear polarization curves for dry and wet pretreatment, respectively. The values of R_{ct} and i_o were estimated by a curve fit technique of the PowerSuite software. Also, the i_o was calculated using equation 13. R_{ct} and i_o values at dry and wet conditions are shown in table 9. For the first and second runs for both conditions the estimated R_{ct} values did not vary. However, the third run of both cases present a slight difference, 0.3Ω , which can be attributed to the effect of water content in the cell. As noted in table 9 the Open circuit voltages were relatively constant. The same was observed for the charge transfer resistance. The exchange current was also very consistent. Note that exchange current values reported by curve fitting are very similar to those values calculated using equation 13 with one electron transferred ($n = 1$). The values obtained using this technique are comparable with R_{ct} values estimated using EIS for the 1st runs of both conditions, but are very different from the after runs values. The R_{ct} values from the EIS technique are shown and the exchange current values are presented in Appendix E. Using this technique the memory effects were not evident different to EIS technique which is a helpful tool to understand the effects.

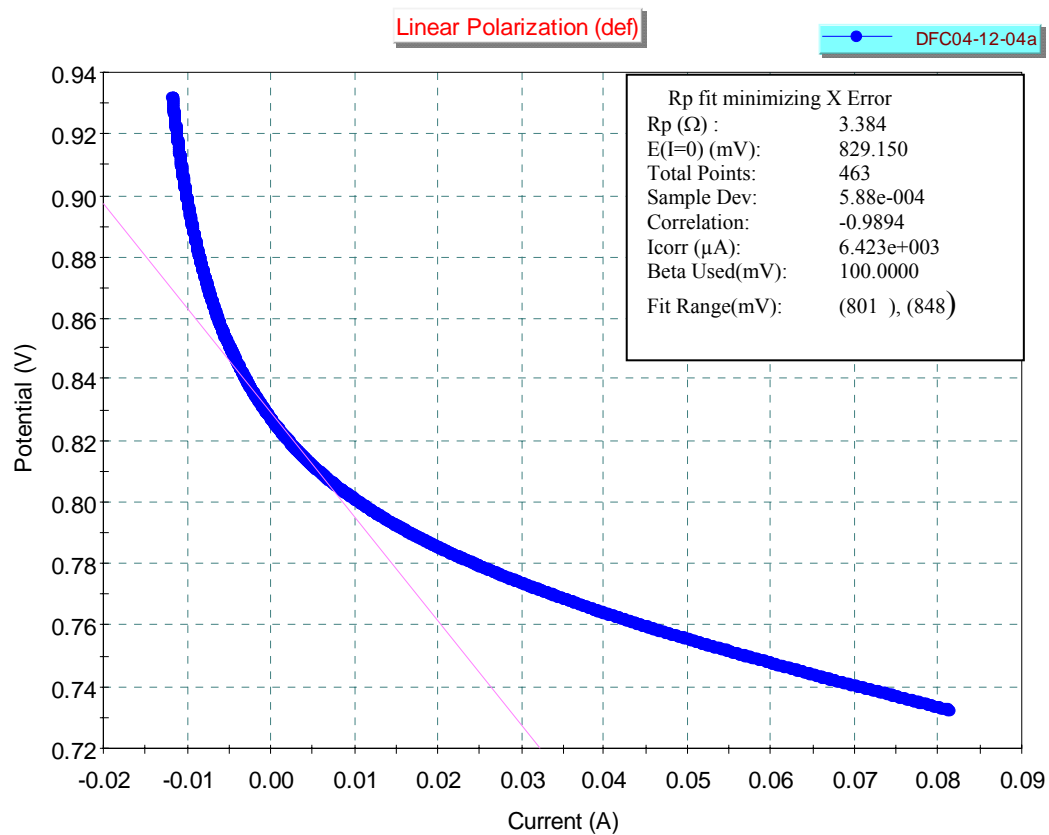


Figure 42. Linear Polarization for PEMFC of 0.3mPt/cm² with Dry Pretreatment.

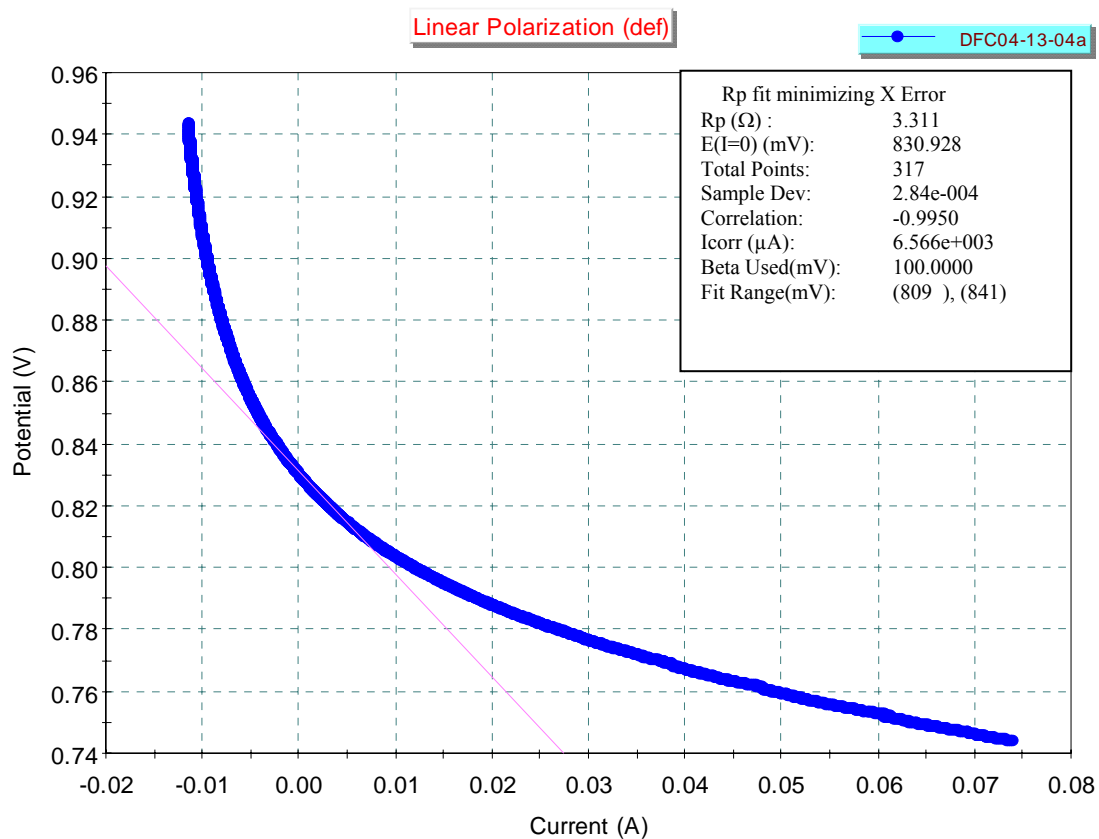


Figure 43. Linear Polarization for PEMFC of $0.3\text{mPt}/\text{cm}^2$ with Wet Pretreatment.

Table 9. Linear Polarization for PEMFC with $0.3\text{mgPt}/\text{cm}^2$

Runs	Open circuit Potential (mV)	Rct (Ω)	i_o (mA) fit	i_o (mA) calc (n=4)	i_o (mA) calc (n=1)
Dry	829.2	3.384	6.423	1.898	7.592
	818.5	3.063	7.097	2.097	8.387
	816.4	3.372	6.447	1.905	7.619
Wet	830.9	3.311	6.566	1.940	7.759
	822.5	3.085	7.047	2.082	8.327
	825.4	3.640	5.973	1.764	7.058

CHAPTER VI: CONCLUSIONS

Electrochemical Impedance Spectroscopy is a very useful tool to understand the electrochemical process occurring in an electrolytic or galvanic cell. Studying the real and imaginary components of electrochemical cell impedance, as represented by the Nyquist Plot, one can obtain valuable information of the interfacial charge transfer resistance, membrane resistance, contact resistance, oxygen diffusion, proton transport and water transport resistances. In this study we intended to understand the difference between a PEM cells operated in electrolysis (electrolytic) mode or fuel cell (galvanic) mode. Both cells were successfully examined and compared. The membrane resistance of the PEM fuel cell was larger than the PEM electrolyzer. It was attributed to the fact that the conductivity of Nafion® membrane is increased with the water content. The PEM Electrolyzer is always in contact with water to perform the electrolytic reaction, while the fuel cell needs to be operated with the optimal water quantity in the anode and cathode side. The water to the fuel cell is supplied by external means, the water carried by the humidified reactant gases, water generated by the ORR at the cathode or water carried by the protons. Another finding was that the charge transfer resistance was lower for the PEM electrolyzer indicating faster kinetics than for the fuel cell. The Warburg impedance was obtained only for the fuel cell, which implicates that the charge transfer is affected by the proton transport. The PEM Electrolyzer apparently was not affected by mass transport effects but it could be masked by the high value of the double layer capacitance. For both cells a high frequency semicircle was found indicating that the cells have other resistance properties, which are attributed to grain dispersion, surface irregularities, or

electrode electronic properties. The value of this resistance was not dependent on potential. It should be an integral part of any study to improve the performance of the cells. Apparently, it is related to better catalyst dispersion, and the best materials to construct the electrode of the cells.

Considering the amount of catalyst loading the results demonstrated that the PEMFC with $0.3\text{mgPt}/\text{cm}^2$ has better water management properties. The memory effects were evaluated by running the PEMFC in a consecutive run, and named after runs. The lower charge transfer resistances values obtained was for the PEMFC with $0.3\text{mgPt}/\text{cm}^2$. Analyzing the charge transfer resistance behavior it is noted that the PEMFCs resistances increased as the operating time passed. This would result in lower current densities with time. The best operational condition found in this study was for the PEMFC of $0.3\text{mgPt}/\text{cm}^2$ at wet 1st run condition. The memory effects of the PEMFCs were found to be related to the water content and management in the cells and they were more evident at low overpotentials.

CHAPTER VII: RECOMMENDATIONS

In order to better understand the memory effects, more replicates are needed including another experimental design where the humidity percent of the gases and membrane will be monitored. The initial conditions of the PEMFC must be well controlled to obtain reproducible data. It is also recommended to apply the same pretreatments to other PEMFCs with different electrode area, membrane thickness, and catalyst loading.

To improve the performance is necessary to decrease the charge transfer resistance with the operational conditions and water management. It is recommended to design the PEMFC with the best water and proton transport qualities. The semicircle at very high frequencies need to be studied further, because it is constant at different potentials and its origin is not well understood. The study of this resistance needs a closer inspection of the Nyquist Plot.

BIBLIOGRAPHY

1. Andreaus, B., McEvoy, A.J., and Scherer, G.G. "Analysis of performance losses in polymer electrolyte fuel cells at high current densities by impedance spectroscopy" Electrochimica Acta 47 (2002): 2223-2229
2. "Analyzing PowerSINE Data" Electrochemistry PowerSuite HTML User Help Manual. Feb 2002. Princeton Applied Research. Jan 2003.
3. Ayala, R. "Polymer Electrolyte Fuel Cell Experimental and Characterization Studies Using Electrochemical Impedance Spectroscopy" MS Thesis, UPRM (2001)
4. Bard, Faulkner. "Techniques Based on Concepts of Impedance" Electrochemical Methods: Fundamentals and Applications, Wiley & Sons. (2000): 376-387
5. "Basic of AC Impedance Measurements." Princeton Applied Research. 2003. Advance Measurements Technology, Inc. 9 Dec. 2003
<http://www.princetonappliedresearch.com/applications/application_notes/appnotes.htm>
6. Brett D. J. L., Atkins S., Brandon N., Vesovic V., Vasileiadis N., and Kiernak A. "Localized Impedance Measurements along a Single Channel of Solid Polymer Fuel Cell" Electrochemical and Solid-State Letters 6 (2003): A63-A66.
7. Cho, E., Ko, J., Ha, H.Y., Hong, S., Lee, K., Lim, T., and I. Oh. "Characteristics of the PEMFC Repetitively Brought to Temperatures Below 0°C" Journal of The Electrochemical Society 150 (2003): A1667-A1670
8. Costamagna, Paola. "Transport Phenomena in polymeric membrane fuel cells" Chemical Engineering Science 56 (2001): 323-332
9. "Dismantable Fuel Cell." Fuelcellstore. Feb 2004
<<http://www.fuelcellstore.com/cgi-bin/fuelweb/view=Item/cat=9/product=36>>
10. "Eco H2/Air Set." fuelcellstore.com. 10 Oct. 2002
<<http://www.fuelcellstore.com/cgi-bin/fuelweb/view=Item/cat=/product=61>>
11. Eikerling, M., Kornyshev, A.A. "Electrochemical impedance of the cathode catalyst layer in polymer electrolyte fuel cells" Journal of Electroanalytical Chemistry 475 (1999): 107-123

12. Fischer, A., Jindra, J., and H. Wendt. "Porosity and catalyst utilization of thin layer cathode in air operated PEM-fuel cells" Journal of Applied Electrochemistry 28 (1998): 277-282
13. Freire, T.J.P., Gonzalez, E.R. "Effect of membrane characteristics and humidification conditions on the impedance response of polymer electrolyte fuel cells" Journal of Electroanalytical Chemistry 503 (2001): 57-68.
14. "Fuel Cells: How the PEM Fuel Cell Works." Howstuffworks. 5 Jan 2003
<<http://www.humboldt.edu/~serc/fc.html>>
15. "Fuel Cell Performance." Fuel Cell Handbook, EG&G Services, Parson Inc (2000): 2-1 – 2-26
16. "Fuel Cell: Understanding electricity production" h-tec education. 22 Jul. 2003
<<http://www.h-tec.com/education/eng>>
17. Genies, L., Bultel, Y., Faure, R., and Durand R. "Impedance study of oxygen reduction on platinum nanoparticles in alkaline media" Electrochimica Acta 48 (2003): 3879-3890
18. Gode, P., Jaouen F., Lindberg, G., Lundblad, A. and Sundholm G. "Influence of the composition on the structure and electrochemical characteristics of the PEC cathode" Electrochimica Acta 48 (2003): 4175-4187
19. Gottesfeld, S., Zawodzinski, T.A. "Polymer Electrolyte Fuel Cells" Advances in Electrochemical Science and Engineering, Wiley-Vch. 5 (1996): 195-301
20. "Greenwinds" Pege. 20 Oct. 2003
<<http://www.pege.org/greenwinds/electrolyzer.htm>>
21. Guangehun, L., and Pickup, P. "Ionic Conductivity of PEMFC Electrodes" Journal of The Electrochemical Society, 150 (2003): C745-C752
22. Guo, Q., Cayetano, M., Tsou, Y., De Castro, E., and White R. "Study of Ionic Conductivity Profiles of the Air Cathode of a PEMFC by AC Impedance Spectroscopy" Journal of The Electrochemical Society 150 (2003): A1440-A1449
23. "How does a Fuel Cell work?" FuelCellStore. 2003. 3 Mar 2004
<http://www.fuelcellstore.com/information/how_fuelcells_work.htm>
24. "Identifying a Warburg Impedance." Electrochemistry Resources. 18 Aug 2003
<<http://www.consultrsr.com/resources/eis/warburg1.htm>>

25. Jaouen, F., Lindbergh, G. and K. Wiezell. "Transient Techniques for Investigating Mass Transport Limitations in Gas Diffusion Electrodes" Journal of The Electrochemical Society 150 (2003): A1711-A1717
26. Kordesch, Simader. "Fuel for the Fuel Cell Technology" Fuel Cells and Their Applications Vch. (1996): 297
27. Lefebvre, M.C., Martin, R.B., and Peter G. Pickup. "Characterization of Ionic Conductivity Profiles within Proton Exchange Fuel Cell Gas Diffusion Electrodes by Impedance Spectroscopy" Electrochemical and Solid-State Letters 2 (1999): 259-261
28. MacDonald J. R. "Fundamentals of Impedance Spectroscopy" Impedance Spectroscopy (1987): 1-20
29. MacDonald J. R. "Impedance Spectroscopy: Old Problems and New Developments", Electrochimica Acta 35 (1990): 1483-1492
30. Murgia, G., Pisani, L., Valentini, M. and D'Aguanno B. "Electrochemistry and Mass Transport in Polymer Electrolyte Membrane Fuel Cells I. Model" Journal of The Electrochemical Society 149 (1) (2002): A31-A38
31. Paganin, V. A., C. L. F. Oliviera, E.A. Ticianelli, T. E. Springer, and E.R. Gonzalez "Modelistic interpretation of the impedance response of a polymer electrolyte fuel cell", Electrochimica Acta 43 (1998): 3761-3766.
32. "PARSTAT 2263." Princeton Applied Research. 10 Oct. 2002
<http://www.princetonappliedresearch.com/pdf/parstat_ds.pdf>
33. Parthasarathy, D., Srinivasan, A., and Martin, J. "The Platinum Microelectrode/Nafion Interface: An Electrochemical Impedance Spectroscopic Analysis of Oxygen Reduction Kinetics and Nafion Characteristics" Journal of The Electrochemical Society 139 (1992): 134-140
34. Plambeck, J. "Electrical Concepts and Units" Electroanalytical Chemistry, John Wiley & Sons (1982): 11-16
35. "Polymer Electrolyte Fuel Cell" Fuel Cell Handbook, EG&G Services, Parson Inc (2000): 3-1 – 3-14
36. Song, J.M., Cha, S.Y. and Lee W.M. "Optimal Composition of Polymer electrolyte fuel cell electrodes determined by the AC impedance method", Journal of Power Sources 94 (2001): 78-84.

37. "The Electrical Double Layer." Bath University. 9 Dec.2003
<<http://www/bath.ac.uk>>
38. Vetter, K. "Total Overvoltage – AC Polarization Impedance" Electrochemical Kinetics, Academic Press (1967): 345-348
39. Wagner, N. "Characterization of membrane electrode assemblies in polymer electrolyte fuel cells using a.c. impedance spectroscopy" Journal of Applied Electrochemistry 32 (2002): 859-863
40. Walsh, F. "Simple Electron (Charge) Transfer" A First Course in Electrochemical Engineering, The Electrochemical Consultancy, (1993): 86-112
41. Zhang, S., Ding, M.S., Xu, K., Allen, J., and T. Richard Jow. "Understanding Solid Electrolyte Interface film Formation on Graphite Electrodes" Electrochemical and Solid-State Letters 4 (2001): A206-A208

APPENDIX

APPENDIX A. PEMFC RESULTS FOR ELECTROLYSIS COMPARATION

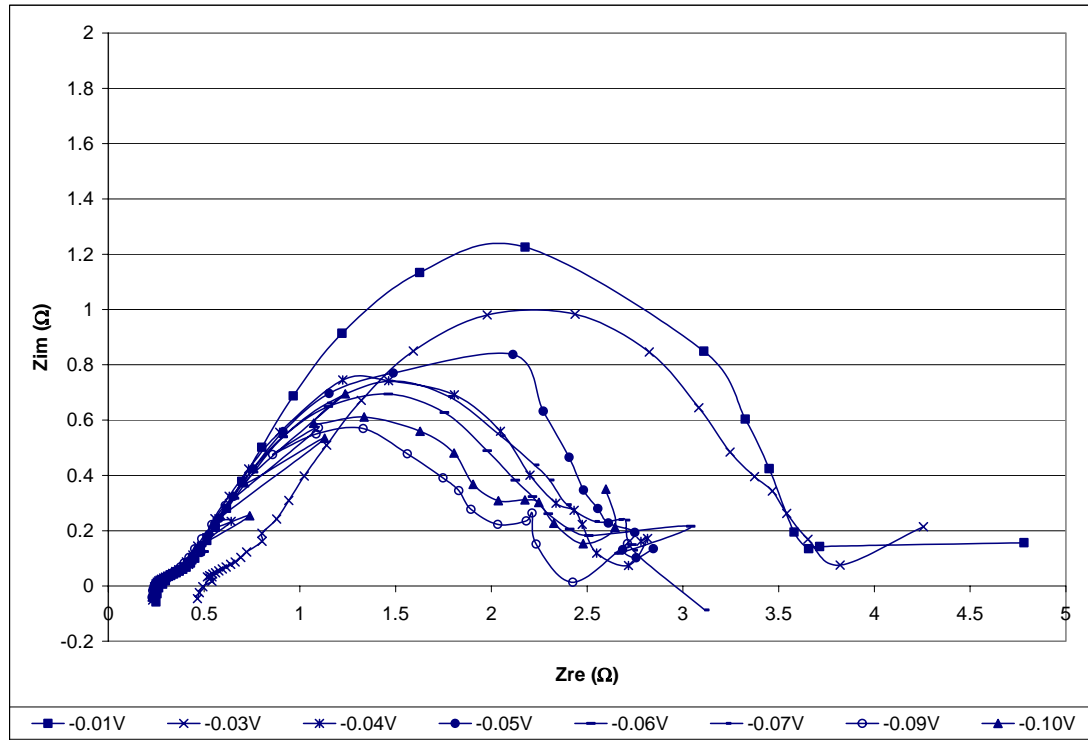


Figure A.1. PEMFC Nyquist Plots at different overpotentials

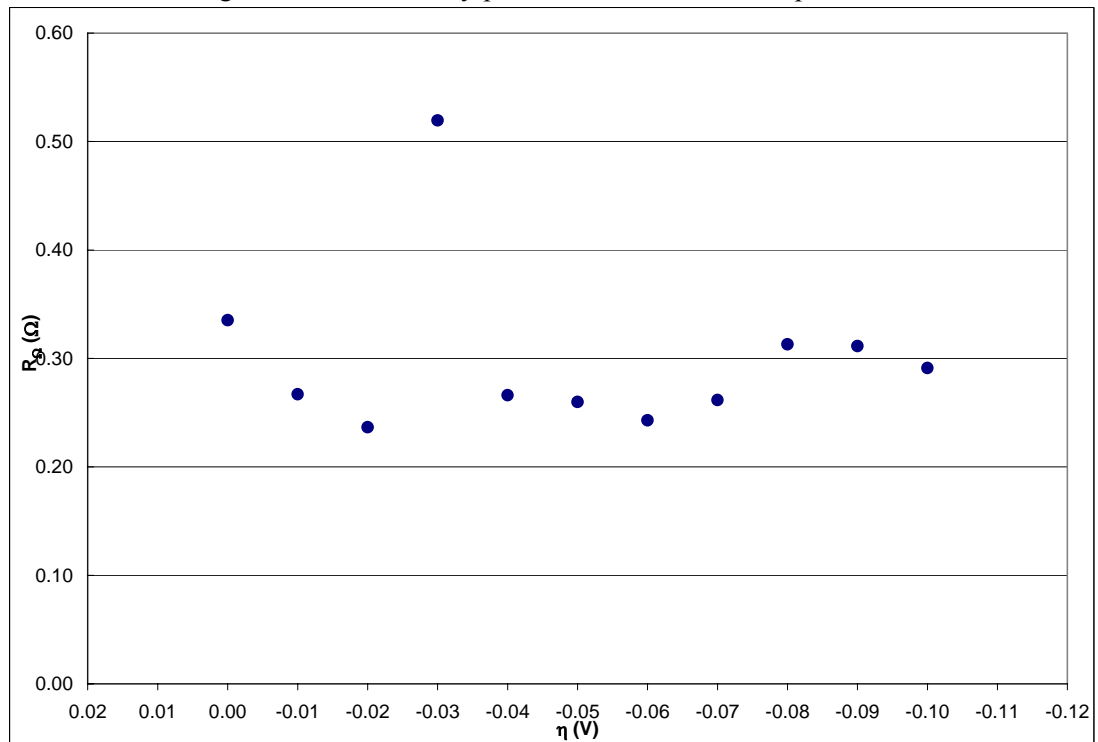


Figure A.2. PEMFC Ohmic Resistance from Bode Plot at different overpotentials

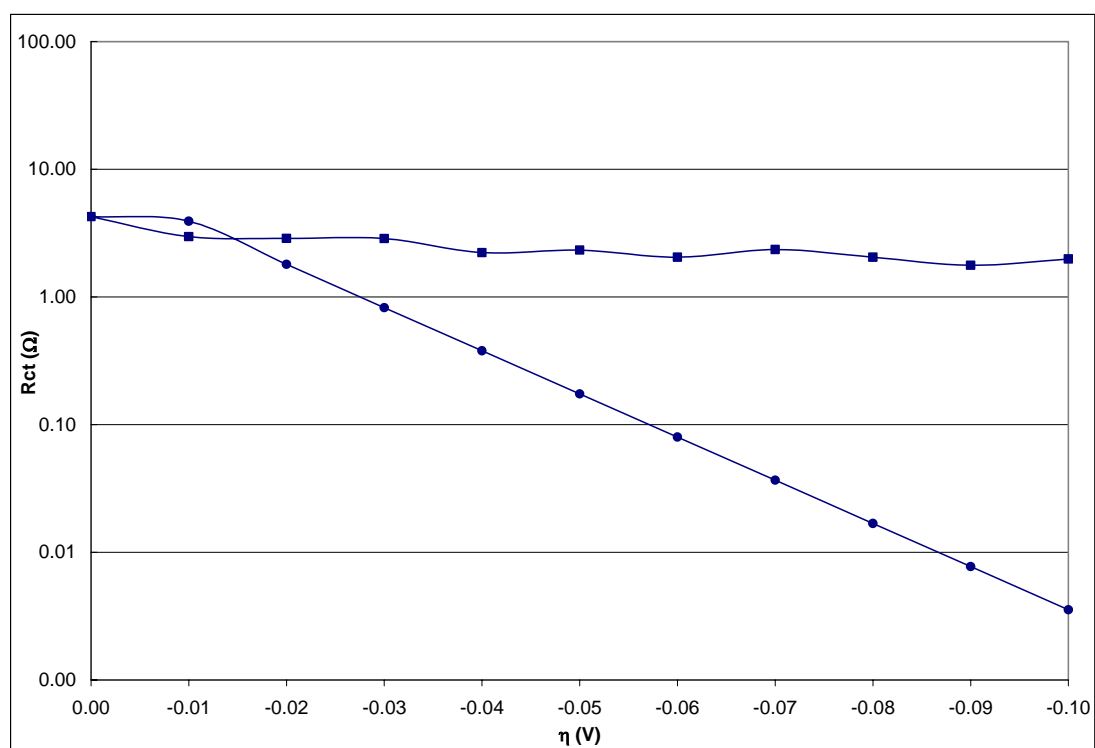


Figure A.3. Charge Transfer Resistance versus potential for PEMFC from Bode Plot; (■) from experimental data; (●) calculated using the i - η Tafel behavior equation

APPENDIX B. PEM ELECTROLYZER

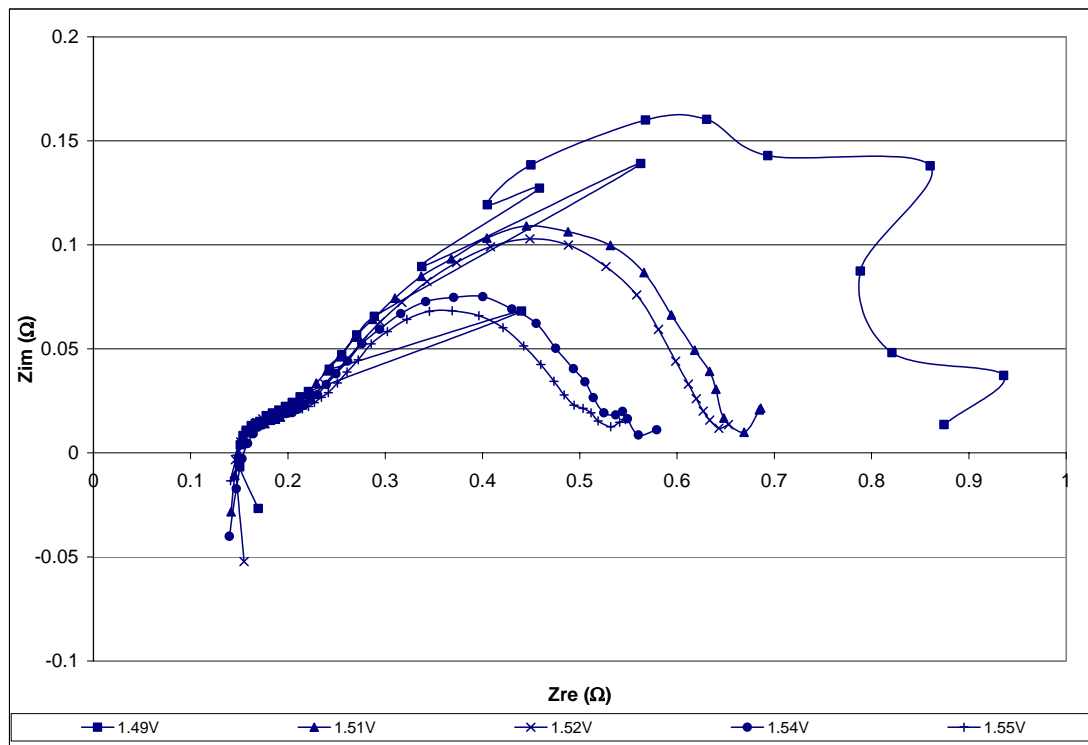


Figure B.1. PEM Electrolyzer Nyquist Plots at different overpotentials

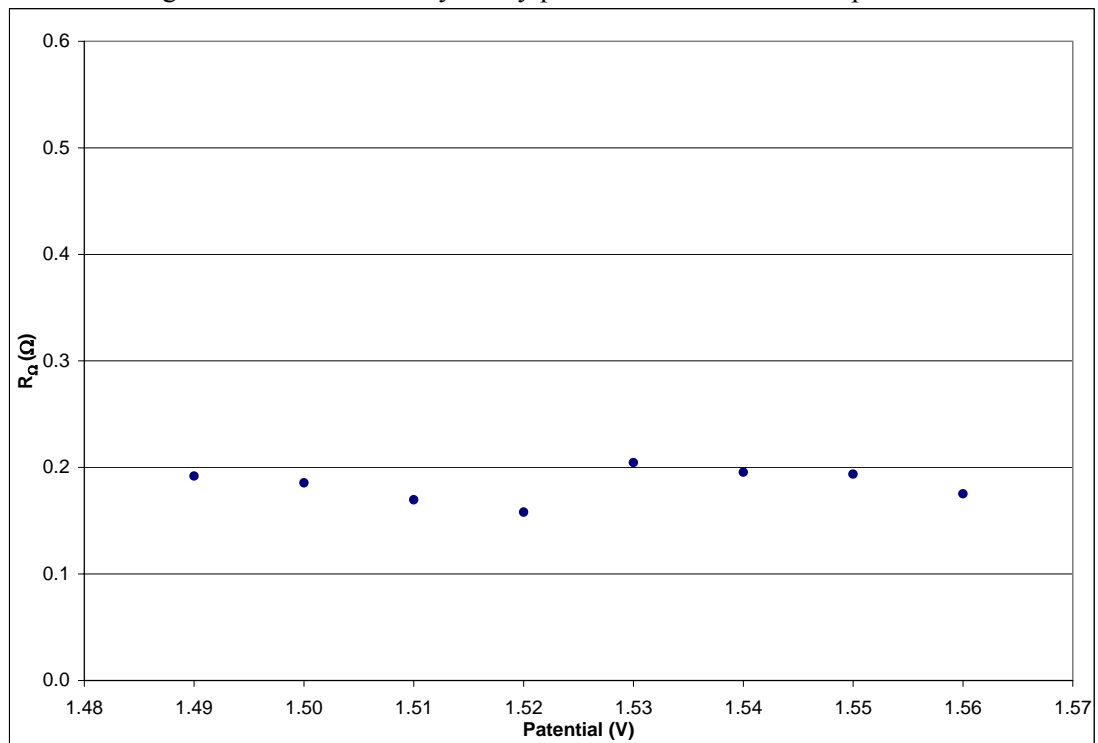


Figure B.2. PEM Electrolyzer Ohmic Resistance from Bode Plot at different overpotentials

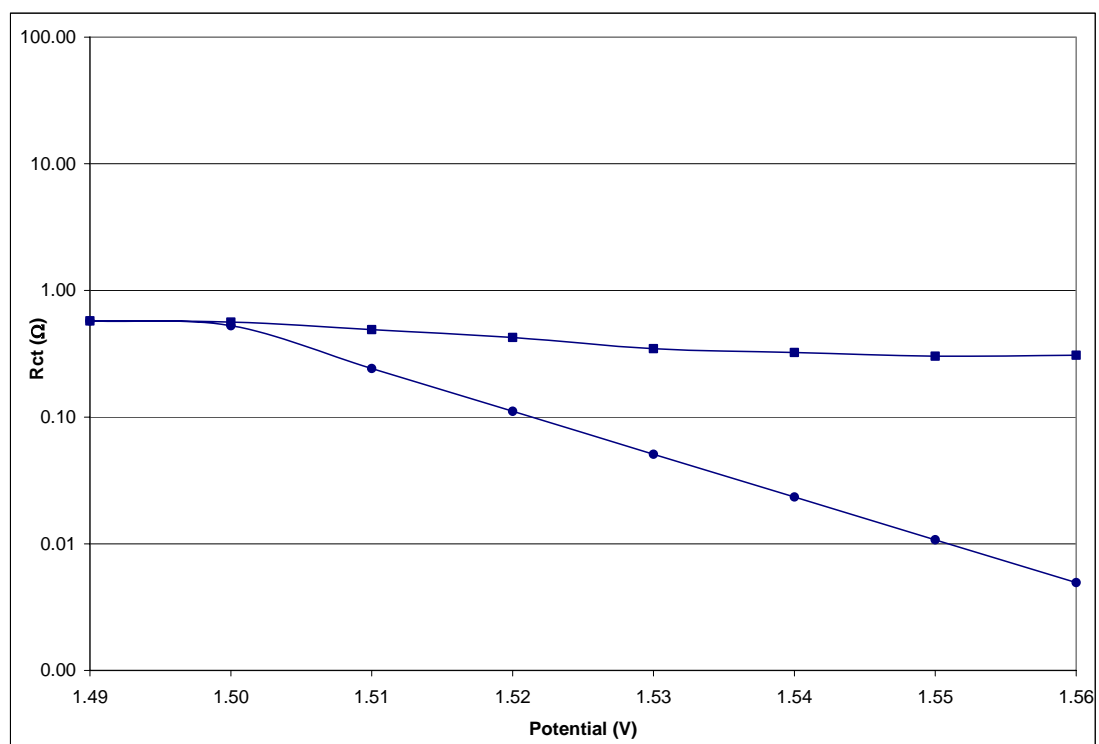


Figure B.3. Charge Transfer Resistance versus potential for PEM Electrolyzer from Bode Plot; (■) from experimental data; (●) calculated using $i-\eta$ equations

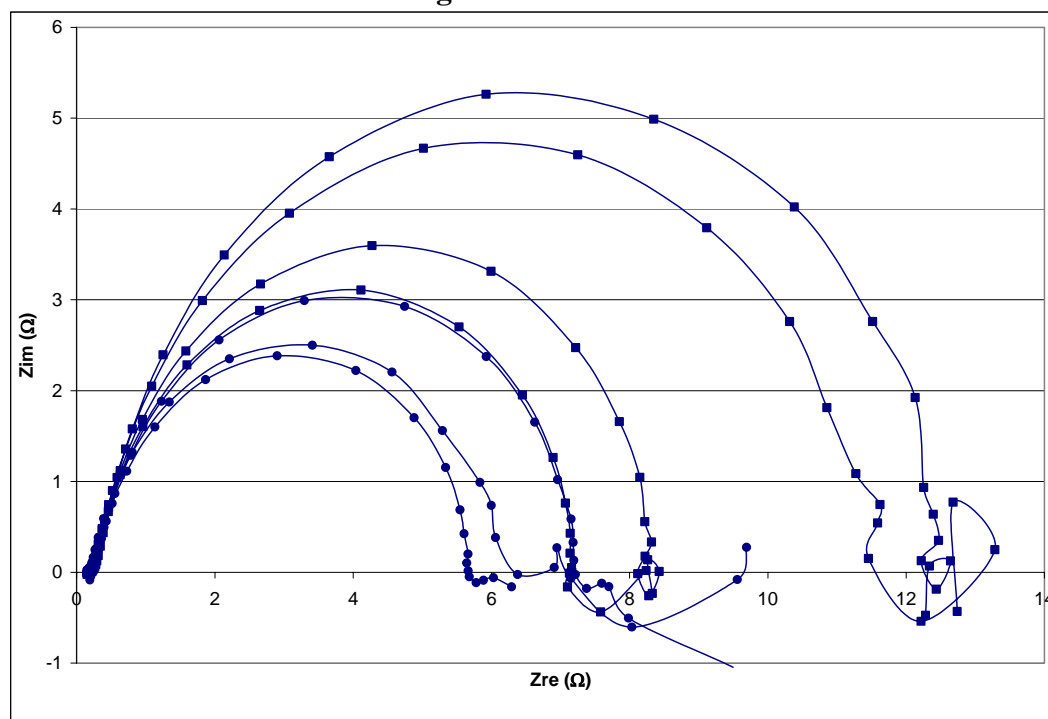
APPENDIX C. PEMFC with $0.1\text{mgPt}/\text{cm}^2$ 

Figure C.1. Nyquist Plots for PEMFC of $0.1\text{mgPt}/\text{cm}^2$ with dry pretreatment at OCP; (■) for after run; (●) for 1st run.

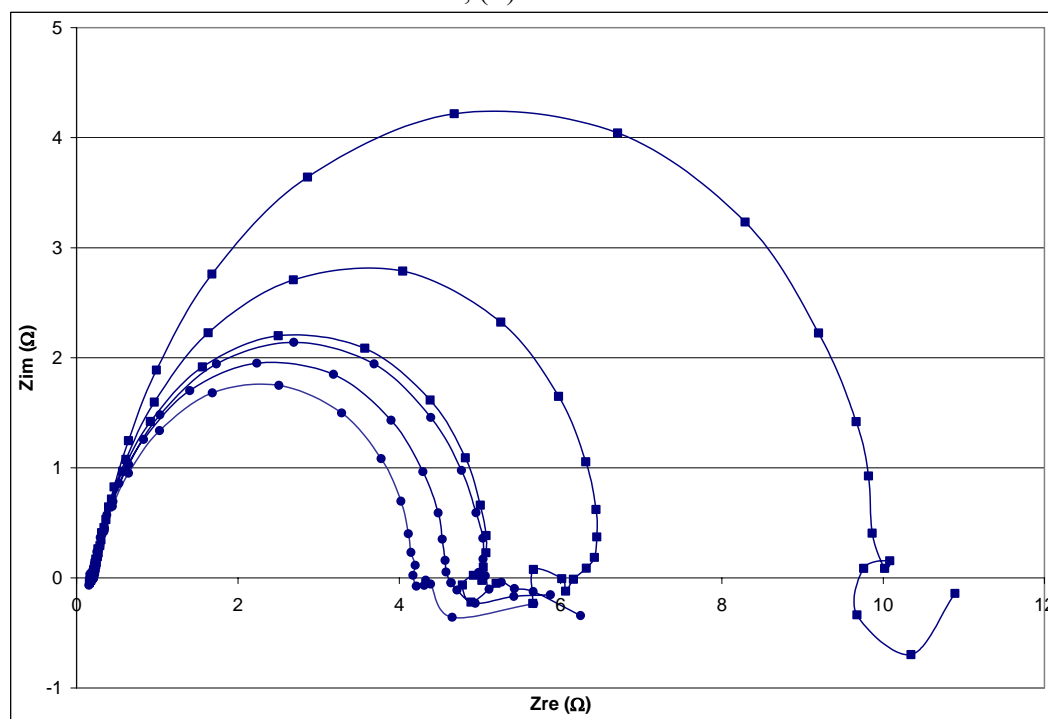


Figure C.2. Nyquist Plots for PEMFC of $0.1\text{mgPt}/\text{cm}^2$ with wet pretreatment at OCP; (■) for after run; (●) for 1st run.

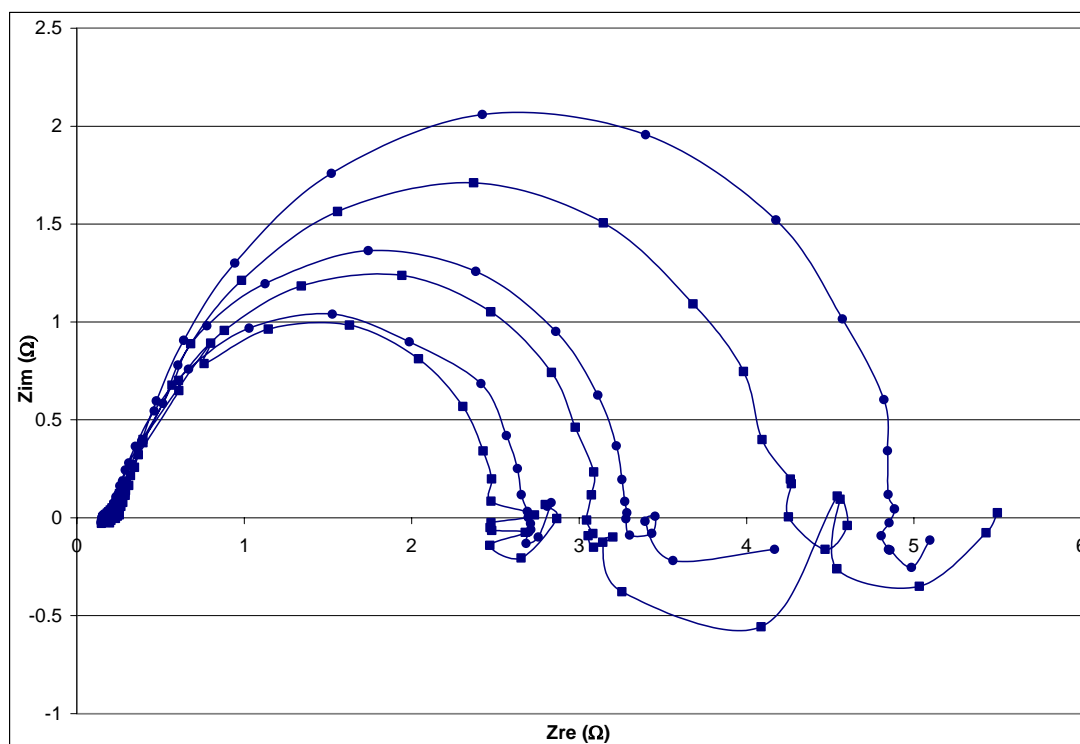


Figure C.3. Nyquist Plots for PEMFC of $0.1\text{mgPt}/\text{cm}^2$ with dry pretreatment at $\eta = -0.05\text{V}$; (■) for after run; (●) for 1st run.

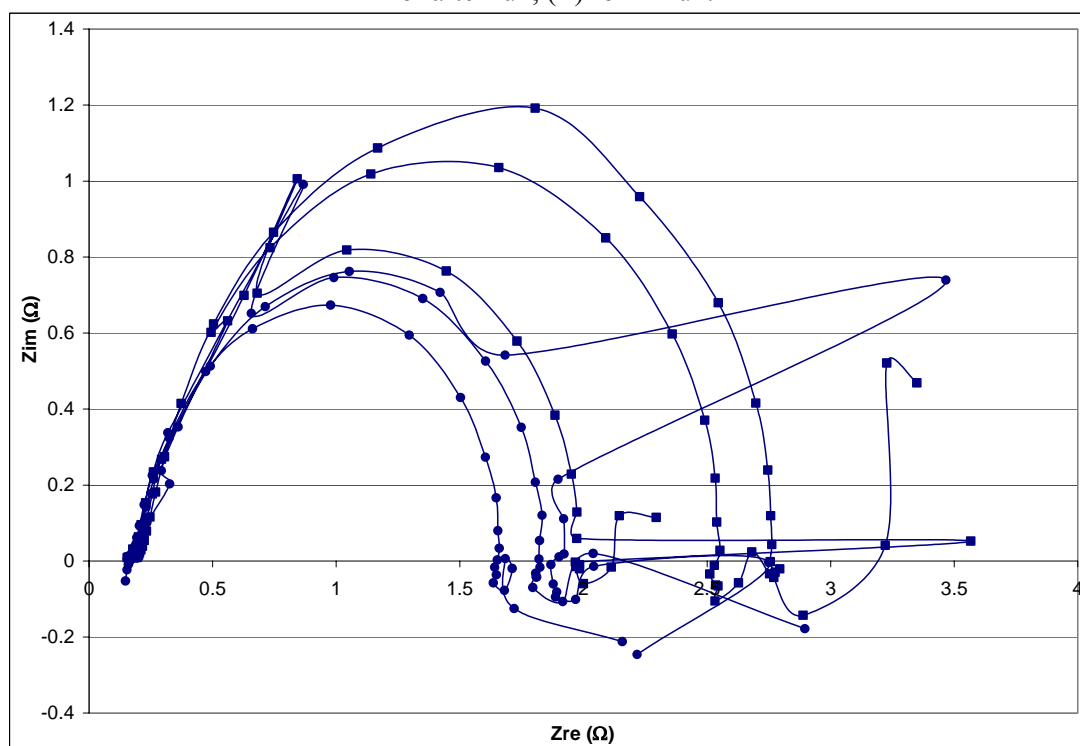


Figure C.4. Nyquist Plots for PEMFC of $0.1\text{mgPt}/\text{cm}^2$ with wet pretreatment at $\eta = -0.05\text{V}$; (■) for after run; (●) for 1st run.

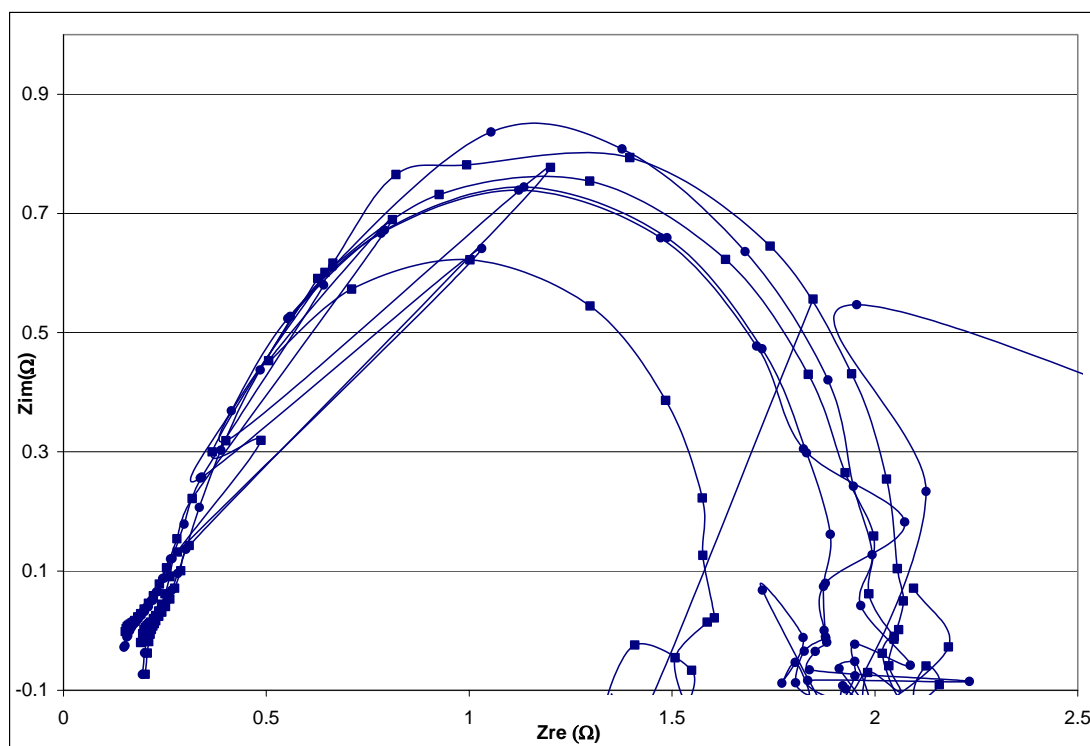


Figure C.5. Nyquist Plots for PEMFC of 0.1mgPt/cm² with dry pretreatment at $\eta = -0.10\text{V}$; (■) for after run; (●) for 1st run.

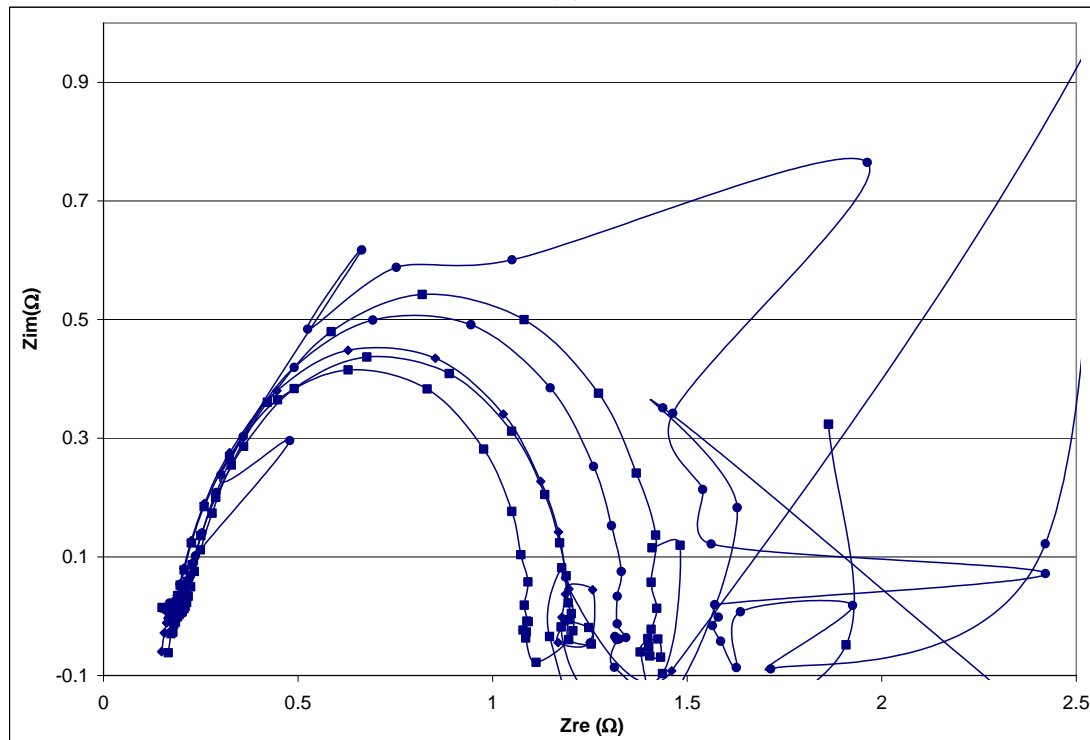


Figure C.6. Nyquist Plots for PEMFC 0.1mgPt/cm² with wet pretreatment at $\eta = -0.10\text{V}$; (■) for after run; (●) for 1st run.

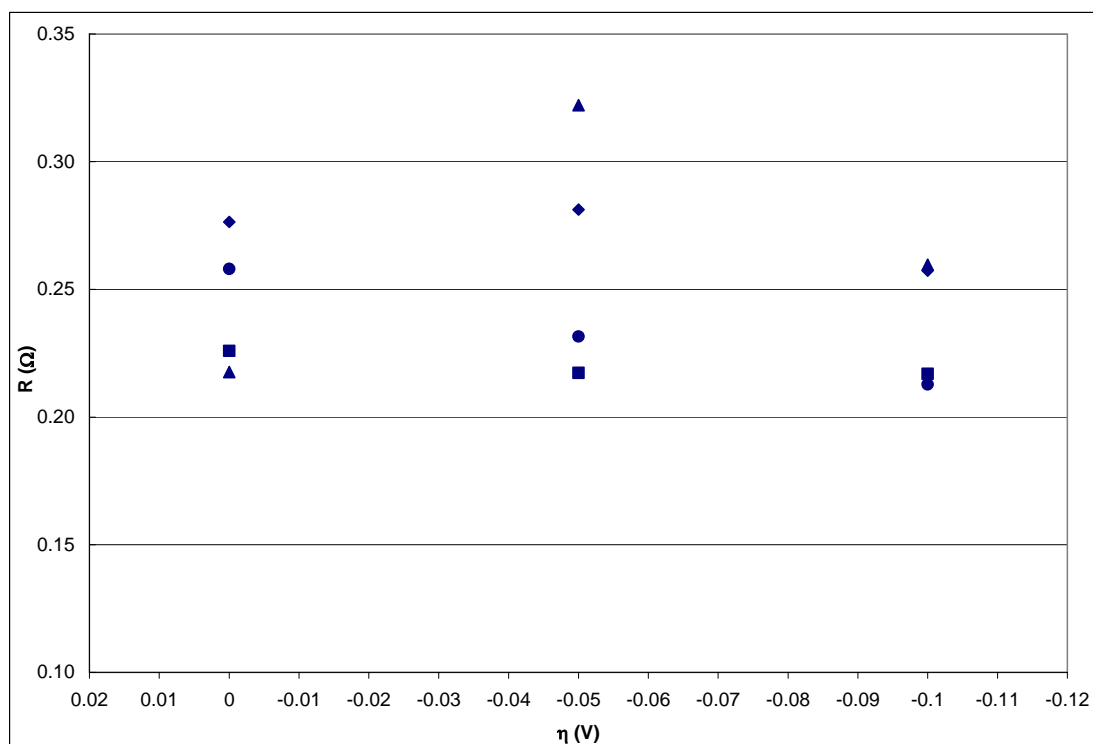


Figure C.7. Ohmic resistance for PEMFC with $0.1\text{mgPt}/\text{cm}^2$ for all initial conditions from Bode Plot; (■) wet 1st run; (●) wet after run; (▲) dry 1st run; (◆) dry after run.

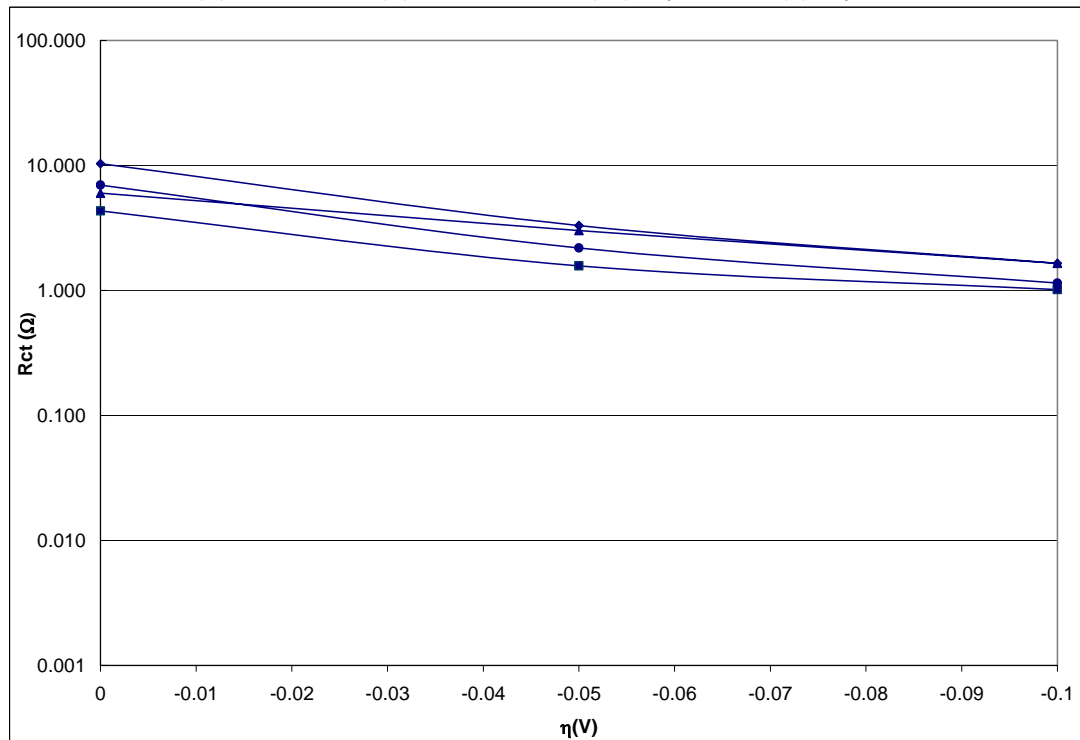


Figure C.8. Experimental Charge Transfer Resistance from Bode Plot for PEMFC of $0.1\text{mgPt}/\text{cm}^2$; (■) wet 1st run; (●) wet after run; (▲) dry 1st run; (◆) dry after run.

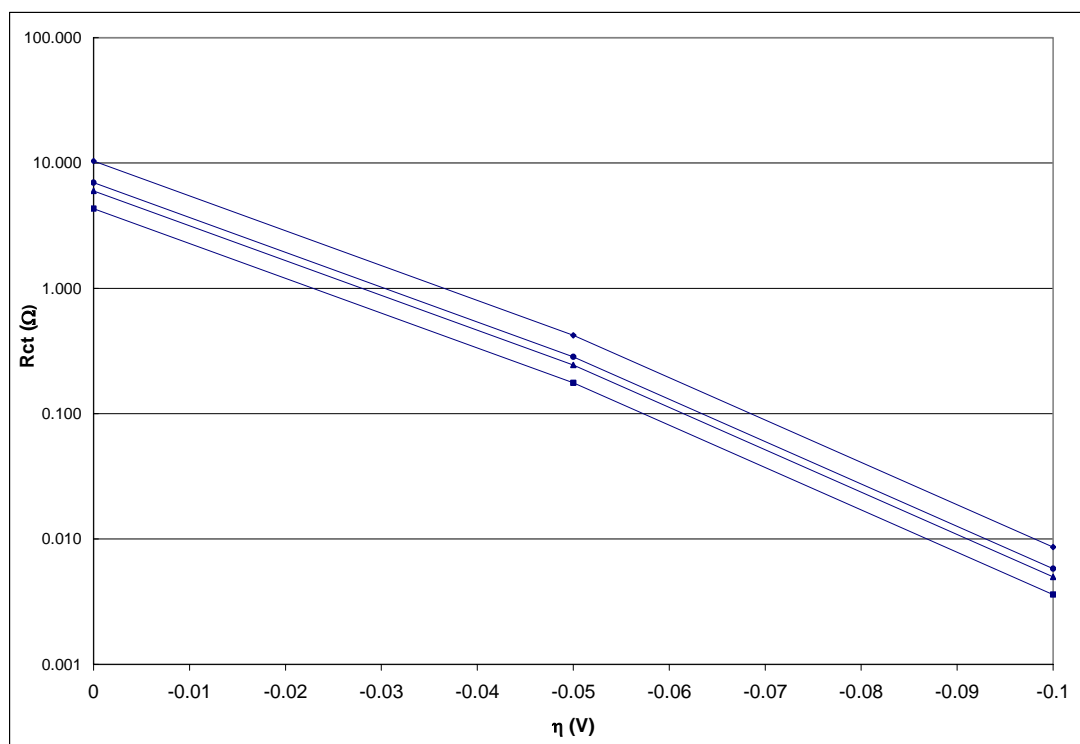


Figure C.9. Charge Transfer Resistance calculated using Tafel equation for PEMFC of $0.1 \text{ mgPt}/\text{cm}^2$ from Bode Plot; (■) wet 1st run; (●) wet after run; (▲) dry 1st run; (◆) dry after run.

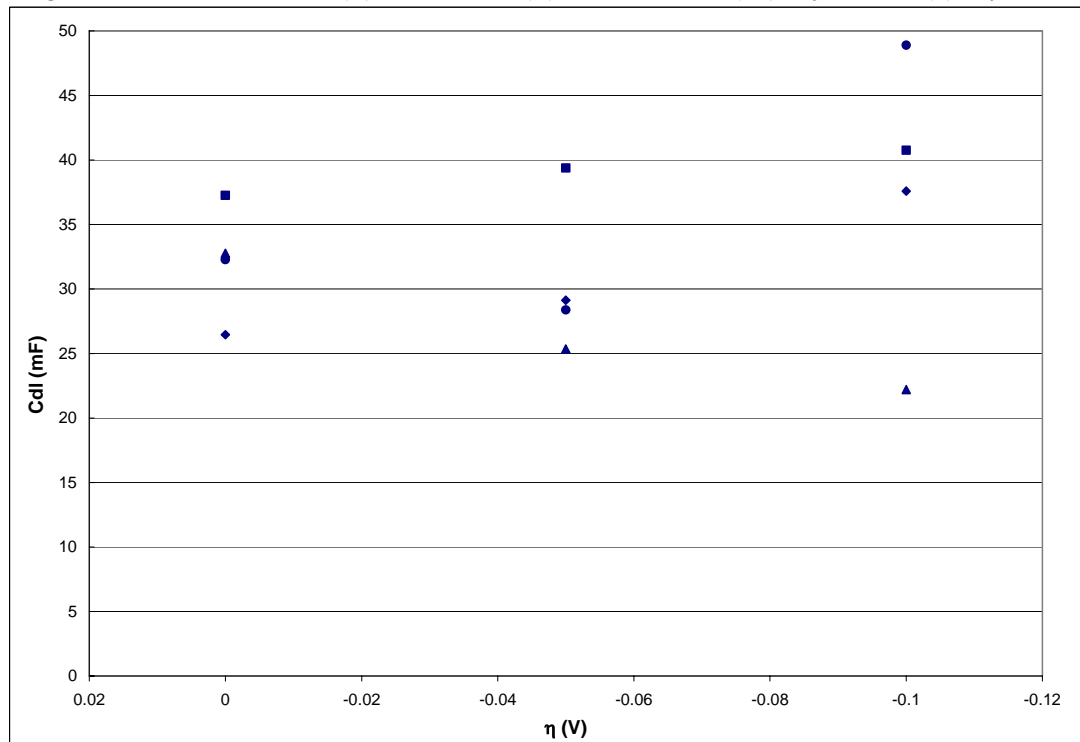


Figure C.10. Double Layer Capacitance versus overpotential for PEMFC of $0.1 \text{ mgPt}/\text{cm}^2$ from Bode Plot; (■) wet 1st run; (●) wet after run; (▲) dry 1st run; (◆) dry after run.

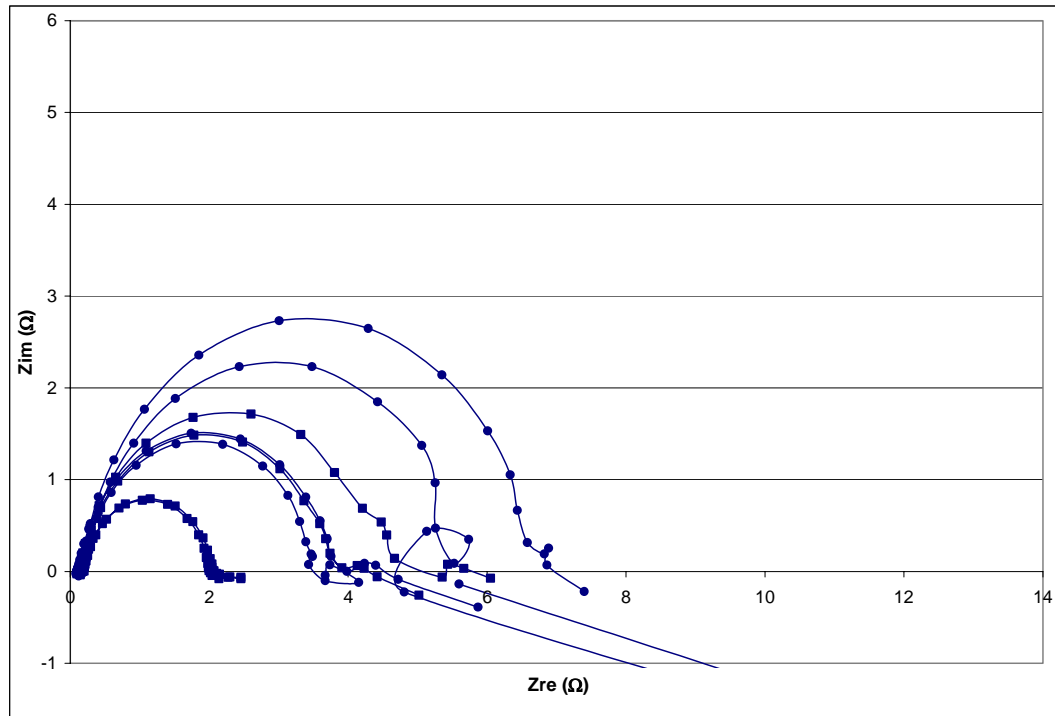
APPENDIX D. PEMFC with $0.3\text{mgPt}/\text{cm}^2$ 

Figure D.1. Nyquist Plots for PEMFC of $0.3\text{mgPt}/\text{cm}^2$ with dry pretreatment at OPC; (■) for after run; (●) for 1st run.

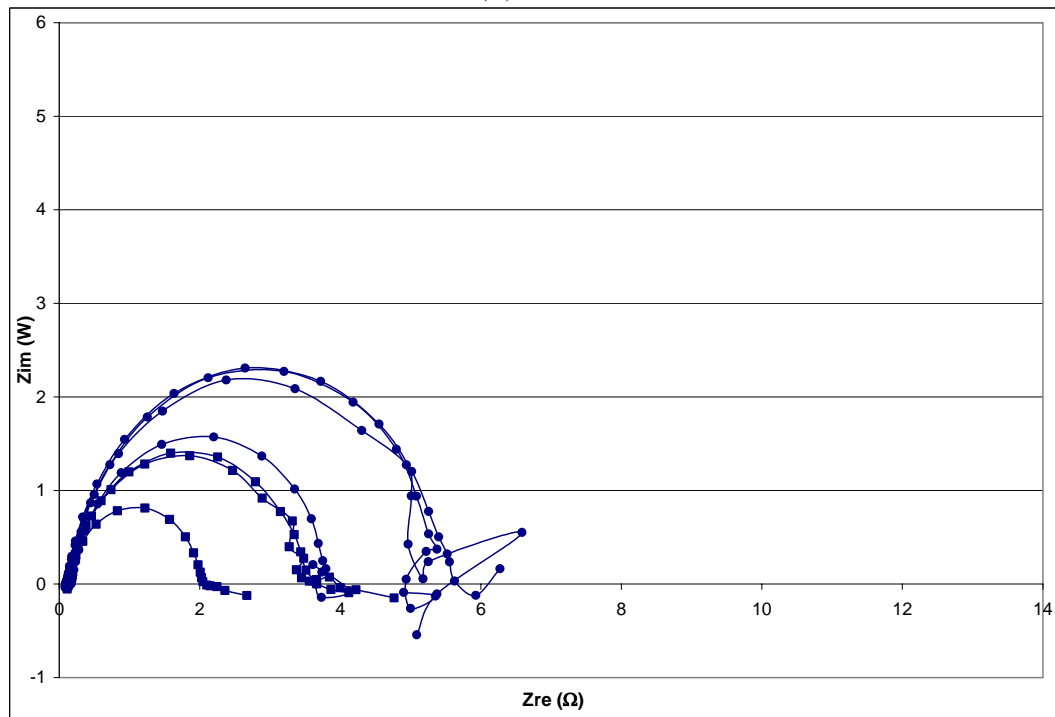


Figure D.2. Nyquist Plots for PEMFC of $0.3\text{mgPt}/\text{cm}^2$ with wet pretreatment at OPC; (■) for after run; (●) for 1st run.

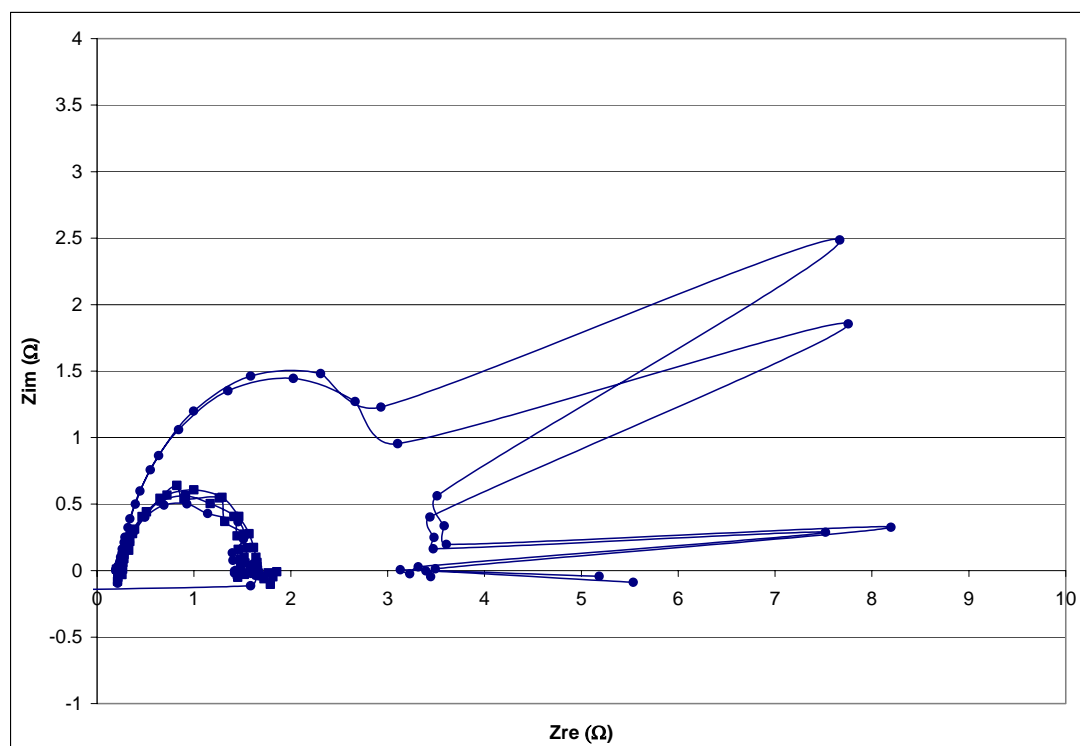


Figure D.3. Nyquist Plots for PEMFC of $0.3\text{mgPt}/\text{cm}^2$ with dry pretreatment at $\eta = -0.02\text{V}$; (■) for after run; (●) for 1st run.

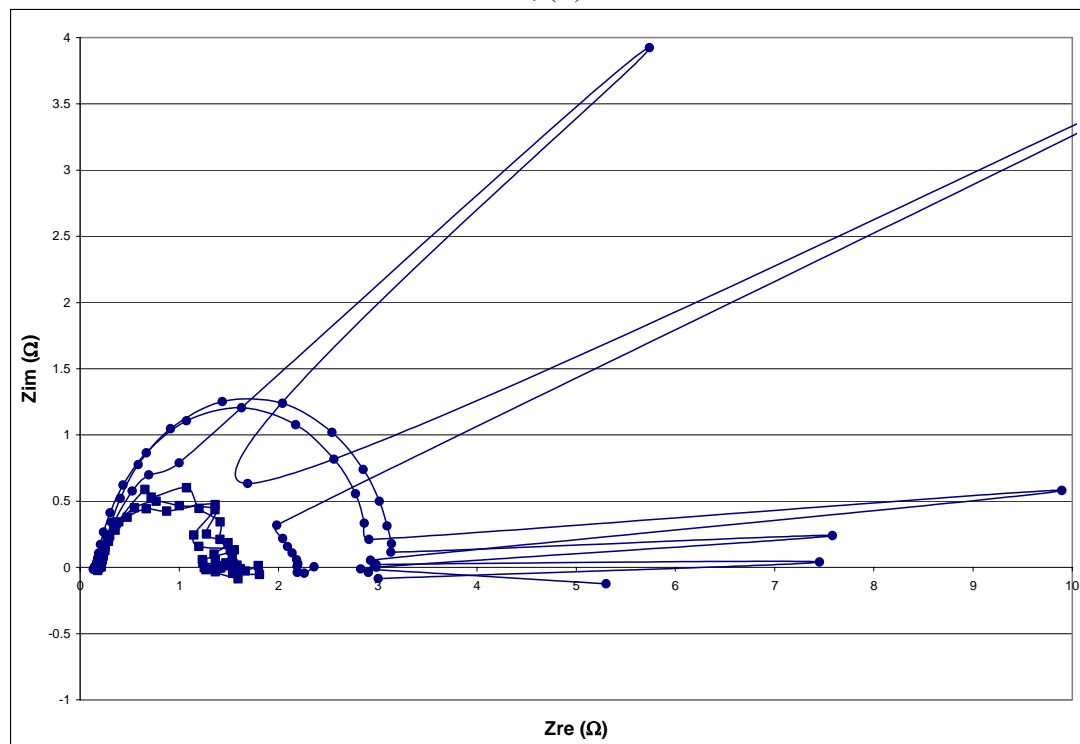


Figure D.4. Nyquist Plots for PEMFC of $0.3\text{mgPt}/\text{cm}^2$ with wet pretreatment at $\eta = -0.02\text{V}$; (■) for after run; (●) for 1st run.

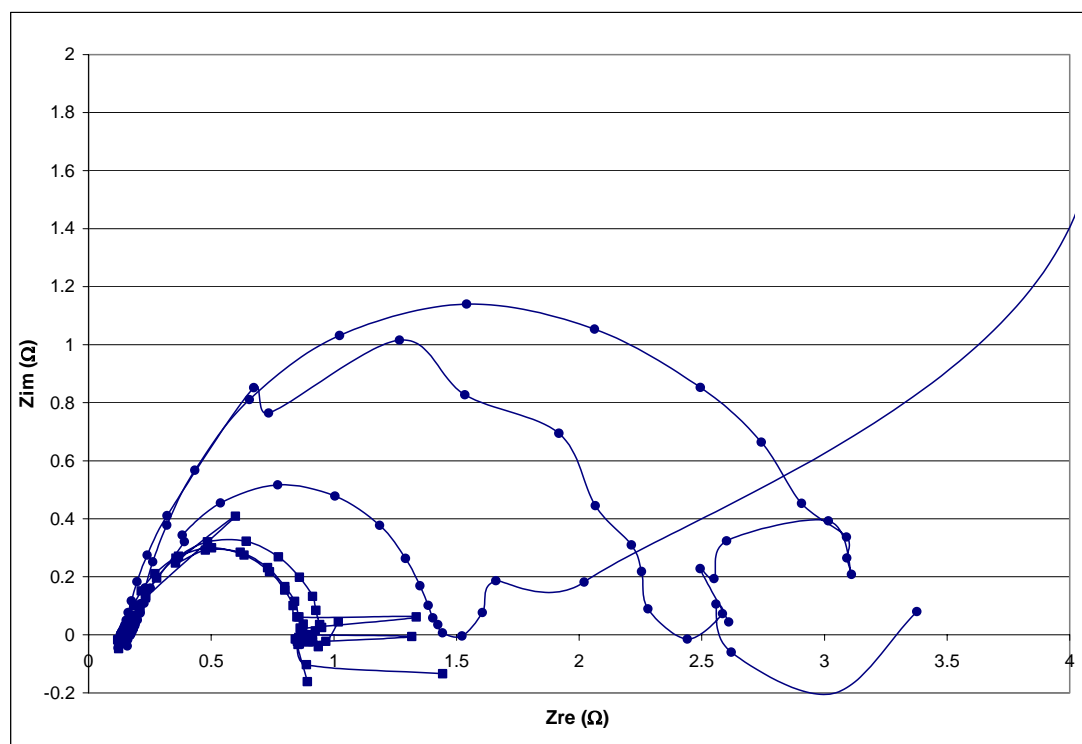


Figure D.5. Nyquist Plots for PEMFC of $0.3\text{mgPt}/\text{cm}^2$ with dry pretreatment at $\eta = -0.05\text{V}$; (■) for after run; (●) for 1st run.

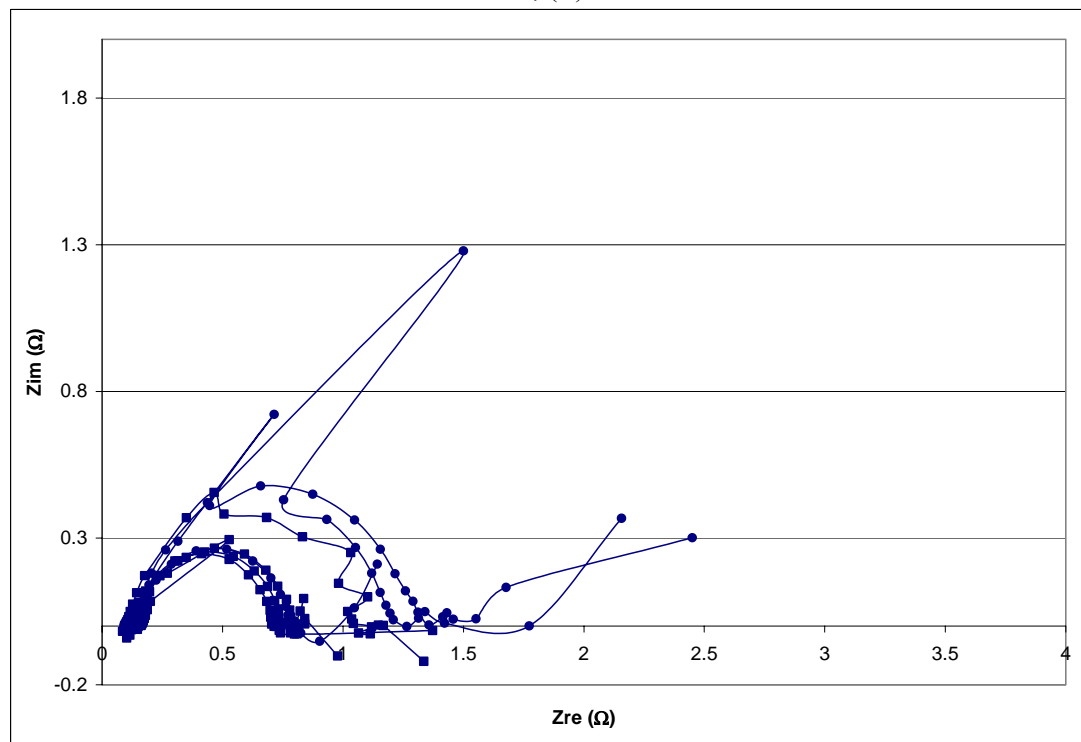


Figure D.6. Nyquist Plots for PEMFC of $0.3\text{mgPt}/\text{cm}^2$ with wet pretreatment at $\eta = -0.05\text{V}$; (■) for after run; (●) for 1st run.

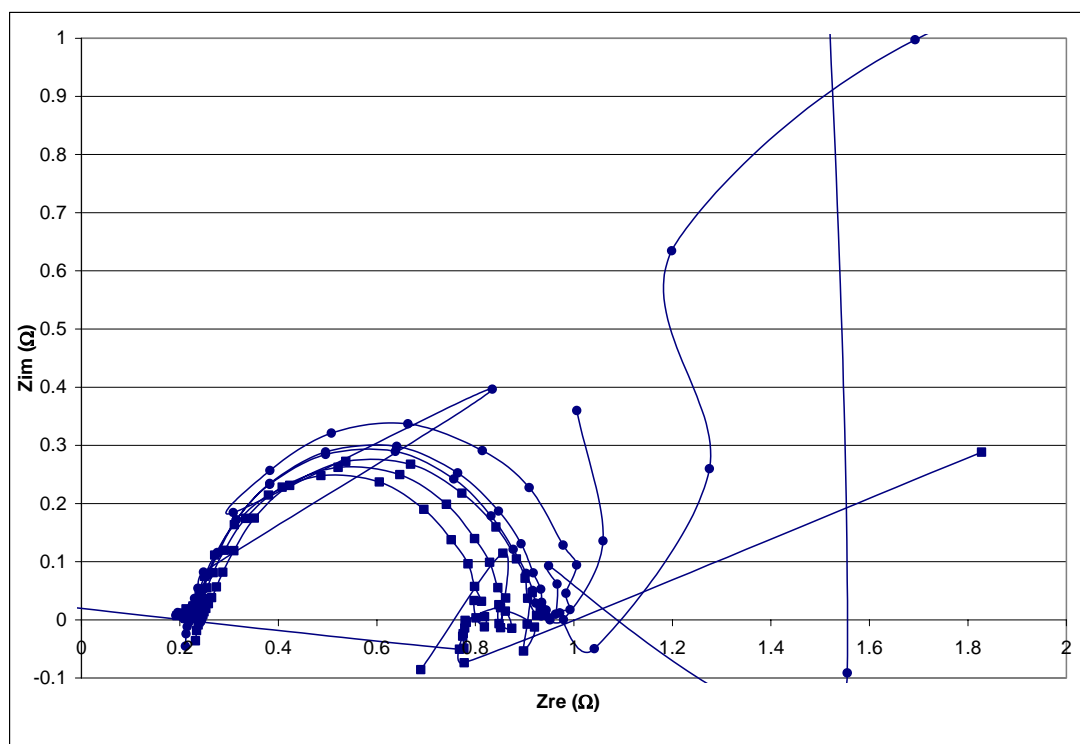


Figure D.7. Nyquist Plots for PEMFC of $0.3\text{mgPt}/\text{cm}^2$ with dry pretreatment at $\eta = -0.08\text{V}$; (■) for after run; (●) for 1st run.

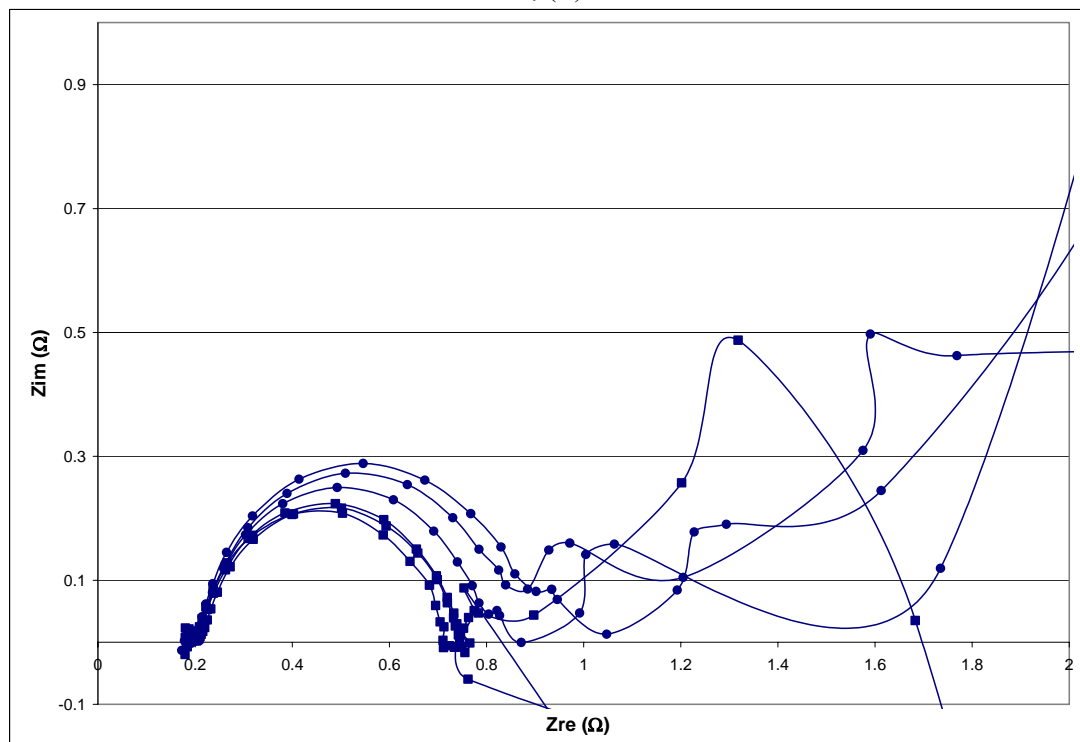


Figure D.8. Nyquist Plots for PEMFC $0.3\text{mgPt}/\text{cm}^2$ with wet pretreatment at $\eta = -0.08\text{V}$; (■) for after run; (●) for 1st run.

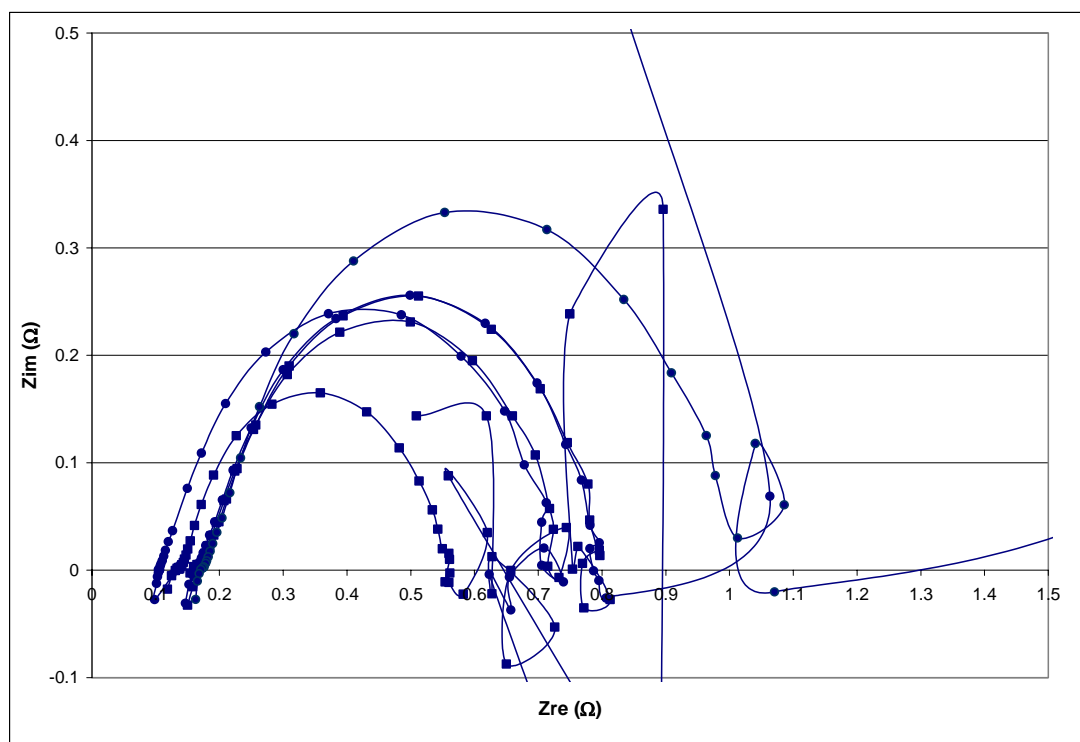


Figure D.9. Nyquist Plots for PEMFC of $0.3\text{mgPt}/\text{cm}^2$ with dry pretreatment at $\eta = -0.10\text{V}$; (■) for after run; (●) for 1st run.

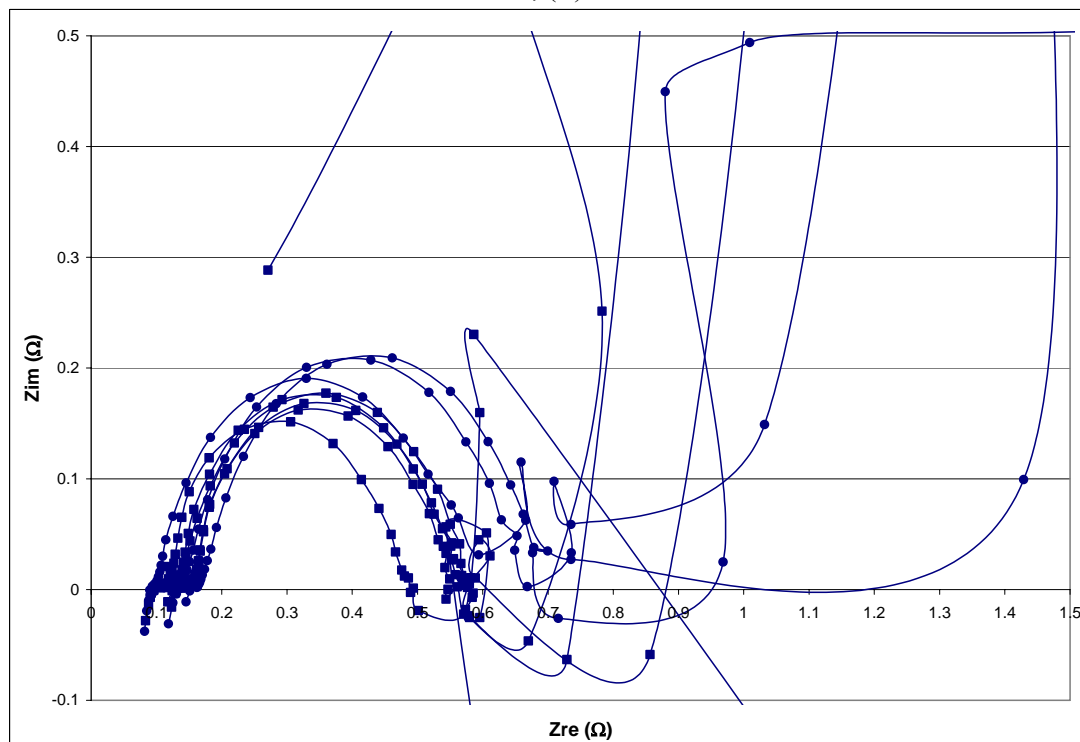


Figure D.10. Nyquist Plot for PEMFC $0.3\text{mgPt}/\text{cm}^2$ with wet pretreatment at $\eta = -0.10\text{V}$; (■) for after run; (●) for 1st run.

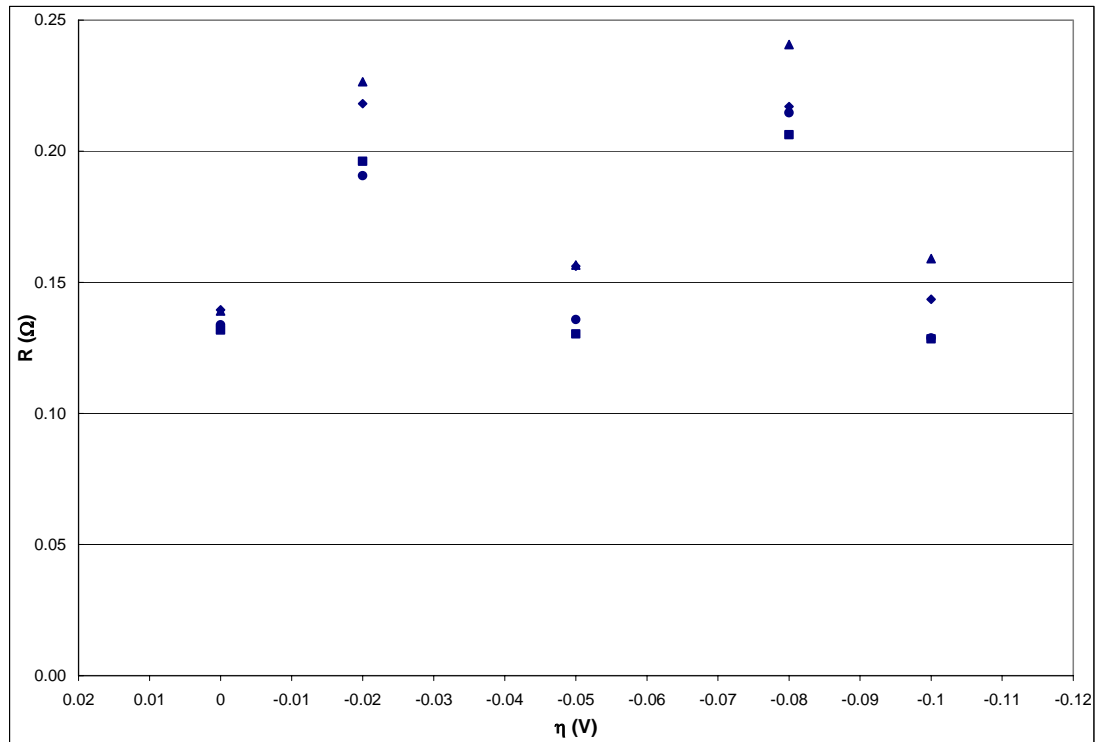


Figure D.11. Ohmic resistance for PEMFC with $0.3\text{mgPt}/\text{cm}^2$ for all initial conditions from Bode Plot; (■) wet 1st run; (●) wet after run; (▲) dry 1st run; (◆) dry after run.

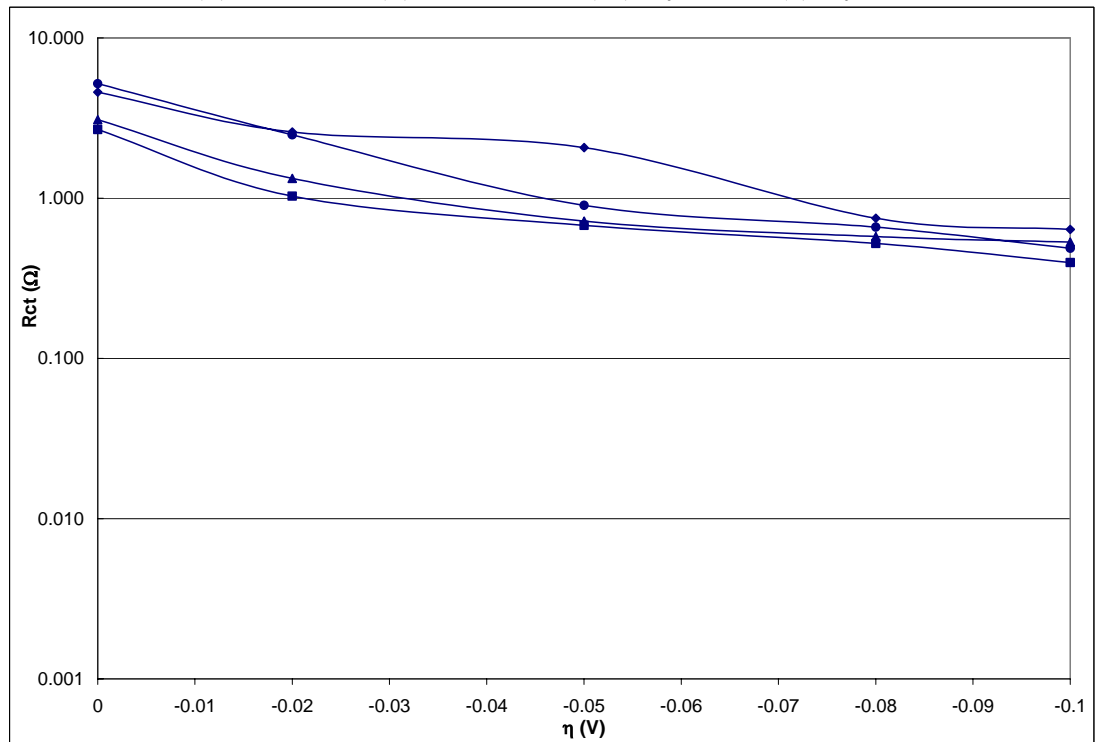


Figure D.12. Experimental Charge Transfer Resistance from Bode Plot for PEMFC of $0.1\text{mgPt}/\text{cm}^2$; (■) wet 1st run; (●) wet after run; (▲) dry 1st run; (◆) dry after run.

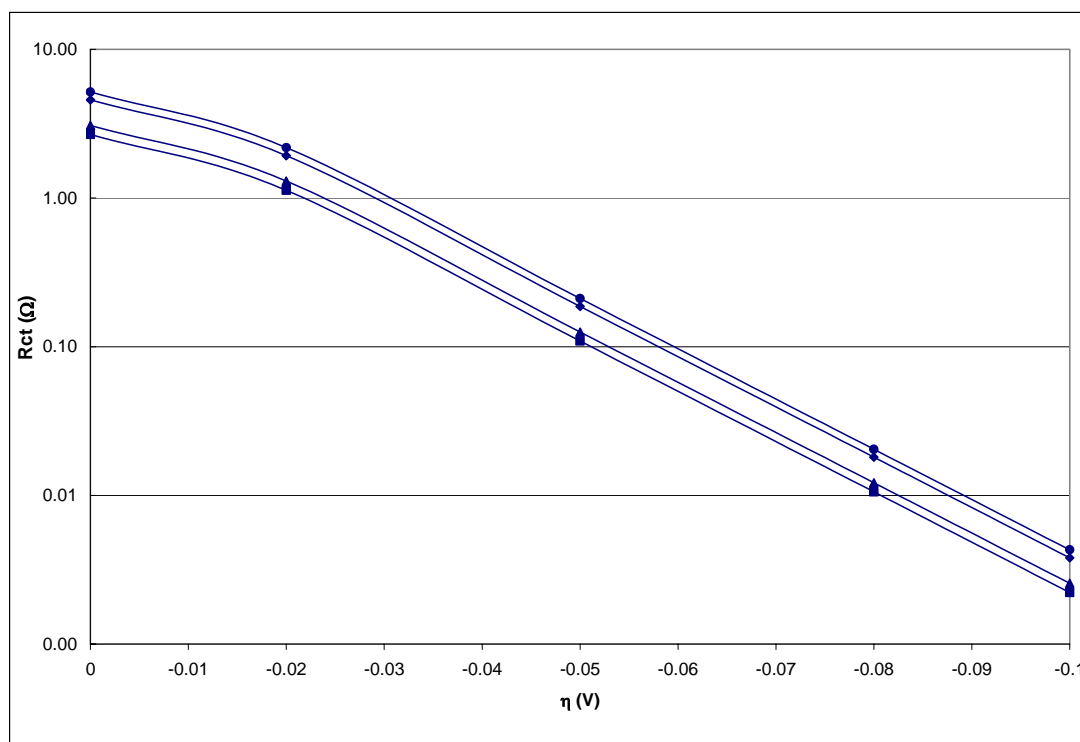


Figure D.13. Charge Transfer Resistance calculated using i - η equations for PEMFC of $0.1\text{mgPt}/\text{cm}^2$ from Bode Plot; (\blacksquare) wet 1st run; (\bullet) wet after run; (\blacktriangle) dry 1st run; (\blacklozenge) dry after run

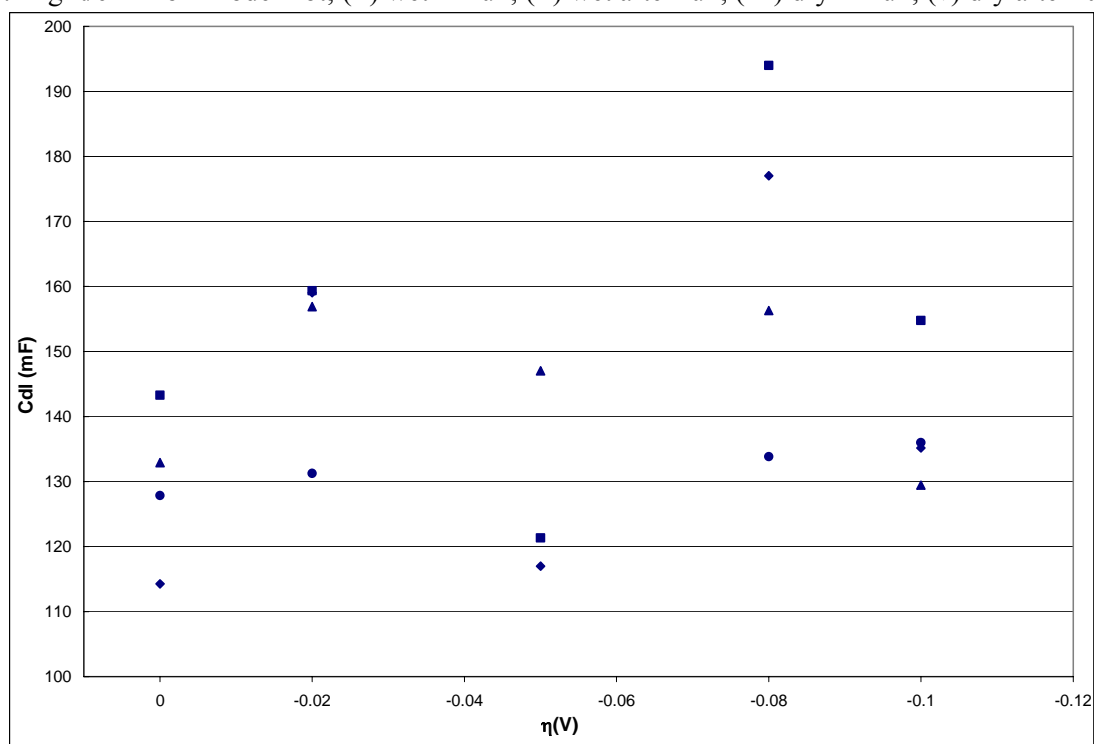


Figure D.14. Double Layer Capacitance versus overpotential for PEMFC of $0.3\text{mgPt}/\text{cm}^2$ from Bode Plot; (\blacksquare) wet 1st run; (\bullet) wet after run; (\blacktriangle) dry 1st run; (\blacklozenge) dry after run.

APPENDIX E. EXCHANGE CURRENT

Table E.1. Exchange current of PEMFC with 0.1mgPt/cm²

0.0V	Pretreatment	Nyquist Plot		Bode plot	
		Rct (ohm)	i0 (mA)	Rct (ohm)	i0 (mA)
Wet	1st run	4.4160	1.45436	4.3236	1.48547
	After run	6.9074	0.92980	6.9615	0.92257
Dry	1st run	6.1301	1.04770	5.9929	1.07169
	After run	10.4867	0.61244	10.3487	0.62061

Table E.2. Exchange current of PEMFC with 0.3mgPt/cm²

0.0V	Pretreatment	Nyquist Plot		Bode plot	
		Rct (ohm)	i0 (mA)	Rct (ohm)	i0 (mA)
Wet	1st run	2.9470	2.17931	2.6770	2.39917
	After run	5.3546	1.19943	5.1814	1.23952
Dry	1st run	3.3080	1.94153	3.0833	2.08302
	After run	4.7108	1.36336	4.5781	1.40287

APPENDIX F. LINEAR POLARIZATION PLOTS FOR PEMFC WITH 0.3mgPt/cm²

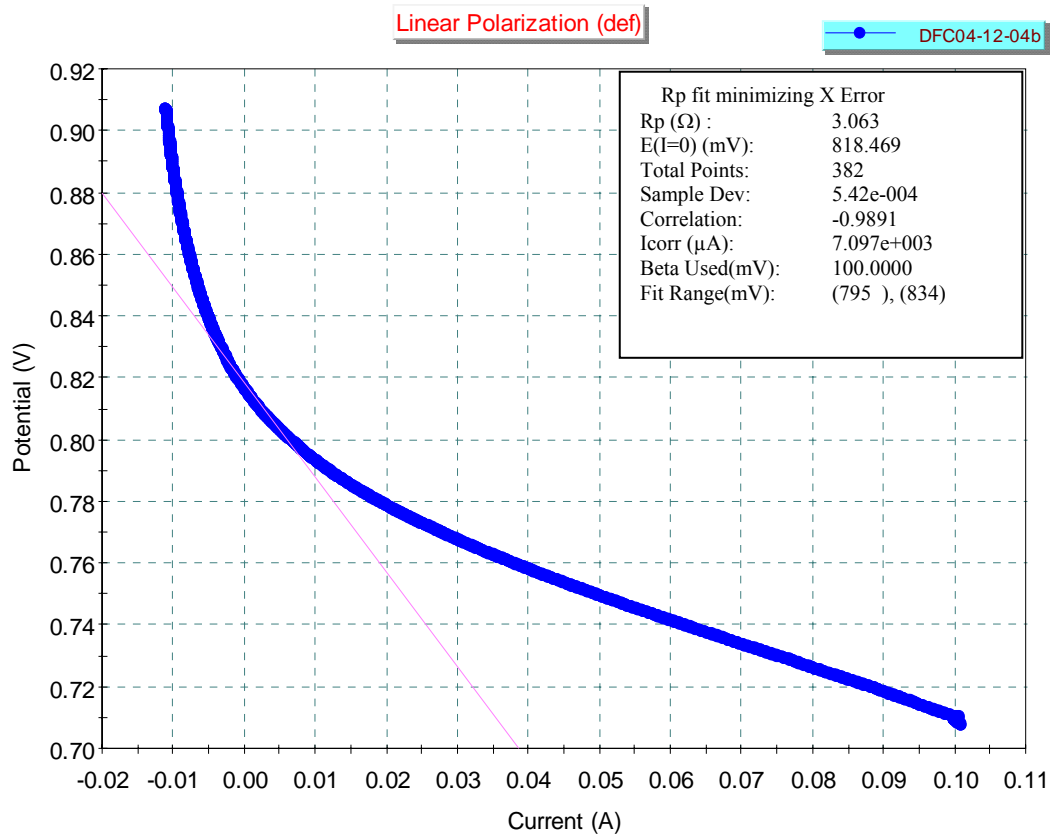


Figure F.1. *E-i* curve for PEMFC of 0.3mgPt/cm² at dry condition

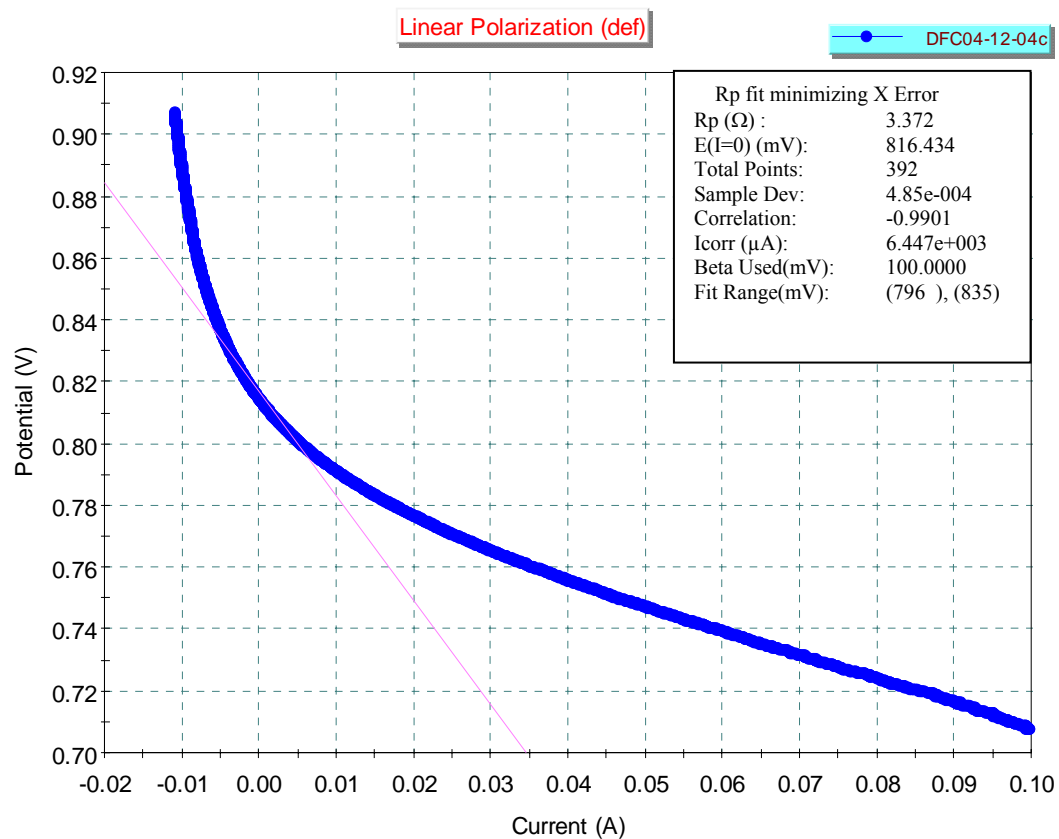


Figure F.2. $E-i$ curve for PEMFC of $0.3\text{mgPt}/\text{cm}^2$ at dry condition

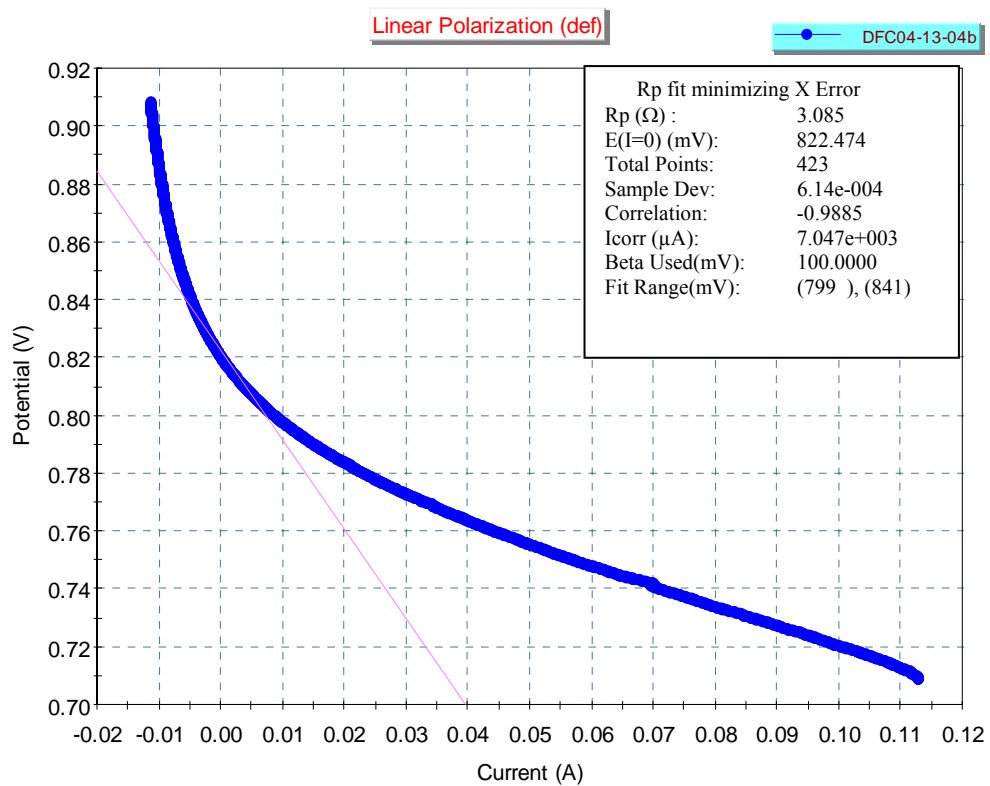


Figure F.3. $E-i$ curve for PEMFC of $0.3\text{mgPt}/\text{cm}^2$ at wet condition

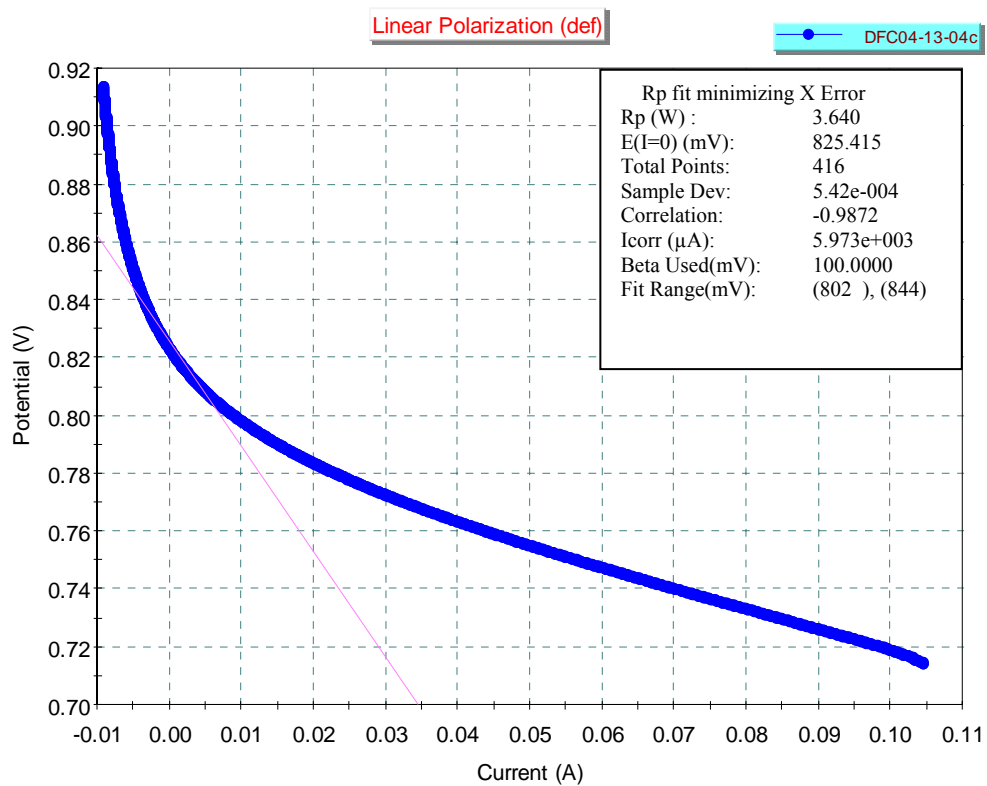


Figure F.4. $E-i$ curve for PEMFC of $0.3\text{mgPt}/\text{cm}^2$ at wet condition

APPENDIX G. PROPERTIES OF NAFION[®]

Properties of Nafion[®] PFSA Membrane

A. Thickness and Basis Weight Properties¹

Membrane Type	Typical Thickness (microns)	Basis Weight (g/m ²)
N-112	51	100
NE-1135	89	190
N-115	127	250
N-117	183	360
NE-1110	254	500

B. Physical and Other Properties

Property ²	Typical Value	Test Method
Physical Properties		
Tensile Modulus, MPa (kpsi)		
50% RH, 23 °C	249 (36)	ASTM D 882
water soaked, 23 °C	114 (16)	ASTM D 882
water soaked, 100 °C	64 (9.4)	ASTM D 882
Tensile Strength, maximum, MPa (kpsi)		
50% RH, 23 °C	43 (6.2) in MD, 32 (4.6) in TD	ASTM D 882
water soaked, 23 °C	34 (4.9) in MD, 26 (3.8) in TD	ASTM D 882
water soaked, 100 °C	25 (3.6) in MD, 24 (3.5) in TD	ASTM D 882
Elongation at Break, %		
50% RH, 23 °C	225 in MD, 310 in TD	ASTM D 882
water soaked, 23 °C	200 in MD, 275 in TD	ASTM D 882
water soaked, 100 °C	180 in MD, 240 in TD	ASTM D 882
Tear Resistance - Initial, g/mm		
50% RH, 23 °C	6000 in MD, TD	ASTM D 1004
water soaked, 23 °C	3500 in MD, TD	ASTM D 1004
water soaked, 100 °C	3000 in MD, TD	ASTM D 1004
Tear Resistance ³ - Propagating, g/mm		
50% RH, 23 °C	>100 in MD, >150 in TD	ASTM D 1922
water soaked, 23 °C	92 in MD, 104 in TD	ASTM D 1922
water soaked, 100 °C	74 in MD, 85 in TD	ASTM D 1922
Specific Gravity	1.98	—
Other Properties		
Conductivity, S/cm	0.083	see footnote ⁴
Acid Capacity, meq/g	0.89	see footnote ⁵

¹Measurements taken with membrane conditioned to 23 °C, 50% relative humidity (RH).

²Where specified, MD - machine direction, TD - transverse direction. Conditioning state of membrane given. Measurements taken at 23 °C, 50% RH.

³Tear resistance (g/mm) of dry membrane increases with thickness. Values given are typical for 0.05 mm membrane.

⁴Conductivity measurement as described by Zawodzinski, et.al, *J. Phys. Chem.*, 95 (15), 6040 (1991). Membrane conditioned in 100 °C water for 1 hour. Measurement cell submerged in 25 °C D.I. water during experiment. Membrane impedance (real) taken at zero imaginary impedance.

⁵A base titration procedure measures the equivalents of sulfonic acid in the polymer, and uses the measurement to calculate the acid capacity or equivalent weight of the membrane.

Properties of Nafion[®] PFSA Membrane

C. Hydrolytic Properties

Property	Typical Value	Test Method
Hydrolytic Properties		
Water content, % water ⁶	5	ASTM D 570
Water uptake, % water ⁸	38	ASTM D 570
Thickness change, % increase		
from 50% RH, 23 °C to water soaked, 23 °C	10	ASTM D 756
from 50% RH, 23 °C to water soaked, 100 °C	14	ASTM D 756
Linear expansion, % increase ⁹		
from 50% RH, 23 °C to water soaked, 23 °C	10	ASTM D 756
from 50% RH, 23 °C to water soaked, 100 °C	15	ASTM D 756

⁶Water content of membrane conditioned to 23 °C, 50% relative humidity (RH), compared to dry weight basis.

⁸Water uptake from dry membrane to water soaked at 100 °C for 1 hour (dry weight basis).

⁹Average of MD and TD. MD expansion is slightly less than TD.